University of Alberta

Permeability Estimation of Fracture Networks

by

Alireza Jafari

A thesis submitted to the Faculty of Graduate Studies and Research
in partial fulfillment of the requirements for the degree of

Doctor of Philosophy

in

Petroleum Engineering

Department of Civil and Environmental Engineering

Edmonton, Alberta
Spring, 2011

In The Name of God, The Most Gracious, The Most Merciful

Dedication to

My patient wife, Marzieh Ganjali, for her love and friendship,

My beautiful and lovely daughter, Dina, for bringing happiness to my life,

My wonderful and supportive parents and also all my sisters and brothers,

and

All my good friends.

Abstract

This dissertation aims to propose a new and practical method to obtain equivalent fracture network permeability (EFNP), which represents and replaces all the existing fractures located in each grid block for the reservoir simulation of naturally fractured reservoirs. To achieve this, first the relationship between different geometrical properties of fracture networks and their EFNP was studied. A MATLAB program was written to generate many different realizations of 2-D fracture networks by changing fracture length, density and also orientation. Next, twelve different 2-D fractal-statistical properties of the generated fracture networks were measured to quantify different characteristics. In addition to the 2-D fractal-statistical properties, readily available 1-D and 3-D data were also measured for the models showing variations of fracture properties in the Z-direction.

The actual EFNP of each fracture network was then measured using commercial software called FRACA. The relationship between the 1-, 2- and 3-D data and EFNP was analyzed using multivariable regression analysis and based on these analyses, correlations with different number of variables were

proposed to estimate EFNP. To improve the accuracy of the predicted EFNP values, an artificial neural network with the back-propagation algorithm was also developed.

Then, using the experimental design technique, the impact of each fracture network parameter including fracture length, density, orientation and conductivity on EFNP was investigated. On the basis of the results and the analyses, the conditions to obtain EFNP for practical applications based on the available data (1-D well, 2-D outcrop, and 3-D welltest) were presented. This methodology was repeated for natural fracture patterns obtained mostly from the outcrops of different geothermal reservoirs. The validity of the equations was also tested against the real welltest data obtained from the fields.

Finally, the concept of the percolation theory was used to determine whether each fracture network in the domain is percolating (permeable) and to quantify the fracture connectivity, which controls the EFNP. For each randomly generated fracture network, the relationship between the combined fractal-percolation properties and the EFNP values was investigated and correlations for predicting the EFNP were proposed. As before, the results were validated with a new set of fracture networks.

Acknowledgments

I would like to express my gratitude to my supervisor Dr. Tayfun Babadagli, for his advice, guidance and support throughout the course of this research.

I would also like to express my appreciation to all committee members of the candidacy and final exams, Dr. Ergun Kuru, Dr. Hassan Safouhi, Dr. Mohamed Al-Hussein and Dr. Koorosh Asghari.

I gratefully acknowledge financial support from NSERC (Discovery Grant No:G121210595), Iranian Ministry of Science, Research and Technology, and also the Institute of Petroleum Engineering (IPE) of Tehran University.

I would like to thank Beicip-Inc. and Schlumberger, for supplying FRACA and Eclipse software packages, respectively.

Once again, I would like to take this opportunity to thank the endless support from my wonderful and respected parents, my kind and lovely wife and beautiful daughter and also all my sisters and brothers.

I also extend my appreciation to all members of the EOGRRC research group at the University of Alberta.

Table of Contents

List of Tables

List of Figures

1 Introduction

1.1 Overview

Mapping fracture networks and estimating their properties such as porosity and permeability to be used as input data in simulation studies are two critical steps in the modeling of naturally fractured reservoirs. The data to achieve these two tasks are almost always insufficient and mostly limited to well scale measurements, seismic maps, and outcrop studies. Any quantitative information about fracture networks obtained through these sources would make the accurate preparation of static models possible. It is essential to use limited quantitative data effectively in fracture network studies for accurate estimation of reservoir performance in any subsurface modeling study.

The most challenging parameter of fracture networks to be fed into the flow simulator is permeability. In fact, all fractures placed in each grid block could be replaced by an equivalent permeability value representing all of those existing fractures. Numerical methods to calculate the equivalent permeability values for a given fracture network system exist; however, they could be significantly time consuming, especially in highly fractured-complex reservoirs.

This dissertation focuses on this critical problem, namely practical estimation of fracture network permeability. Chapter 2 covers the application of the fractal geometry for characterizing and analyzing 2-D fracture networks. In this chapter, the relationships between different fractal-statistical properties of fracture network features and equivalent facture network permeability (EFNP) are shown. Also, after quantifying different features of fracture networks using the fractal dimension, the results of conducting an experimental design technique to show the influence of each fracture network property on the EFNP is presented.

In chapter 3, an application of artificial neural networks to improve the accuracy of EFNP is given. This chapter also compares the EFNP values obtained from two different methods, i.e. multivariable regression analysis (MRA) and artificial neural networks (ANN). The models were developed using natural fracture patterns and validated using synthetic fracture patterns. Statistical and fractal characteristics of twenty natural fracture patterns collected from the outcrops of geothermal reservoirs were measured and then correlated to the EFNP using MRA and several empirical equations with different numbers of variables were proposed. Next, synthetic fracture networks were generated and used for validation purposes. The EFNP of these synthetic fracture networks were predicted using the derived empirical equations. As a final effort, we took advantage of the capability of ANN to improve the correlations obtained through the MRA.

Chapter 4 explains the proposed procedure for calculating the EFNP for a set of fracture patterns mapped from the outcrops of geothermal reservoirs in

southwestern Turkey. Their EFNP values were predicted using the new method proposed in the thesis and it is shown that the computed permeability values are comparable to those obtained with a commercial software package and actual permeability values obtained through field tests.

Chapter 5 extends the previous works to fracture network permeability estimation using the statistical and fractal properties data conditioned to welltest information based on the existing strong correlation between the statistical and fractal parameters of 2-D fracture networks and their permeability shown in previous chapters.

In chapter 6, a more complex and realistic 3-D network system is considered. Variation of fracture network characteristics in the z-direction was presented by a multi-layer system representing three different facieses with different fracture properties. Using available 1-D, 2-D, and 3-D data, MRA was performed to obtain EFNP correlations and then the derived equations were validated against a new set of synthetic fracture networks. Next, minimal amount of 1-D, 2-D and 3-D data needed to accurately map fracture network permeability was determined for different fracture network characteristics.

In chapter 7, the concepts of percolation theory and fractal geometry are combined to define the connectivity characteristics of 2-D fracture networks and a new approach to estimate the EFNP is introduced. The fractal dimensions of different fracture network features (intersection points, fracture lines, connectivity index, and also the fractal dimensions of scanning lines in X- and Y- directions), and the dimensionless percolation density of fracture

networks are computed. The method is based on the proposed correlations between the EFNP and a percolation term, $(\rho'-\rho'_c)$. This term is obtained using the relationships with the fractal and statistical properties of fracture networks mentioned above. The method introduced was validated using different fracture patterns representing a wide range of fracture and length values. In addition, a correlation between the number of fractures in the domain and the minimum size of the fracture length is presented to estimate the shortest or minimum fracture length required to have a percolating system for a given number of fractures in the domain.

As this is a paper-based thesis, each chapter has its own conclusions. In chapter 8, the major contributions of this dissertation and also recommendations for future works are presented.

1.2 Literature review

The natural fractures in the subsurface reservoirs strongly control the fluid flow, as fluid along these fractures can flow more quickly and over larger distances than it could flow through the matrix itself (Murphy et al., 2004) unless they are sealed with later depositions. The correct estimation of the flow properties of fractured rocks is crucial in modeling of hydrocarbon reservoirs, nuclear waste repositories, and geothermal reservoirs. Despite the extensive work on characterizing fractured rocks conducted over the last few decades, predicting fluid flow within the host rocks is still a challenging work (Berkowitz, 1995). Literature relevant to the research done in this dissertation is reviewed under several different titles as given below.

1.2.1 Modeling approaches for naturally fractured reservoirs

Two well-known modeling approaches commonly used in simulating flow in naturally fractured reservoirs (NFR) are dual-porosity and discrete fracture network (DFN) models. The dual-porosity approach was first presented by Barenblatt and Zheltov (1960) and Barenblatt et al. (1960) to model NFRs. In this approach, each medium, i.e. a porous matrix and the fracture network, is superimposed and mutually communicating (Bogdanov et al. 2003). Warren and Root (1963) later modeled fractured porous media as an idealized two equivalent fracture and matrix media consisted of identical rectangular matrix blocks separated by an orthogonal network of fractures. In this model, fluid flow occurs in the fracture network and the matrix blocks feed these networks. Dual-porosity models are limited in capturing the complex structure of fracture networks; though, they are useful in describing the complex process of matrix-fracture interaction.

Later, Pruess and Narasimhan (1985) introduced the MINC (multiple interacting continua) model, which discretizes the matrix block into smaller units. This approach is often used to simulate fractured geothermal systems. The major problem associated with the dual porosity and MINC approaches is the specification of equivalent hydraulic properties, especially permeability, for the fracture network.

On the other hand, the discrete fracture network (DFN) models are more useful in describing the complex structure of fracture networks (Narr et al. 2006; Parney et al. 2000). The DFN models are more capable in addressing the connectivity characteristics of fracture networks compared to the dual-porosity

models (Dershowitz et al. 2000). However, they are limited in modeling complex dynamic processes.

Generally, a simulation grid block containing fractures acts as an effective medium whose properties can be represented by equivalent values, for instance an equivalent fracture network permeability tensor (Long et al, 1982). For any kind of dynamic modeling approach, one needs to define the equivalent fracture network permeability values for each grid block and the accuracy of the simulation strongly depends on this parameter (Bourbiaux et al., 1998).

The influence of fracture properties in particular is significant on the results as the fracture system preferentially controls the hydrodynamics of fractured reservoir (Mourzenko et al. 2001). In fact, fracture network permeability is one of the critical input data to the simulator and controlled by topological and geometrical properties of the networks. A great deal of effort has been devoted to characterize those properties (Berkowitz, 1994). Despite remarkable efforts to characterize fractured reservoirs properly and to simulate their performances, due to complex fracture network geometry, modeling of such systems is still considered to be a difficult task. In other words, this complex geometry prevents direct feeding into the reservoir simulators (Bourbiaux et al., 1998, 1999). As a result, at a crucial stage in the simulation modeling of these reservoirs, this geometry (with all its defined properties) must be scaled up i.e. converted into essential parameters for running any simulator, and the results for instance equivalent permeability could be then fed into single or dual porosity (or dual porosity-permeability) simulators (Petrel Manual, 2007). However, one of the big challenges in numerical simulations of this type of

reservoirs is the specification of those equivalent permeability values for the fracture network.

1.2.2 Estimation of effective fracture network permeability values

Several methods have been proposed to calculate effective (equivalent) fracture network permeability (EFNP). Oda (1985) introduced a method for calculating equivalent permeability tensor of a fractured reservoir using the geometry of fracture network. The method does not require a flow simulator to obtain the permeability tensor; also it does not account for the fracture connectivity; and thus, it is limited to well-connected fracture networks. In other words, it would underestimate equivalent fracture permeability when fracture density is low.

Long et al. (1985) and Cacas et al. (1990) developed 3D fracture flow models and then Massonnate and Manisse (1994) introduced a 3D fracture flow model which takes into account the matrix permeability. Lough et al. (1996) developed a 2D fracture flow model taking into account the contribution of 3D matrix flows. Odling (1992) introduced a 2D model by considering the matrix permeability. Later, Bourbiaux et al. (1998) proposed a method to calculate the equivalent permeability by applying a pressure drop between the two sides of the parallelepiped network with a specific boundary condition. Using their model, the equivalent permeability for incompressible steady-state flow through the actual 3D fracture network can be calculated.

Min et al. (2004) presented a method to calculate equivalent fracture permeability tensor of fractured rocks using stochastic representative elementary volume (REV) approach. In their method, the equivalent permeability values were calculated using the two-dimensional distinct element code UDEC (Itasca, 2000). Nakashima et al. (2000 and 2001) presented an up-scaling technique by the boundary element method to estimate the effective permeability of naturally fractured reservoirs. Teimoori et al. (2003) used the same method to improve the computation of effective permeability tensor in naturally fractured reservoirs.

Semi-quantitative analyses have shown that fracture network characteristics have direct implications on fracture network permeability. Basically, fracture connectivity, length, density, aperture, and orientation are the crucial parameters of each fracture network controlling the permeability of the network. For instance, Babadagli (2001) speculated that perpendicular fractures to the direction of the flow probably reduce the permeability. Also, as fracture length and density increase, the connectivity of a fracture network will increase (Rossen et al., 2000); and the hydraulic properties of fractured reservoirs are primarily dependent on the degree of fracture interconnection. A fracture network must have a percolating cluster to be permeable. Hence, the connectivity is of the primary importance in this analysis. Zhang et al (1996) showed that with an increase in fracture aperture and density, permeability of the network also increases.

Fracture connectivity controls many principle properties of fractured reservoirs and the permeability is the most critical one (Berkowitz, 1995). For example,

Long and Billaux (1987) observed that, due to low fracture connectivity at a field site in France, roughly 0.1% of fractures contribute to the overall fluid flow (i.e., permeability). This parameter, however, is difficult to quantify and embedded in the fracture network permeability correlations. Other parameters including fracture length, density, aperture and orientation also play a critical role on the equivalent fracture network permeability.

1.2.3 Fractal properties and the fracture networks

Along with the statistical properties such as distribution functions of fracture network properties, fractal characteristics are used for quantification purposes since the natural fracture patterns were observed to be fractal objects (Barton and Larsen, 1985; La Pointe, 1988; Barton and Hseih, 1989). The fractal dimension, which is a non-integer value, shows the tendency of an object to spread or fill in the space where it is located (Berkowitz and Hadad, 1997).

Later, a limited number of studies reported that fractal properties have implications on the equivalent fracture network permeability. For example, La Pointe (1997) stated that flux and mass fractal dimension of discrete fracture networks have a linear proportionality which implies that fractal dimension probably is a useful index of the flow properties of fractured rocks.

The fractal dimensions of different network properties such as length, density and orientation of fracture needs to be measured as these parameters control the hydraulic properties of fracture networks. For example, higher fractal dimension means more complex and denser fracture network (Matsumoto et al.

1992; Babadagli, 2001) and the denser networks yield higher fracture permeability.

It is expected that the fractal dimension of different network properties yields different values even if the same technique is applied. Also, the fractal dimension of the same fracture network property can be estimated using different techniques such as box-counting, sand-box and scanline and they may yield different values as those techniques measure different fractal characteristics (Babadagli, 2001).

There are a few techniques to measure fractal dimension. The standard technique proposed to quantify the spatial distribution of irregular objects is called box-counting (Mandelbrot, 1982). In this methodology, different box sizes are selected and overlaid on fracture network. Then, the number of boxes filled with fracture lines is counted. The number boxes filled with fracture lines vs. box sizes are plotted on log-log scale and the slope yields the fractal dimension (Barton and Larsen, 1985).

The mass dimension (sand-box) technique is also used to measure fractal dimension. In this method, a circle with a specific size and center was overlaid on the fracture domain and the number of features (fractures or points) located inside the circle is counted. The procedure is continued increasing the size of the circle with the same center. Then, the number of counts is plotted against the size of circle, on a log-log scale and the slope of the straight line yields mass fractal dimension (Bunde and Havlin, 1995).

The quantification of fracture orientation is critical in assessing the equivalent fracture network permeability. For example, it is expected that perpendicular fractures to fluid flow direction have negative effects on the network permeability, while parallel ones cause an increase in permeability (Babadagli, 2001). The scanline method proposed by Babadagli (2001) was used to consider the effect of orientation. In this method, a number of squares with different size but the same centre was used. The number of fractures touched by a scanline in a specific direction in an L-size square was counted. This procedure was repeated for each square of different sizes. Then on a double logarithmic scale, the size of squares, *L*, was plotted against the total number of the counts. The slope yields the fractal dimension.

The lacunarity is related to the degree of gappiness (or hole or porosity) or texture of an irregular object and can be used to differentiate fractal objects with exactly the same fractal dimension but different appearances. In fact, two fractal objects may look different despite having the same fractal dimension. In this case, fractal dimension may not be sufficient to differentiate between the two patterns, and other characteristics of the network need to be considered. Lacunarity is a useful tool for this purpose (Hamida and Babadagli, 2005 and 2007).

1.2.4 Use of artificial neural networks (ANN) in fracture network analysis

When the relationships between variables are nonlinear and complicated, it is believed that multivariable regression analysis may not be capable of fully

capturing these relationships. In these situations, the artificial neural networks (ANN) are preferred. Artificial neural networks (ANN) are computer models that mimic the functions of the human nervous system through some parallel structures comprised of non-linear processing nodes which are connected by weights. These weights establish a relationship between the input and output of each node in the ANN (Nikravesh et al., 2003). These systems process the data and then learn the relationships between the given data in a parallel and distributed pattern. This characteristic makes the ANN capable of capturing the complex relationships among many different parameters (White et al., 1995).

ANNs have a layer-based structure. The first and last layers are called input and output layers, which contain artificial neurons or so-called processing elements (PEs) exactly equal to the number of input and output parameters respectively. There is another layer called a hidden layer located between the two previous layers. Although all ANNs have generally the same layer-based topology, the number of hidden layers and PEs in these three kinds of layers varies depending on the problem (Rezaee et al., 2006).

For permeability estimation problems, supervised algorithms are generally preferred (Wiener 1995). Therefore, a supervised back propagation neural network (BPNN) with given both the input and output values during the learning (training) process is suitable (Wong and Nikravesh, 2001).

1.2.5 Percolation theory and fracture network

In addition to fractal geometry, the percolation theory has been turned out to be useful for analyzing fracture networks. The percolation theory is a powerful

concept for studying different phenomena in disordered media, especially for analyzing the transport properties of random systems.

Significant amount of work has been performed to solve network related problems in different areas of science and engineering using the classical theory of percolation since it was first introduced by Broadbent and Hammersley (1957). Scaling equations and universal constants and exponents are well defined for systematic lattices (Kirkpatrick, 1971; Stauffer, 1979; Sahimi, 1993; Berkowitz and Ewing, 1998). Fracture networks are random systems and the continuum percolation was introduced as an alternative to the lattice percolation.

First attempts on modeling fracture networks were on lattice networks (Stauffer and Aharony, 1994). However, due to the nature of fracture distribution within host rocks, percolation of fracture networks needed another class of percolation called continuum percolation (Mourzenko et al., 2005). The necessity of this approach was justified by Khamforoush et al. (2008) as the transport properties of fractured networks are affected not only by the individual properties of fractures and but also their connectivity properties.

Berkowitz (1995) reported that fracture connectivity could be used to study most of the fundamental properties of fracture networks which can be mathematically modeled by percolation theory (King et al., 2002). The most important characteristics of the continuum percolation is an appropriate density parameter equivalent to occupancy probability in the lattice percolation (Mourzenko et al., 2005).

An appropriate density parameter equivalent to occupancy probability in the lattice percolation was defined in the continuum percolation (Mourzenko et al., 2005). Also, Balberg et al. (1984) introduced the excluded volume (in 3D) concept which could play a critical role in continuum percolation. It is defined as the volume into which the center of other similar objects should not be placed in order not to have any overlap (intersection). However, it should be mentioned that this definition is valid if the objects are placed uniformly in space (Adler and Thovert, 1999). Mourzenko et al. (2004) combined fracture density in a unit cell with excluded volume and ended up with a dimensionless density. Since this dimensionless density is related to the excluded volume, the macroscopic properties of the fracture networks are independent of fracture shape (Koudina et al., 1998; Bogdanov et al., 2003a and 2003b; Mourzenko et al., 2004; Huseby et al., 1997; Huseby et al., 2001).

Mourzenko et al. (2004 and 2005) studied a 3-D model containing 2-D fracture planes (polygons) with power-law size distribution uniformly located in the space. Then, they triangulated each fracture network to solve flow equations and calculate permeability. They stated that a dimensionless fracture density is an appropriate equivalent parameter in continuum percolation which is independent of fracture shape. They also proposed a general equation by combining fracture density weighted by fracture conductivities and a universal function of a dimensionless fracture density which takes into account fracture shape and size distribution.

King et al. (1999) used percolation theory to estimate the distribution of the shortest path between two wells and also the distribution of the breakthrough

times and associated uncertainty by simple algebraically calculation rather than the traditional time-consuming numerical simulation.

Odagaki et al. (1999) investigated the 2-D systems with correlated distribution for a model granular system and a lattice gas and found that correlated distribution of percolating objects affects the percolation properties in both statistic structure and dynamic processes.

Nolte et al. (1989) studied the effect of contact areas of fractures on their flow properties and showed that the effect of tortuosity of the flow path on fluid transport is controlled by the proximity of the distribution of these paths to a percolation threshold. They also presented a model which could be used to determine how far the systems are located above the percolation threshold.

Very recently, more emphasis was given to the estimation of fracture network permeability through the percolation theory. Khamforoush et al. (2008) studied the percolation threshold and permeability of anisotropic 3-D fracture networks. They found that the percolation threshold in the X- and Y-directions decreases as anisotropy increases but in the Z-direction an opposite trend can be seen. Koudina et al. (1998) calculated the permeability of a 3-D network consisting of polygonal fractures and studied the data relative to the percolation threshold and found that permeability exponent, i.e., "t" ($K \approx (\rho' - \rho'c)^t$) in 3-D, was in very good agreement with the universal exponent in 3-D reported by Stauffer and Aharony (1994); the effect of the fracture shape was also investigated.

Zhang and Sanderson (2002) studied the connectivity of 2-D fractures in terms of fracture density, orientation and length. They found that fracture density is the controlling parameter of the percolation threshold and fracture connectivity is dependent only on this parameter as long as the fractures have much a smaller length relative to the size of the region of interest. Also, at or above this critical point, i.e., percolation threshold, the permeability of the system increases with an increase in fracture density.

Masihi et al. (2005) applied the percolation theory concepts on fractured reservoirs to analyze the reservoir performance and showed that the performance parameters can be predicted very quickly by some semi-analytical universal curves. Later, Masihi et al. (2007) determined the two scaling curves of connectivity of isotropic fracture systems which could be used to estimate fracture connectivity and its associated uncertainty very quickly. They also applied the percolation concepts to a field example from the Bristol Channel basin.

The percolation threshold of different simple systems in the percolation continuum has been determined by different researchers; for example, the percolation threshold of randomly oriented sticks in 2-D in terms of dimensionless density (ρ') has been reported to be 3.6 (Adler and Thovert, 1999). For analyzing any fracture system, the percolation threshold needs to be estimated theoretically and compared with the actual density of fractures in the system (Berkowitz and Balberg, 1993).

Conventional methods of fracture network modeling, more specifically

permeability estimation, suggest generating many different -random- realizations of possible fracture network configurations and then flow simulation for each one has to be performed. Having a practical technique to quickly estimate the equivalent fracture network permeability using available fracture network properties and percolation theory will reduce the computational work needed in the conventional characterization and simulation of fractured systems.

1.3 Statement of the problem

Despite the recent efforts to characterize fractured reservoirs properly, simulation of flow in such systems has remained a difficult task mainly due to complex fracture network geometry.

Petrophysicists, hydrogeologists, and reservoir engineers are interested in measuring permeability values of complex subsurface reservoirs as input data for simulation studies. Direct measurements of permeability using wireline devices or welltest methods are rarely applicable in fractured reservoirs and are usually expensive. Even if these tools are available at acceptable costs, direct permeability measurements are usually unevenly and sparsely distributed. Although they might be useful in homogeneous reservoirs, it is difficult to obtain meaningful permeability values of fracture networks for the whole reservoir structure through these techniques.

In practice, the only source of high resolution data to aid in permeability estimation is provided by well logging. However, due to the complexity of the

fractured reservoirs, to the best of our knowledge, no universally applicable method of estimating fracture network permeability from well logging data exists. The main problem is that the fracture systems are random in nature and limited 1-D (well) data is not sufficient to represent the whole (3-D) system. Single well data provide information in 1-D, which naturally lacks the information about the length of fracture extension and more importantly, connectivity. Network permeability requires this information and limited data (density and aperture) obtained from wells may not be sufficient to obtain meaningful information about 3-D characteristics of fracture networks related to the permeability. 3-D network permeability obtained from pressure transient tests represents an average "global" value and cannot account for the regional changes in permeability, which is a common issue as network characteristics of fractures change in lateral and vertical directions considerably due to their random nature.

In addition, most of the methods mentioned in the "Literature Review" section for calculating the equivalent fracture network permeability (mainly the numerical techniques) require fracture network discretization and a significant computational effort due to a great number of nodes needed for computations, especially when dealing with a highly fractured reservoir. This is an additional cost to the simulation of hydrocarbon and geothermal reservoirs.

Therefore, it is critical to develop simpler and more accurate correlations to predict the equivalent fracture network permeability for practical purposes. Obviously, the new technique proposed should be based on different scenarios (possibility) of all available information on fracture networks for practical

purposes including core (1-D), outcrop (2-D) and welltest (3-D) data. Often times, they all may not be available and one has to utilize the existing data for permeability estimation.

1.4 Solution methodology

The objective of this thesis work was to propose a practical and accurate approach to estimate equivalent fracture network permeability (EFNP) values for 2-D networks. To define correlations for the EFNPs, extensive quantification of fracture network properties are needed. For this purpose, fractal and percolation characteristics of randomly generated 2-D fracture networks (in the MATLAB environment), were defined and tested against "actual" EFNPs obtained from an existing software package (FRACA). This software package is one of the very limited commercially available tools to perform fracture network modeling and simulation applications. Our solutions rely on the accuracy of this software package and there is no any other possible and practical way to create significant number of experimental trials of EFNP calculations to eventually generate correlations. This software package has been tested (Bourbiaux et al., 1998) and commonly used in the industry (Veire et al., 2007).

All possible combinations of fracture network properties and many different random realizations of them were used in the analysis in this dissertation. After this experimentation process, correlations were obtained using multivariable regression and artificial neural network methods. A validation process was applied at the end using fracture configurations that were not used in the

correlation development exercise. The methodology proposed was also applied on natural fracture systems and validated against unbiased samples of fracture networks.

Through the methodology, a relatively simpler approach was proposed for practical estimation of EFNP at different scales using any possible combination of available data including 1-D (well related) and 2-D (outcrop) and even 3-D (well test) data to be eventually fed into the flow simulators.

2 Effective Parameters on Fracture Network Permeability

2.1 Overview

Fracture network mapping and estimation of its permeability constitute two major steps in static model preparation of naturally fractured reservoirs. The equivalent fracture network permeability (FNP) is controlled by many different fracture network parameters such as fracture length, density, orientation, aperture, and single fracture connectivity.

The objective of this chapter was to determine the relative importance of the different fracture network parameters using the experimental design approach (2- and 3-level design). Five different 2-D fracture data sets were generated for random and systematic orientations. In each data set, twenty different combinations of fracture density and length for different orientations were tested. For each combination, ten different realizations were generated. The results were presented as Pareto charts.

A version of this chapter has been published

Jafari, A. and Babadagli, T.: "A Sensitivity Analysis for Effective Parameters on 2-D Fracture Network Permeability," June 2009 SPE Reservoir Evaluation & Engineering Journal.

2.2 Generation of fracture network models

To generate 2-D random fracture networks in square domains, a numerical algorithm was developed. Each fracture network is composed of linear fractures with fracture centers distributed randomly according to a uniform distribution. In this algorithm, the fracture length was considered as a categorical variable. Either a constants value for it (20m, 40m, 60m and 80m) was used or a distribution was assigned (normal distribution with a mean value of 20m, 40m, 60m or 80m). The fracture density (as the number of fractures per 100x100 m^2 area) was defined also as a categorical variable (50, 100, 150, 200, and 250). The orientation was considered creating two fracture sets in each domain with different directions as follows: (1) NS-EW, (2) NW-SE & NE-SW, and (3) totally random orientation (**Table 2.1**).

Table 2.1 The variability of the each fracture network parameters used in the generation of fracture network models.

Fracture Parameter	Value
Length(m)	Constant (20, 40, 60, 80)
	Variable (Normal distribution with a mean value of 20, 40, 60, 80)
Density(#/domain)	50, 100, 150, 200, 250
Orientation	N-S & E-W
	NW-SE & NE-SW
	Random

Jafari, A. and Babadagli, T.: "A Sensitivity Analysis for Effective Parameters on 2-D Fracture Network Permeability," June 2009 SPE Reservoir Evaluation & Engineering Journal.

The conductivity (aperture) of fractures was kept constant in the derivation of the FNP correlation. For further sensitivity analysis, it was changed for a few cases to clarify its effects on the FNP.

In total, five different data sets were generated: (1) N-S & E-W fractures with fixed length (2) N-S & E-W fractures with variable length (3) NW-SE & NE-SW fractures with fixed length (4) NW-SE & NE-SW fractures with variable length and (5) random orientation with fixed length. **Figure 2.1**, **Figure 2.2** and **Figure 2.3** show examples of these two-dimensional patterns with different orientation. Each figure represent 100x100 m^2 plane.

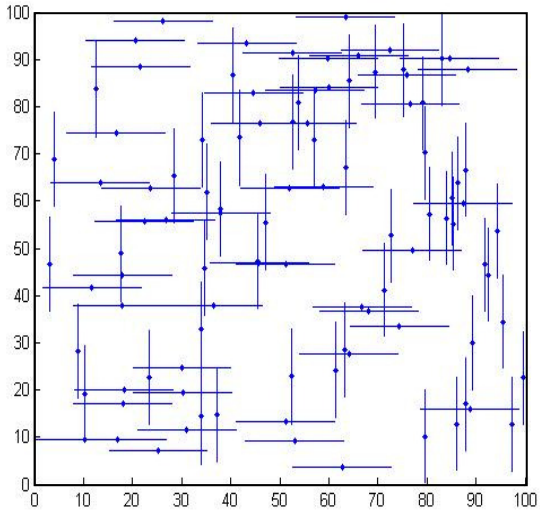

Figure 2.1 Fracture network with two fracture sets, N-S & E-W and fixed length.

Jafari, A. and Babadagli, T.: "A Sensitivity Analysis for Effective Parameters on 2-D Fracture Network Permeability," June 2009 SPE Reservoir Evaluation & Engineering Journal.

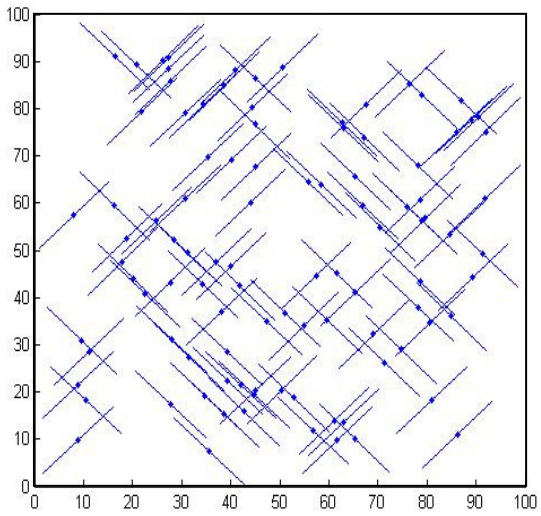

Figure 2.2 Fracture network with two fracture sets, NW-SE & NE-SW and fixed length.

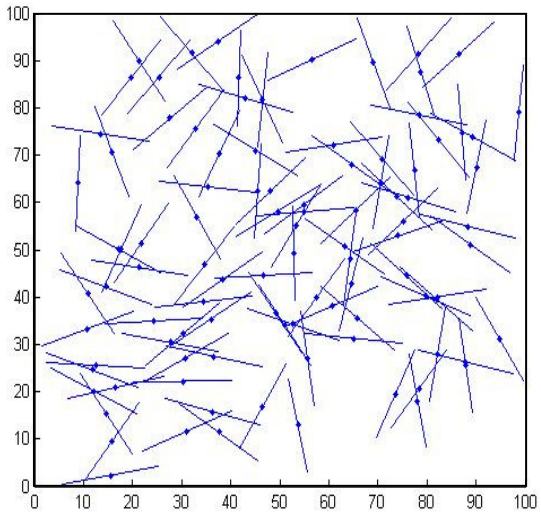

Figure 2.3 Fracture network with random orientation and fixed length.

Jafari, A. and Babadagli, T.: "A Sensitivity Analysis for Effective Parameters on 2-D Fracture Network Permeability," June 2009 SPE Reservoir Evaluation & Engineering Journal.

Each data set has twenty different scenarios which cover a wide range of possible combinations of length and density values as shown in **Table 2.2** and **Table 2.3**. Each scenario has ten different realizations generated using different random seeds which yield a total of 200 runs. Those runs were repeated for the five different cases listed above (three different orientations and fracture length distribution types with the same and variable length). Eventually, the total number of runs turned out to be 1000.

Table 2.2 Two fracture sets in the domain with directions NW-SE & NE-SW and fixed length (FD: Fractal dimension).

Length (m)	Density	Box Counting FD		Sandbox Counting FD		Scanline FD (in X direction)	Scanline FD (in Y direction)	Connectivity Index	Maximum Touch with X Scanline	Maximum Touch with Y Scanline	Box Counting FD	Permeability (mD)
		Intersection Point	Mid Point	Intersection Point	Mid Point						Lines	
20	50	1.08	1.408	1.328	1.555	1.605	1.437	0.616	7072.2	7070.8	1.293	8.322
20	100	1.555	1.638	1.604	1.707	1.318	1.324	1.199	14142.2	14145.9	1.465	22.247
20	150	1.74	1.733	1.551	1.503	1.338	1.317	1.812	21212.8	21216.3	1.552	71.728
20	200	1.835	1.817	1.681	1.491	1.347	1.37	2.477	28282.4	28283.2	1.62	131.307
20	250	1.878	1.857	1.856	1.541	1.363	1.365	2.976	35350	35354.3	1.648	177.957
40	50	1.564	1.401	1.65	1.366	1.131	1.145	2.902	14140.2	14142.5	1.429	69.346
40	100	1.803	1.647	1.565	1.404	1.112	1.113	5.911	28283.3	28285	1.583	176.614
40	150	1.867	1.745	1.671	1.428	1.118	1.115	8.776	42427	42426.6	1.651	297.858
40	200	1.911	1.817	1.886	1.352	1.132	1.134	11.499	56569.2	56571.8	1.7	403.728
40	250	1.915	1.854	1.935	1.403	1.126	1.122	14.575	70714.1	70710.6	1.737	527.569
60	50	1.703	1.398	1.59	1.265	0.93	0.932	7.444	21213.1	21213.2	1.457	124.91
60	100	1.812	1.641	1.531	1.198	0.94	0.934	14.875	42426.5	42424.9	1.596	269.127
60	150	1.841	1.754	1.7	1.241	0.929	0.932	22.666	63638.5	63639.4	1.682	389.361
60	200	1.849	1.823	1.62	1.342	0.934	0.936	30.224	84852.2	84850.3	1.722	534.268
60	250	1.855	1.859	1.632	1.286	0.928	0.929	37.907	106066.6	106062.6	1.76	685.512
80	50	1.727	1.401	1.903	1.501	0.86	0.859	12.064	28282.7	28284.9	1.456	134.642
80	100	1.78	1.638	1.773	1.903	0.859	0.859	24.008	56568.4	56567.6	1.586	287.947
80	150	1.8	1.754	1.771	2.122	0.859	0.859	36.095	84852.8	84855	1.665	430.228
80	200	1.801	1.817	1.671	1.788	0.859	0.859	47.925	113136.7	113137.6	1.705	603.897
80	250	1.804	1.86	1.74	1.808	0.859	0.859	59.979	141420.9	141422.2	1.73	731.907

Jafari, A. and Babadagli, T.: "A Sensitivity Analysis for Effective Parameters on 2-D Fracture Network Permeability," June 2009 SPE Reservoir Evaluation & Engineering Journal.

Table 2.3 Two fracture sets in the domain with directions NW-SE & NE-SW and variable length (FD: Fractal dimension).

Length (m)	Density	Box Counting FD		Sandbox Counting FD		Scanline FD (in X direction)	Scanline FD (in Y direction)	Connectivity Index	Maximum Touch with X Scanline	Maximum Touch with Y Scanline	Box Counting FD	Permeability (mD)
		Intersection Point	Mid Point	Intersection Point	Mid Point						Lines	
20	50	1.083	1.396	1.423	1.524	1.348	1.409	0.594	7014.1	7011.7	1.312	7.039
20	100	1.524	1.633	1.729	1.622	1.383	1.377	1.16	13903.6	13902.2	1.45	23.709
20	150	1.738	1.751	1.802	1.584	1.327	1.324	1.719	20569.7	20570.9	1.538	69.25
20	200	1.818	1.814	1.917	1.511	1.368	1.38	2.267	27661.5	27661	1.599	118.259
20	250	1.881	1.849	1.856	1.6	1.322	1.344	2.885	34549.9	34553.1	1.645	167.823
40	50	1.565	1.402	1.935	1.444	1.189	1.188	2.826	14001.2	14001.1	1.42	65.471
40	100	1.805	1.637	1.78	1.45	1.141	1.142	5.585	27884.7	27884.1	1.558	184.384
40	150	1.872	1.748	1.758	1.431	1.117	1.111	8.522	41616.6	41611.6	1.652	280.764
40	200	1.911	1.814	1.723	1.473	1.111	1.111	11.283	55866.7	55869.7	1.697	411.096
40	250	1.922	1.86	1.802	1.437	1.124	1.128	14.131	69860.4	69863.6	1.735	495.838
60	50	1.69	1.401	1.531	1.2	0.933	0.93	7.172	20897.1	20894.9	1.465	121.551
60	100	1.807	1.625	1.57	1.289	0.926	0.929	14.851	41982.3	41980.1	1.612	250.268
60	150	1.849	1.749	1.838	1.29	0.928	0.928	22.493	63175.1	63173.1	1.672	399.481
60	200	1.862	1.815	1.7	1.367	0.929	0.926	29.096	83946.2	83945.6	1.719	545.515
60	250	1.87	1.853	1.717	1.414	0.927	0.928	36.994	104983.9	104981.8	1.755	678.4
80	50	1.713	1.399	1.676	2	0.856	0.857	11.862	28040.4	28042	1.453	131.304
80	100	1.785	1.625	1.762	1.86	0.857	0.857	23.747	55972.4	55971.5	1.582	293.921
80	150	1.795	1.736	1.7	1.815	0.857	0.858	35.561	84288.3	84287.4	1.664	402.936
80	200	1.801	1.808	1.69	1.686	0.857	0.857	47.435	112088	112088.8	1.715	552.664
80	250	1.805	1.841	1.676	1.778	0.857	0.857	58.932	139992.2	139992	1.745	740.174

2.3 Fractal analysis of 2-D fracture models

Natural fracture patterns show fractal behavior (Barton and Larsen, 1985; La Pointe, 1988; Barton and Hseih, 1989). In their pioneering work, Barton and Larsen, (1985) and later Barton (1995) analyzed the fractal dimension of fracture trace maps from a different tectonic settings and lithologies using box-

Jafari, A. and Babadagli, T.: "A Sensitivity Analysis for Effective Parameters on 2-D Fracture Network Permeability," June 2009 SPE Reservoir Evaluation & Engineering Journal.

counting technique. Bonnet et al. (2001) later concluded that the geometry of a fracture system cannot be completely defined by a single fractal dimension and the fractal dimension of other geometrical parameters such as density, length and orientation and aperture and fracture surface roughness needs to be considered.

It is expected that the fractal dimension of different network properties yields different values even if the same technique is applied. Also, the fractal dimension of the same fracture network property can be estimated using different techniques such as box-counting, sand-box and scanline and they yield different values as those techniques measure different fractal characteristics (Babadagli, 2001). Hence, different methods should be used to measure the fractal dimension of different fracture properties.

The connectivity of fracture networks is very critical parameter controlling the fluid flow in impermeable or low permeable formations (Long and Balliaux, 1987; Margolin et al., 1998). Therefore, we started with measuring the fractal dimension of the distribution of the fracture intersection and mid-points that represent the connectivity and density of the network, respectively, using different methods. The fractal dimensions of other network properties such as length, density and orientation of fracture were also measured as these parameters control the hydraulic properties of fracture networks. For example, higher fractal dimension means more complex and denser fracture network (Matsumoto et al. 1992; Babadagli, 2001) and the denser networks yield higher fracture permeability.

Jafari, A. and Babadagli, T.: "A Sensitivity Analysis for Effective Parameters on 2-D Fracture Network Permeability," June 2009 SPE Reservoir Evaluation & Engineering Journal.

The fractal techniques we applied in this study are briefly described below:

2.3.1 Box dimension (box-counting) method

This is a standard technique proposed to quantify the spatial distribution of irregular objects (Mandelbrot, 1982). In this methodology, different box sizes are selected and overlaid on fracture network. Then, the number of boxes filled with fracture lines is counted. The number boxes filled with fracture lines vs. box sizes are plotted on log-log scale and the slope yields the fractal dimension (Barton and Larsen, 1985). Using this technique, the fractal dimensions of intersection points, mid-point and fracture lines were measured. The following equation shows the relationship between the box size, number of filled box and fractal dimension:

$$N(r) \alpha r^{-D} \qquad \textbf{(1)}$$

where $N(r)$ is the number of the filled boxes and r is the box sizes and D is fractal dimension.

2.3.2 Mass dimension (sandbox) method

In this method, a circle with a specific size and center was overlaid on the fracture domain and the number of features (fractures or points) located inside the circle is counted. The procedure is continued increasing the size of the circle with the same center. Then, the number of counts, $M(r)$, is plotted against the size of circle, r, on a log-log scale and the slope of the straight line yields mass fractal dimension (Bunde and Havlin, 1995):

Jafari, A. and Babadagli, T.: "A Sensitivity Analysis for Effective Parameters on 2-D Fracture Network Permeability," June 2009 SPE Reservoir Evaluation & Engineering Journal.

$$M(r) \alpha r^{Dm} \quad \textbf{(2)}$$

The mass dimension method was used to measure the fractal dimension of fracture intersection points and mid-point.

2.3.3 The scanline method

Fracture orientation is one of the critical parameters that affects the hydraulic properties of fracture networks. For example, it is expected that perpendicular fractures to fluid flow direction have negative effects on the network permeability, while parallel ones cause an increase in permeability. Therefore, the quantification of orientation is critical in assessing the FNP (Babadagli, 2001).

The scanline method proposed by Babadagli (2001) was used to consider the effect of orientation. In this method, a number of squares with different size but the same centre was used. The number of fractures touched by a scanline in a specific direction in an L-size square was counted. This procedure was repeated for each square of different sizes. Then on a double logarithmic scale, the size of squares, *L*, was plotted against the total number of the counts. The slope yields the fractal dimension. In this study, two scanline directions (X and Y) were considered.

Jafari, A. and Babadagli, T.: "A Sensitivity Analysis for Effective Parameters on 2-D Fracture Network Permeability," June 2009 SPE Reservoir Evaluation & Engineering Journal.

2.4 Analysis of the results and derivation of FNP correlation

Fracture network permeability (FNP) values for each scenario in different data sets were obtained using a software package (FRACA). The generated fracture network data was imported to the software and the network permeability was determined for each case.

The equivalent permeability of a fracture network in this software is determined by discretizing each fracture of the fracture network into fracture elements such as rectangles, and defining a number of nodes representing interconnected fracture elements. In the next step, while imposing boundary pressure conditions and fluid transmissivities to each couple of neighboring nodes, fluid flow through the discretized network is determined. The flow rate solution is unique and by using the Darcy's law, the equivalent permeability in the considered direction can be determined (Bourbiaux et al, 1998; Cacas et al. 2000).

In this exercise, the fracture aperture (conductivity with the unit of mD-m) was fixed for all fractures initially. For the sensitivity analysis, the conductivity term was also changed. The last column in **Table 2.2** and **Table 2.3** shows the results for different cases. There are totally four data sets but only the two cases with fixed length are presented (**Table 2.2** and **Table 2.3**). The magnitude of permeability is dependent on measurement direction. Hence, the permeability measurement is a vector quantity (Nelson, 2001). In this chapter, we consider permeability in only x-direction.

Jafari, A. and Babadagli, T.: "A Sensitivity Analysis for Effective Parameters on 2-D Fracture Network Permeability," June 2009 SPE Reservoir Evaluation & Engineering Journal.

In addition to the fractal properties, a few other network characteristics were included in the analysis. The connectivity index was defined as a ratio of the number of intersection points to the total number of lines. We also considered the maximum number of touches of the scanlines in both x- and y-directions. This corresponds to the number of touches obtained for the whole fracture network that was obtained during the scanline fractal dimension measurement.

As seen in **Table 2.2** and **Table 2.3**, the fractal dimensions of all data sets lie between 1 and 2 which indicates the fractal nature of the networks. If the fractal dimension of a fracture network is close to one, strongly directional flow anisotropy is expected (Barton and Larsen, 1985). The fractal dimension typically increases with increasing fracture density and length.

Six network properties were determined as the most influential parameters through an extensive regression analysis for each data set. **Figure 2.4** through **Figure 2.8** show the relationship between those parameters and the FNP. Only the cases with two fracture sets in NW-SE & NE-SW directions and fixed length are included in those figures. Since the other data sets show a similar trend between the parameters and fracture network permeability, their plots are not presented here.

Jafari, A. and Babadagli, T.: "A Sensitivity Analysis for Effective Parameters on 2-D Fracture Network Permeability," June 2009 SPE Reservoir Evaluation & Engineering Journal.

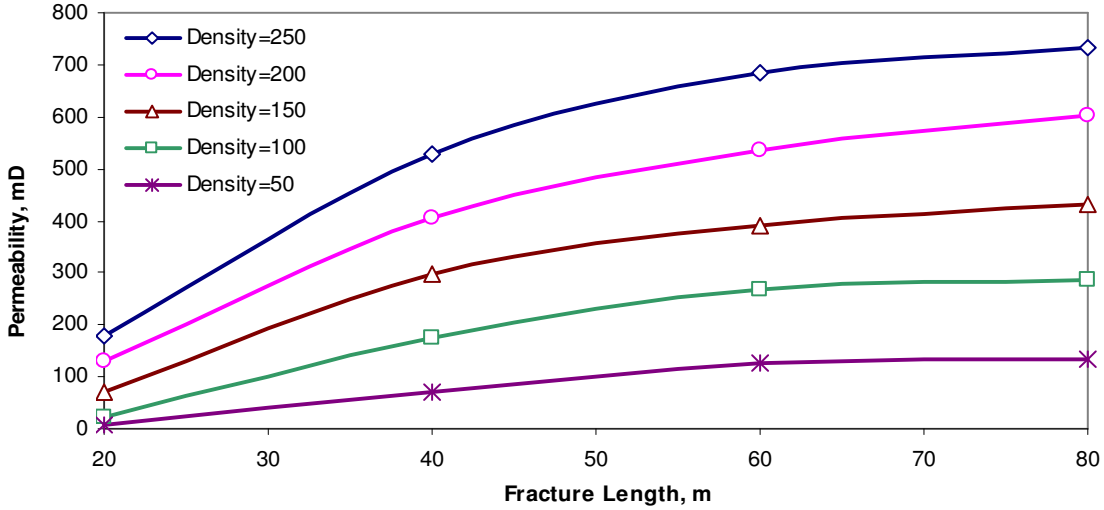

Figure 2.4 Fracture length vs. FNP for the model with two fracture sets in NW-SE & NE-SW directions and fixed length.

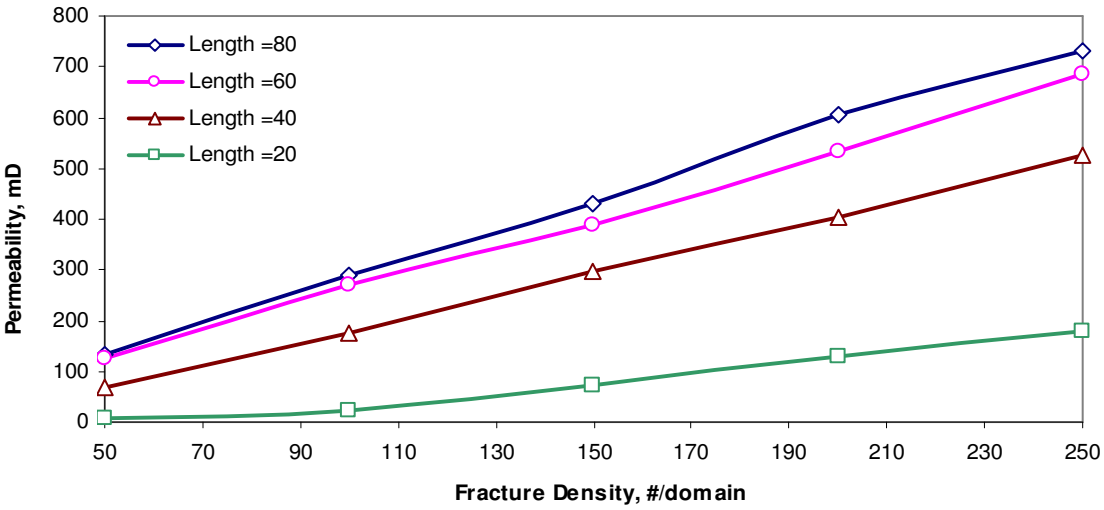

Figure 2.5 Fracture density vs. FNP for the model with two fracture sets in NW-SE & NE-SW directions and fixed length.

Jafari, A. and Babadagli, T.: "A Sensitivity Analysis for Effective Parameters on 2-D Fracture Network Permeability," June 2009 SPE Reservoir Evaluation & Engineering Journal.

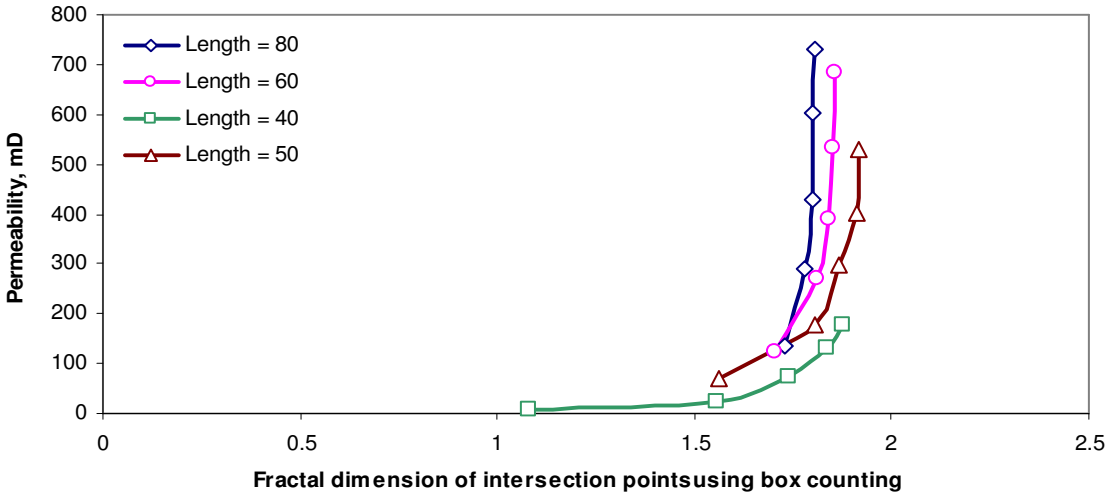

Figure 2.6 The fractal dimension of intersection points obtained using the box-counting vs. FNP for the model with two fracture sets in NW-SE & NE-SW directions and fixed length.

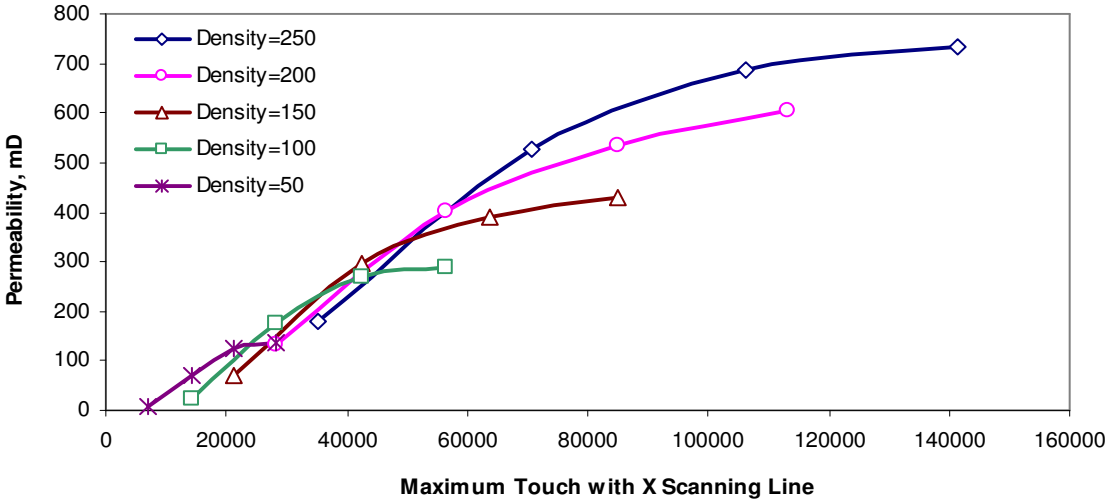

Figure 2.7 Maximum touch with scanlines in X direction vs. FNP for the model with two fracture sets in NW-SE & NE-SW directions and fixed length.

Jafari, A. and Babadagli, T.: "A Sensitivity Analysis for Effective Parameters on 2-D Fracture Network Permeability," June 2009 SPE Reservoir Evaluation & Engineering Journal.

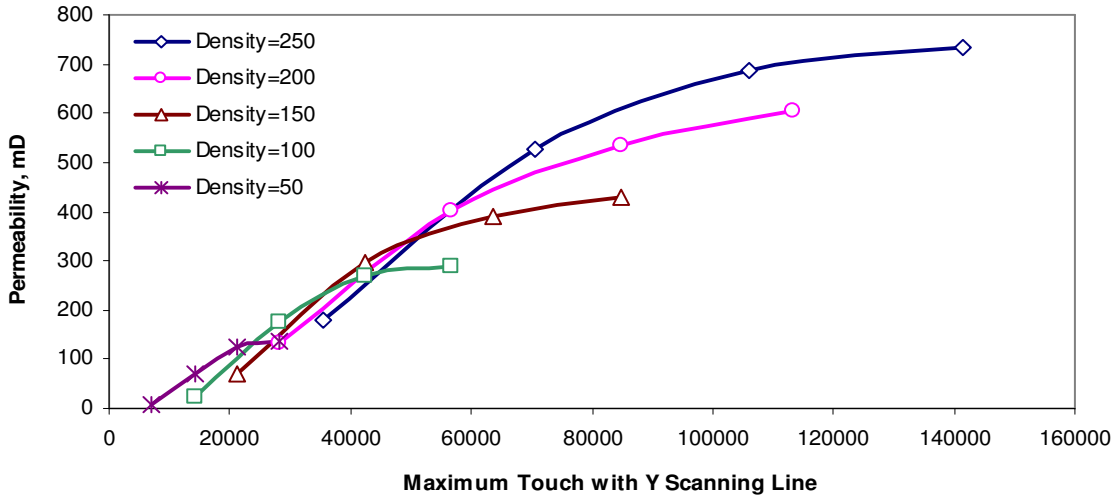

Figure 2.8 Maximum touch with scanlines in Y direction vs. FNP for the model with two fracture sets in NW-SE & NE-SW directions and fixed length.

As seen in each class, the FNP increases with increasing fracture length systematically but the relationship is not linear (**Figure 2.4**). This non-linearity is more significant for higher fracture densities. The relationship between the FNP and fracture density is linear for the given length range (**Figure 2.5**). Through those observations, one can conclude that the effect of fracture density on the FNP could be more significant than that of the fracture length depending also on the orientation. This is expected as the fracture density (number of fracture) increases, the connectivity will increase for random networks and as a result, the FNP increases. A detailed analysis on the relative importance of fracture parameters on the FNP will be provided later in the "Sensitivity analysis using experimental design" section.

Jafari, A. and Babadagli, T.: "A Sensitivity Analysis for Effective Parameters on 2-D Fracture Network Permeability," June 2009 SPE Reservoir Evaluation & Engineering Journal.

The relationship between the FNP and the fractal dimension of intersection points (obtained by box-counting) is shown in **Figure 2.6** for different lengths. The shortest fracture length case (20 m) yields a wider range of fractal dimensions. For higher fracture length cases, the relationship becomes more linear.

Figure 2.8 shows an increase in the FNP with increasing maximum touch with scanline in X and Y directions. This relationship is also non-linear.

Figure 2.9 shows the relationship between the FNP and the box-counting fractal dimension of fracture lines for different densities. It is interesting to note that the change is similar for all density cases and all the curves are almost overlapped.

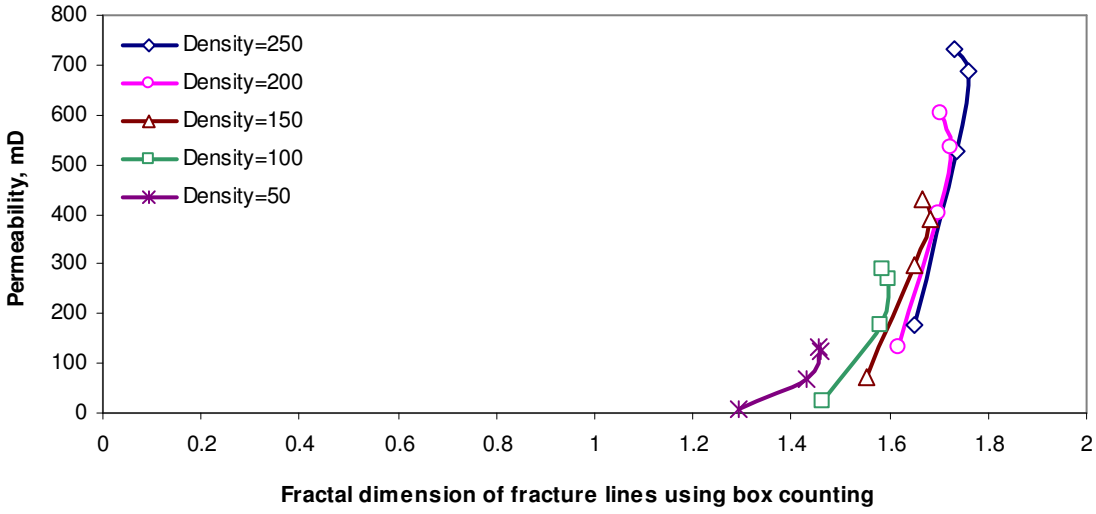

Figure 2.9 Fractal dimension of fracture lines using box counting vs. FNP for the model with two sets in NW-SE & NE-SW directions and fixed length.

Jafari, A. and Babadagli, T.: "A Sensitivity Analysis for Effective Parameters on 2-D Fracture Network Permeability," June 2009 SPE Reservoir Evaluation & Engineering Journal.

Figure 2.10 shows the comparison of the FNPs of different data sets. As the density and length increase, the FNP increases. Note that the fracture models oriented in N-S & E-W directions have higher FNP compared to the other models with fractures in NW-SE & NE-SW directions.

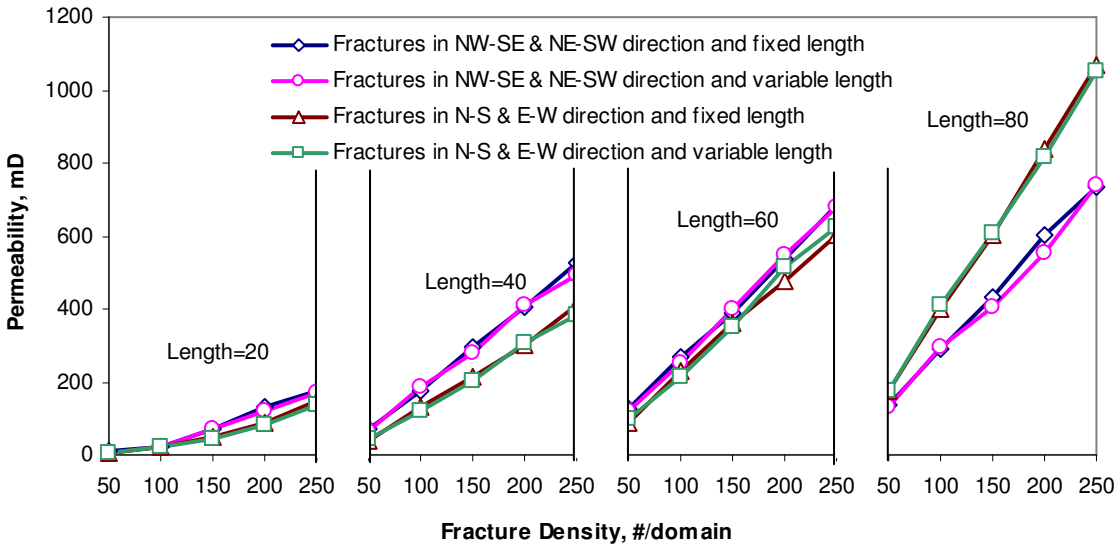

Figure 2.10 Comparison of FNPs with different directions regarding to fracture length and density.

The data sets with orientations other than NW-SE & NE-SW showed the same four fracture network properties to be the most influential ones on the FNP. In the next step, a non-linear multivariable regression equation correlating the FNP to the parameters listed above was developed. Note that, for the sake of universality, the density and length terms were not considered. Hence, only the four parameters given in **Figure 2.6** through **Figure 2.9** were correlated to the

Jafari, A. and Babadagli, T.: "A Sensitivity Analysis for Effective Parameters on 2-D Fracture Network Permeability," June 2009 SPE Reservoir Evaluation & Engineering Journal.

FNP. Eventually, the following equation was observed to be the best correlation between the fracture network properties and the FNP:

$$Y = ae^{bx_1} + c\ln(x_2) + d\ln(x_3) + \ln(x_4) + f \quad \textbf{(3)}$$

where Y denotes logarithm of permeability, x_1 is the fractal dimension of intersection points using box counting, x_2 is the maximum touch with scanlines in X direction, x_3 is the maximum touch with scanlines in Y direction, x_4 is the box-counting fractal dimension of fracture lines. The constants *a, b, c, d* and *f* are the empirical constants which are 25.0081, 0.0462, 2.8952, -1.7052 and -34.6746, respectively.

To validate **Eq. 3**, another data set with random fracture orientation was created (**Table 2.4**).

Jafari, A. and Babadagli, T.: "A Sensitivity Analysis for Effective Parameters on 2-D Fracture Network Permeability," June 2009 SPE Reservoir Evaluation & Engineering Journal.

Table 2.4 Fractures with random orientation and fixed length used to verify Eq. 3 (FD: Fractal dimension).

Length (m)	Density	Box Counting FD		Sandbox Counting FD		Scanline FD (in X direction)	Scanline FD (in Y direction)	Connectivity Index	Maximum Touch with X Scanline	Maximum Touch with Y Scanline	Box Counting FD	Permeability (mD)
		Intersection Point	Mid Point	Intersection Point	Mid Point						Lines	
20	50	1.162	1.389	1.471	1.666	1.565	1.592	0.732	6271	6411.7	1.336	5.609
20	100	1.577	1.623	1.930	1.834	1.424	1.522	1.435	12781.8	12668.2	1.504	27.343
20	150	1.778	1.737	1.722	1.689	1.746	1.692	2.225	18925	19273.1	1.595	74.673
20	200	1.868	1.806	1.827	1.865	1.546	1.530	2.853	25203.4	25366.6	1.657	124.025
20	250	1.905	1.851	1.673	1.695	1.444	1.405	3.640	31793.3	31533.5	1.701	161.214
40	50	1.605	1.384	1.623	1.381	1.180	1.204	3.478	12518.6	12937.7	1.501	77.643
40	100	1.843	1.608	1.667	1.526	1.223	1.223	6.530	25526.4	24957.6	1.647	155.048
40	150	1.913	1.717	1.786	1.695	1.236	1.237	9.439	37071.3	38459.9	1.722	266.795
40	200	1.941	1.772	1.690	1.628	1.220	1.225	13.395	49687.1	52065.4	1.769	395.592
40	250	1.957	1.815	1.747	1.683	1.177	1.167	16.858	64215.3	62891.1	1.798	459.049
60	50	1.747	1.374	1.571	1.423	1.038	1.029	8.096	19184.8	18615.6	1.588	120.310
60	100	1.912	1.581	1.575	1.531	1.052	1.059	15.968	37746	38245.3	1.714	274.240
60	150	1.940	1.681	1.745	1.513	1.039	1.044	24.705	55872	57694.6	1.774	424.930
60	200	1.964	1.722	1.762	1.573	1.039	1.041	32.229	75284.6	76324.5	1.814	583.337
60	250	1.970	1.758	1.611	1.555	1.041	1.029	40.944	98140.7	92938.3	1.838	696.129
80	50	1.839	1.344	1.605	1.518	0.979	0.969	13.702	26071.7	24958.9	1.641	185.112
80	100	1.941	1.516	1.583	1.438	0.993	0.984	27.270	51452.3	49982	1.761	384.561
80	150	1.967	1.591	1.653	1.474	0.980	0.982	41.930	75965.5	77090.8	1.816	621.084
80	200	1.980	1.653	1.589	1.467	0.980	0.980	56.216	101970.6	102215.2	1.847	825.885
80	250	1.984	1.660	1.566	1.434	0.986	0.981	70.622	128651.7	125923.1	1.866	1018.037

Then, the FNP value of this fracture data set was predicted using the derived equation (**Eq. 3**) and plotted against actual FNP given in the last column of **Table 2.4** (**Figure 2.11**). A seen, a good agreement was obtained between the actual and predicted FNPs.

Jafari, A. and Babadagli, T.: "A Sensitivity Analysis for Effective Parameters on 2-D Fracture Network Permeability," June 2009 SPE Reservoir Evaluation & Engineering Journal.

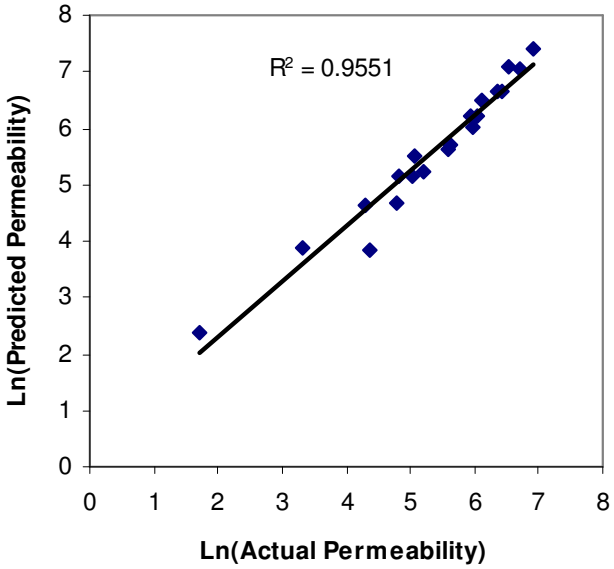

Figure 2.11 Actual vs. predicted fracture network permeability (FNP) plot to validate Eq. 3.

2.5 Sensitivity analysis using experimental design

Experiments can be used as a screening device to determine the importance of each variable and their combinations on the results (Cox and Reid, 2000). The full factorial and fractional factorial designs are used to determine the importance of each input variable on the output of the experiment or process (Saxena and Vjekoslav, 1971).

In order to perform a sensitivity analysis and determine the relative importance of the network properties used in the above analysis considering the interaction among those network properties, the experimental design technique was

Jafari, A. and Babadagli, T.: "A Sensitivity Analysis for Effective Parameters on 2-D Fracture Network Permeability," June 2009 SPE Reservoir Evaluation & Engineering Journal.

applied. We begin this analysis using the network properties only with fixed single fracture conductivity (aperture). Then, we changed the conductivity of single fractures in the network to investigate its effect compared to the network properties.

In general, when the objective of the study is to determine which variable has the largest impact on the result of the process; the full factorial and fractional factorial design are preferred. The factorial design can be used as a screening device to evaluate quickly the importance of each variable and their combinations on the results and to keep the size of the experiment manageable (Cox and Reid, 2000). In this analysis, only two levels of each variable are considered. The factorial design has certain advantages over the commonly used method known as 'one variable at a time' where the levels of one variable are changed at a time but other variables are kept fixed. The factorial design requires fewer experiments; hence is less expensive and less time consuming and also makes it possible to determine the 'interactions' which is the combined effect of two or more variables.

Two levels is a special case of factorial designs where each variable is studied at the two extreme levels and the number of the experiments is written as:

$$2^K = Number\ of\ Factorial\ design\ runs \quad \textbf{(4)}$$

where 2 stands for the number of levels of each variable and K is the number of the variables (Saxena and Vjekoslav, 1971). If the effect of one variable is positive, it means that increasing the value of that variable from low to high

Jafari, A. and Babadagli, T.: "A Sensitivity Analysis for Effective Parameters on 2-D Fracture Network Permeability," June 2009 SPE Reservoir Evaluation & Engineering Journal.

level will increase the response. If the effect is negative, it means that the response will decrease by increasing the value of that variable from low to high level (Montgomery, 2005). When the number of variables increases (e.g. exceed six), according to above correlation, the number of required runs increase significantly that makes the process unfeasible. In these situations, fractional factorial design can be used (Saxena and Vjekoslav, 1971).

2.5.1 Sensitivity analysis- 1

In this chapter, four variables, i.e. length, density, orientation, and conductivity were considered for two level full factorial designs. High and low levels of the values listed in **Table 2.2** and **Table 2.3** were considered (optimistic and pessimistic cases) for simplicity and they were presented by 1 and -1, respectively. Since we used permeability in X direction, we assumed that fracture permeability in the case with fractures in N-S & E-W direction is higher (optimistic case) than that in NW-SE & NE-SW direction (pessimistic case) (**Table 2.5**).

Table 2.5 Levels for three fracture parameters (sensitivity analysis -1).

Variable	Optimistic (1)	Pessimistic (-1)
Length	80	20
Density	250	50
Orientation	N-S & E-W	NW-SE & NE-SW
Conductivity	1500	1000

Jafari, A. and Babadagli, T.: "A Sensitivity Analysis for Effective Parameters on 2-D Fracture Network Permeability," June 2009 SPE Reservoir Evaluation & Engineering Journal.

Sixteen tests (or runs) are needed for all possible combinations of two levels of these four variables (K) to form the matrix of runs (design matrix) according to the following relationship:

$$2^K = 2^4 = 16 \quad Number\ of\ Factorial\ design\ runs \qquad \textbf{(5)}$$

Once the design matrix is built, the experiment is performed (Saxena and Vjekoslav, 1971). **Table 2.6** shows the uncoded design matrix with corresponding results. No two rows are identical; and **Table 2.7** shows the equivalent design matrix with coding.

Table 2.6 Uncoded two level factorial design matrix of runs with results.

Run No.	Length (m)	Density (#/area)	Orientation	Conductivity (mD.m)	Permeability (mD)
1	20	50	NW-SE & NE-SW	1000	8.322
2	80	50	NW-SE & NE-SW	1000	134.642
3	20	250	NW-SE & NE-SW	1000	177.957
4	80	250	NW-SE & NE-SW	1000	731.907
5	20	50	N-S & E-W	1000	3.809
6	80	50	N-S & E-W	1000	177.507
7	20	250	N-S & E-W	1000	149.451
8	80	250	N-S & E-W	1000	1066.250
9	20	50	NW-SE & NE-SW	1500	19.725
10	80	50	NW-SE & NE-SW	1500	228.451
11	20	250	NW-SE & NE-SW	1500	252.487
12	80	250	NW-SE & NE-SW	1500	1057.600
13	20	50	N-S & E-W	1500	15.048
14	80	50	N-S & E-W	1500	246.611
15	20	250	N-S & E-W	1500	287.985
16	80	250	N-S & E-W	1500	1683.890

Jafari, A. and Babadagli, T.: "A Sensitivity Analysis for Effective Parameters on 2-D Fracture Network Permeability," June 2009 SPE Reservoir Evaluation & Engineering Journal.

Table 2.7 Coded two level factorial design matrix of runs with results.

Run No.	L	D	O	C	Kx
1	-1	-1	-1	-1	8.322
2	1	-1	-1	-1	134.642
3	-1	1	-1	-1	177.957
4	1	1	-1	-1	731.907
5	-1	-1	1	-1	3.809
6	1	-1	1	-1	177.507
7	-1	1	1	-1	149.451
8	1	1	1	-1	1066.250
9	-1	-1	-1	1	19.725
10	1	-1	-1	1	228.451
11	-1	1	-1	1	252.487
12	1	1	-1	1	1057.600
13	-1	-1	1	1	15.048
14	1	-1	1	1	246.611
15	-1	1	1	1	287.985
16	1	1	1	1	1683.890

As mentioned earlier, one of the advantages of the full factorial design is that in addition to the determination the effect of each variable, the effect of combination of these variables (interaction) can be evaluated (Saxena and Vjekoslav, 1971). There are eleven combinations for these four variables.

Table 2.8 shows the calculation matrix of four variables and their combinations, where L, D, O and C stand for length, density, orientation and conductivity, respectively. Their all different possible combinations such as LD, LO, LC, DO, DC, OC, LDO, LDC, LOC, DOC, and LDOC were included in the sensitivity analysis.

Jafari, A. and Babadagli, T.: "A Sensitivity Analysis for Effective Parameters on 2-D Fracture Network Permeability," June 2009 SPE Reservoir Evaluation & Engineering Journal.

Table 2.8 Calculation matrix with the result of four variables (L=Length, D=Density, O=Orientation and C=Conductivity) and the combinations of these variables.

Run No.	L	D	O	C	LD	LO	LC	DO	DC	OC	LDO	LDC	LOC	DOC	LDOC	Kx
1	-1	-1	-1	-1	1	1	1	1	1	1	-1	-1	-1	-1	1	8.322
2	1	-1	-1	-1	-1	-1	-1	1	1	1	1	1	1	-1	-1	134.642
3	-1	1	-1	-1	-1	1	1	-1	-1	1	1	1	-1	1	-1	177.957
4	1	1	-1	-1	1	-1	-1	-1	-1	1	-1	-1	1	1	1	731.907
5	-1	-1	1	-1	1	-1	1	-1	1	-1	1	-1	1	1	-1	3.809
6	1	-1	1	-1	-1	1	-1	-1	1	-1	-1	1	-1	1	1	177.507
7	-1	1	1	-1	-1	-1	1	1	-1	-1	-1	1	1	-1	1	149.451
8	1	1	1	-1	1	1	-1	1	-1	-1	1	-1	-1	-1	-1	1066.250
9	-1	-1	-1	1	1	1	-1	1	-1	-1	-1	1	1	1	-1	19.725
10	1	-1	-1	1	-1	-1	1	1	-1	-1	1	-1	-1	1	1	228.451
11	-1	1	-1	1	-1	1	-1	-1	1	-1	1	-1	1	-1	1	252.487
12	1	1	-1	1	1	-1	1	-1	1	-1	-1	1	-1	-1	-1	1057.600
13	-1	-1	1	1	1	-1	-1	-1	-1	1	1	1	-1	-1	1	15.048
14	1	-1	1	1	-1	1	1	-1	-1	1	-1	-1	1	-1	-1	246.611
15	-1	1	1	1	-1	-1	-1	1	1	1	-1	-1	-1	1	-1	287.985
16	1	1	1	1	1	1	1	1	1	1	1	1	1	1	1	1683.890

The factor effect shows the influence of each factor (variable or combination) on the response of the experiment. Hence, to determine the effect of each variable and their combinations on the response of the experiment, the difference in the average response for the two-level of the factor is calculated as follows (Mason et al. 2003):

$$\textit{Factor effect} = \textit{average response at one level} - \textit{average response at a second level} \quad \textbf{(6)}$$

For example, the effect of fracture length on the fracture network permeability is calculated as follows:

Jafari, A. and Babadagli, T.: "A Sensitivity Analysis for Effective Parameters on 2-D Fracture Network Permeability," June 2009 SPE Reservoir Evaluation & Engineering Journal.

$$E_L = \left(\frac{134.642 + 731.907 + 177.507 + 1066.250 + 228.451 + 1057.600 + 246.611 + 1683.890}{8}\right) - \left(\frac{8.322 + 177.957 + 3.809 + 149.451 + 19.725 + 252.487 + 15.048 + 287.985}{8}\right) = 551.509$$

The effects of each variable and their combinations are presented in **Table 2.9** as a vector of effects.

Table 2.9 Vector of effects.

Factor	Absolute Effect
Density	571.676
Length	551.509
Length/Density	366.433
Conductivity	167.744
Length/Orientation	127.982
Orientation	127.433
Density/Conductivity	121.355
Density/Orientation	114.474
Length/Density/Orientation	110.428
Length/Conductivity	108.817
Length/Density/Conductivity	73.750
Density/Orientation/Conductivity	47.602
Orientation/Conductivity	41.385
Length/Density/Orientation/Conductivity	31.561
Length/Orientation/Conductivity	25.425

Also the vector of effect is presented in **Figure 2.12** as a Pareto chart. It is observed that, fracture density, length and their combination have the most remarkable effect on the FNP. This effect is quantitatively seen in **Figure 2.12** as relative to the other parameters. In having a percolating fracture network

Jafari, A. and Babadagli, T.: "A Sensitivity Analysis for Effective Parameters on 2-D Fracture Network Permeability," June 2009 SPE Reservoir Evaluation & Engineering Journal.

with random orientation, the fracture density and fracture length mutually play a critical role.

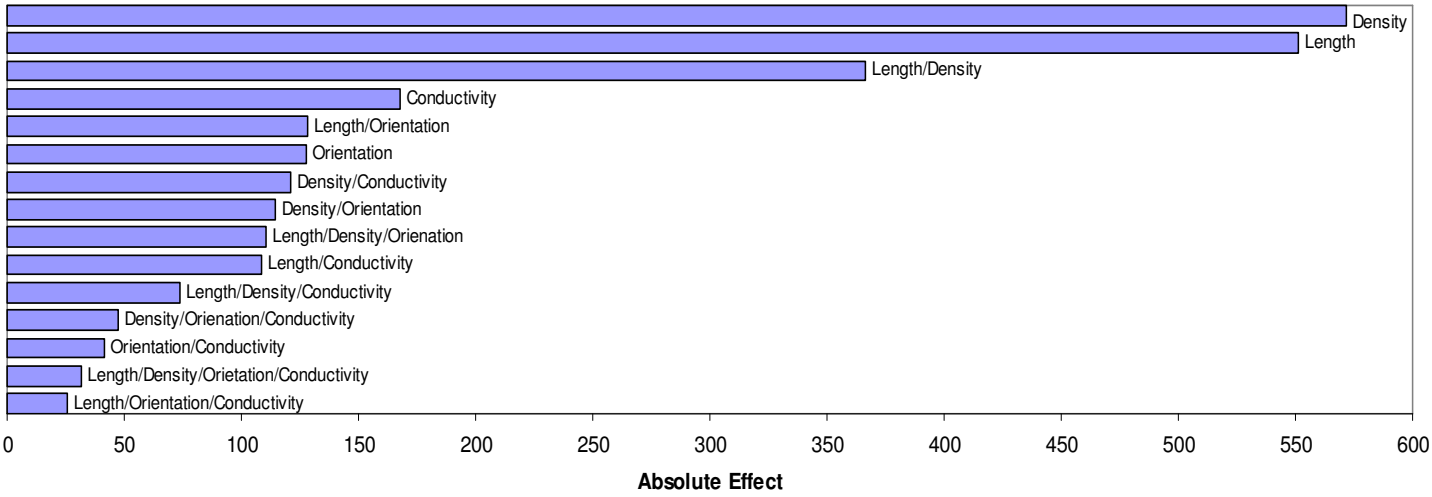

Figure 2.12 Pareto chart of the absolute effect of different variables and their combinations for the case given in Table 2.5.

2.5.2 Sensitivity analysis- 2

In the next sensitivity analysis, we reduced the number of parameters to three by taking the top three single most influential parameters in **Figure 2.12** (density, length, and conductivity). We generated another model where fractures are only in E-W(X) direction to minimize the orientation effect. They are distributed in E&W direction with angles between 0^o and 10^o. For this case, we considered three variables of which the extreme values are presented in **Table 2.10**.

Jafari, A. and Babadagli, T.: "A Sensitivity Analysis for Effective Parameters on 2-D Fracture Network Permeability," June 2009 SPE Reservoir Evaluation & Engineering Journal.

Table 2.10 Three variables and their extreme levels (sensitivity analysis -2).

Variable	Optimistic(1)	Pessimistic(-1)
Length	80	20
Density	250	50
Conductivity	1500	1000

The result of the factorial design is shown in **Figure 2.13** as a Pareto chart. The fracture length has higher effect on the FNP than fractures density. One can infer that, as fractures preferentially are oriented in one direction, the fracture length is more critical in having a percolating network compared to the fracture density.

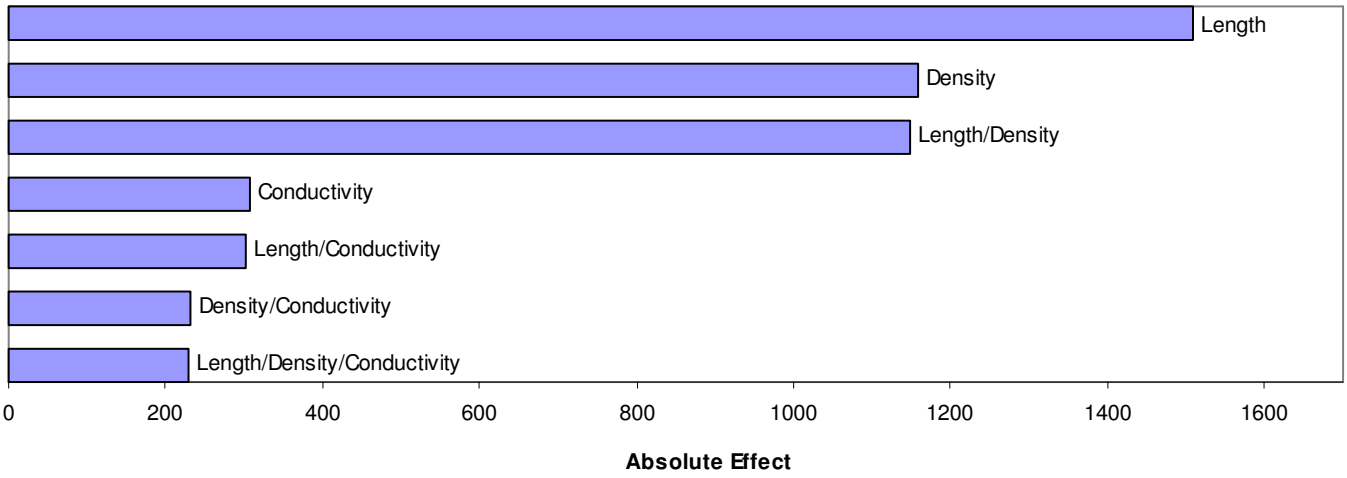

Figure 2.13 Pareto chart of the absolute effect of different variables and their combinations for the case given in Table 2.10.

Jafari, A. and Babadagli, T.: "A Sensitivity Analysis for Effective Parameters on 2-D Fracture Network Permeability," June 2009 SPE Reservoir Evaluation & Engineering Journal.

2.5.3 Sensitivity analysis- 3

In the third sensitivity analysis, we defined another data set where maximum length, density and conductivity were different from the previous data set and also the fracture orientation defined in N-S & E-W direction only. These properties are presented in **Table 2.11**.

Table 2.11 Levels for three fracture parameters (sensitivity analysis -3).

Variable	Optimistic(1)	Pessimistic(-1)
Length	60	40
Density	150	50
Conductivity	2000	500

The results are presented in a Pareto chart (**Figure 2.14**). As seen, the conductivity has the most influence on the fracture network permeability because the range of conductivity variation (from 500 to 2000 mD.m) is high.

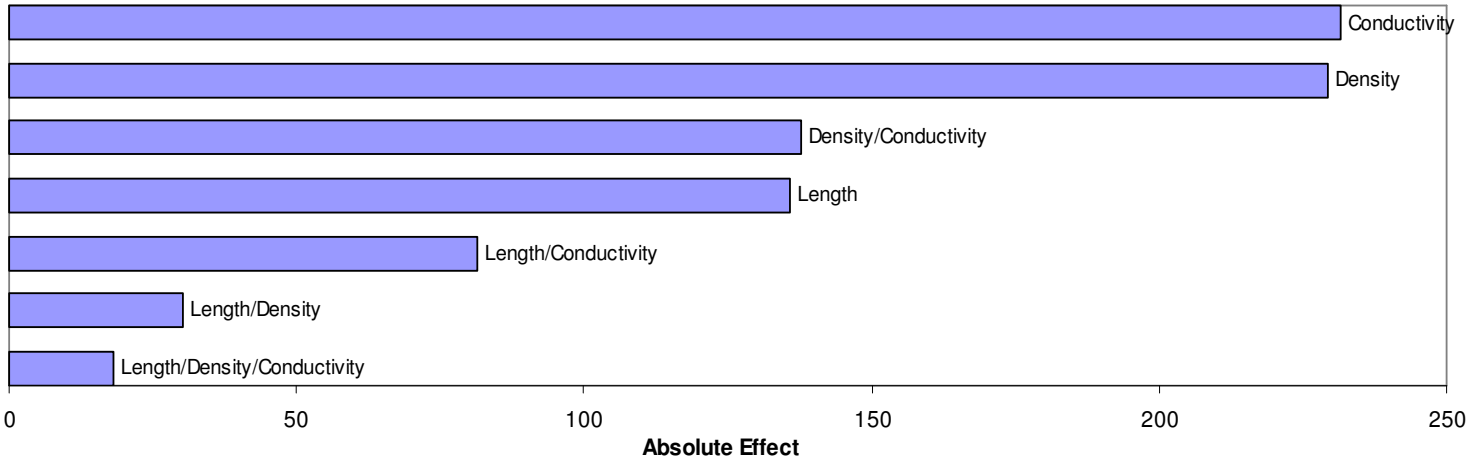

Figure 2.14 Pareto chart of the absolute effect of different variables and their combinations for the case given in Table 2.11.

Jafari, A. and Babadagli, T.: "A Sensitivity Analysis for Effective Parameters on 2-D Fracture Network Permeability," June 2009 SPE Reservoir Evaluation & Engineering Journal.

The three sensitivity analyses done so far imply that there exists a limit where single fracture conductivity (or parameters such aperture, surface roughness that control the conductivity) starts controlling the FNP. This is a critical point as typical practice to determine the FNP is to use 1-D well data and extend it to the whole reservoir. Practitioners typically use the average fracture aperture value and the number of fractures obtained from core and image log data to estimate the FNP and to construct the fracture permeability map. This, however, lacks important information regarding the connectivity and average fracture length to the extent of whole reservoir (2-D or 3-D data). Although the fracture aperture values obtained through core or log data are useful information and could be extrapolated to the rest of the reservoir, the fracture density obtained through these sources is limited to the vicinity of wellbore and may not be representative of the whole system. Hence it is critical to determine beyond which values of single fracture properties like aperture, fracture network properties become the controlling parameters. Beyond this critical value, the wellbore related data may not be useful to determine the FNP for the whole reservoir. A few more sensitivity analyses as similar to the previous ones were performed to eventually determine this limiting characteristic fracture network and single fracture values.

2.5.4 Sensitivity analysis- 4

In this case, the conductivity was kept constant (1000 mD.m). The two levels of each variable were presented in **Table 2.12**.

Jafari, A. and Babadagli, T.: "A Sensitivity Analysis for Effective Parameters on 2-D Fracture Network Permeability," June 2009 SPE Reservoir Evaluation & Engineering Journal.

Table 2.12 Levels for three fracture parameters (sensitivity analysis -4).

Variable	Optimistic(1)	Pessimistic(-1)
Length	80	20
Density	250	50
Orientation	N-S&E-W	NW-SE&NE-SW

The Pareto chart is given in **Figure 2.15**. As seen, like the first sensitivity analysis, the fracture density and length and their combination are the most influential factors on the FNP.

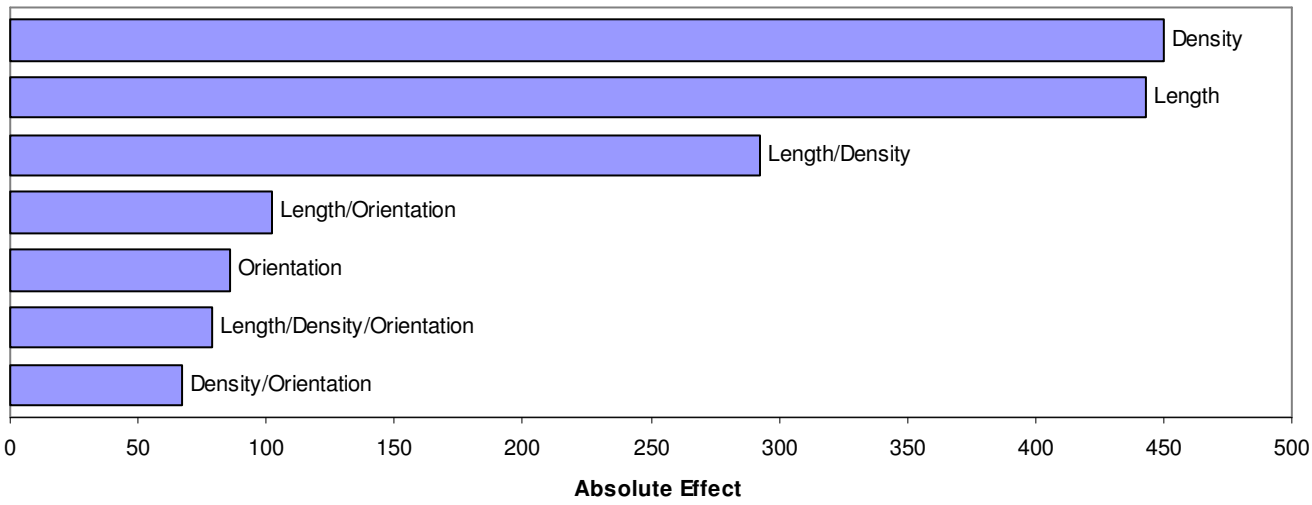

Figure 2.15 Pareto chart of the absolute effect of different variables and their combinations for the case given in Table 2.12.

Jafari, A. and Babadagli, T.: "A Sensitivity Analysis for Effective Parameters on 2-D Fracture Network Permeability," June 2009 SPE Reservoir Evaluation & Engineering Journal.

2.5.5 Sensitivity analysis- 5

This case is exactly the same as the first data set but this time the conductivity range is wider (**Table 2.13**).

Table 2.13 Levels for four fracture parameters (sensitivity analysis -5).

Variable	Optimistic(1)	Pessimistic(-1)
Length	80	20
Density	250	50
Orientation	N-S & E-W	NW-SE & NE-SW
Conductivity	2000	500

The results show that, like sensitivity analysis-1, the fracture density and length are the most influential factors (**Figure 2.16**).

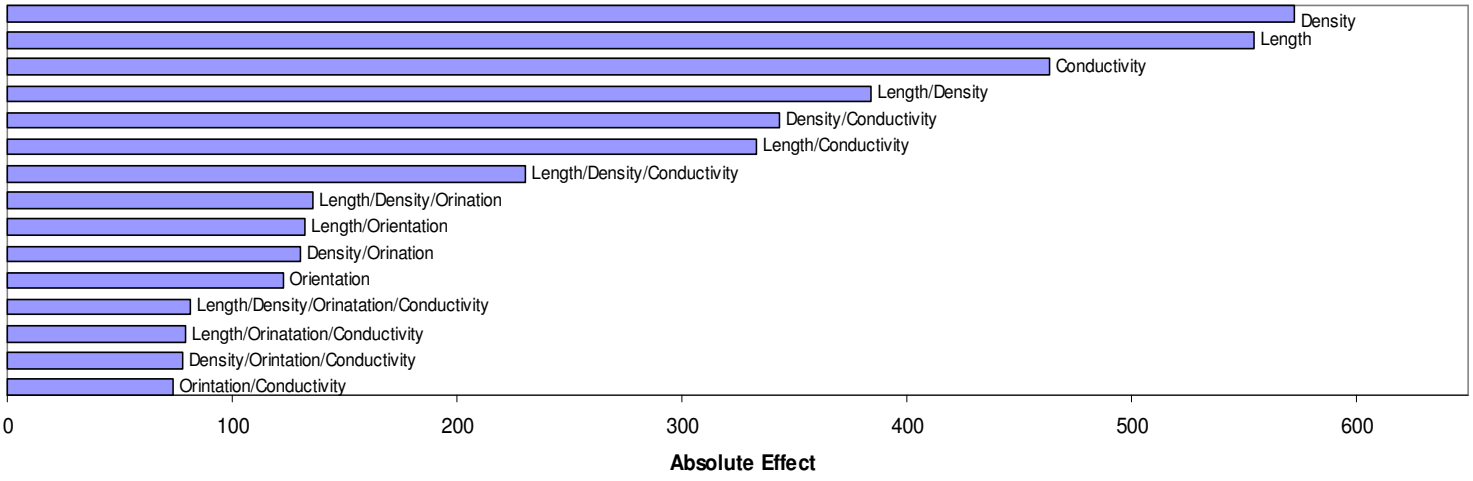

Figure 2.16 Pareto chart of the absolute effect of different variables and their combinations for the case given in Table 2.13.

Jafari, A. and Babadagli, T.: "A Sensitivity Analysis for Effective Parameters on 2-D Fracture Network Permeability," June 2009 SPE Reservoir Evaluation & Engineering Journal.

The conductivity turned out to be more important than the combination of density and length but the density and length individually are still the dominating parameters. Note that this case represents the highest values and the widest range of all four parameters. Although the highest conductivity values were used, the network characteristics still dominate over the single fracture characteristics.

2.5.6 Sensitivity analysis- 6

This data set in terms of orientation is similar to the second data set, but the ranges of length, density and conductivity were decreased to the lowest values (**Table 2.14**).

Table 2.14 Levels for three fracture parameters (sensitivity analysis -6).

Variable	Optimistic(1)	Pessimistic(-1)
Length	40	20
Density	100	50
Conductivity	1000	500

The results are shown as a Pareto chart in **Figure 2.17**. In this case, the density, length, and their combination are still the dominating parameters over single fracture conductivity.

Jafari, A. and Babadagli, T.: "A Sensitivity Analysis for Effective Parameters on 2-D Fracture Network Permeability," June 2009 SPE Reservoir Evaluation & Engineering Journal.

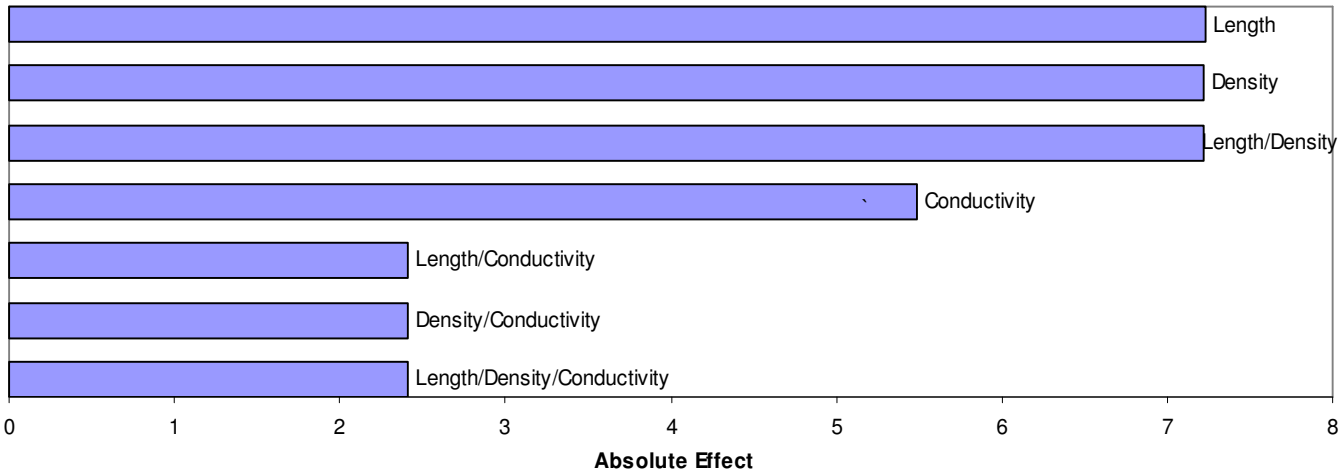

Figure 2.17 Pareto chart of the absolute effect of different variables and their combinations for the case given in Table 2.14.

2.5.7 Sensitivity analysis- 7

This case has the same orientation as the data sets used in the second and sixth sensitivity analyses. Unlike the sixth data set, the highest values of the length, density and conductivity were used (**Table 2.15**).

Table 2.15 Levels for three fracture parameters (sensitivity analysis -7).

Variable	Optimistic (1)	Pessimistic (-1)
Length	80	60
Density	250	200
Conductivity	2000	1000

Jafari, A. and Babadagli, T.: "A Sensitivity Analysis for Effective Parameters on 2-D Fracture Network Permeability," June 2009 SPE Reservoir Evaluation & Engineering Journal.

The Pareto chart given in **Figure 2.18** shows the results. Here, the conductivity became the most influential factor on the FNP.

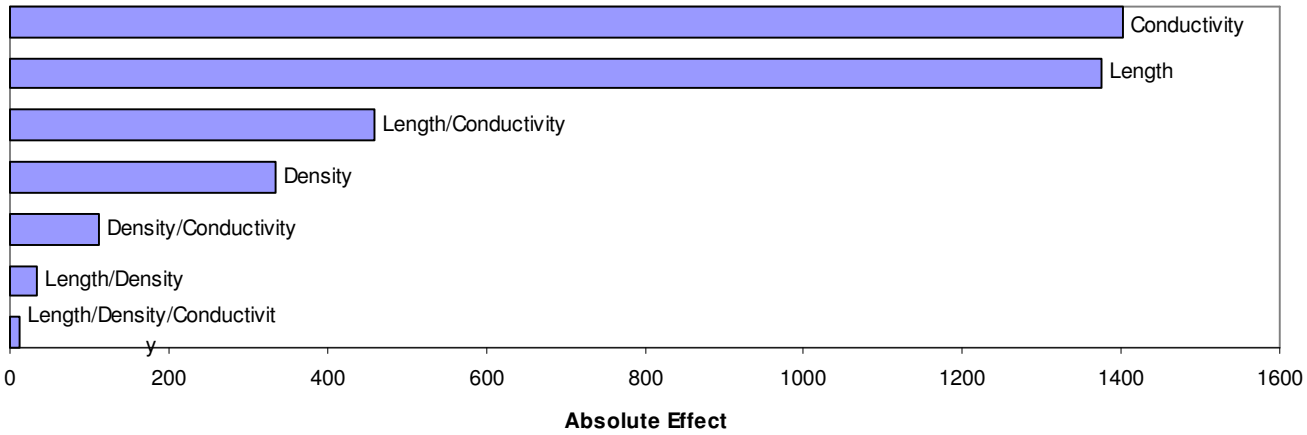

Figure 2.18 Pareto chart of the absolute effect of different variables and their combinations for the case given in Table 2.15.

2.6 Verification of use of two-level design rather than higher levels

Experimental designs with three or more levels of each factor can significantly increase a number of runs. For example, an experiment with four variables and each of them with three-level requires a minimum of $3^4 = 81$ runs. In addition, a very large number of runs in three-level experiments are used to estimate high-order interactions between different factors, but these high-order interactions do not attract the primary interest to evaluate the factor effects (Mason et al. 2003). However, these designs are critical to a lot of non-linear

Jafari, A. and Babadagli, T.: "A Sensitivity Analysis for Effective Parameters on 2-D Fracture Network Permeability," June 2009 SPE Reservoir Evaluation & Engineering Journal.

problems. Fortunately, the authors' 2-D fracture network data set is close to a linear problem. Therefore, the authors decided to use 2-level designs for this problem.

Here we performed a three-level design for a case which is similar to the sensitivity analysis # 5 (**Table 2.13**) in terms of the range of each variable. In this exercise, only three variables (length, density, and conductivity) were assigned three levels and the last one (orientation) has only two levels as given in **Table 2.16**. The results of this experiment are shown in **Figure 2.19**. In this case, the R-squared value is equal to 0.994.

Table 2.16 Levels for four fracture parameters (three-level).

Variable	High	middle	Low
Length	80	40	20
Density	250	150	50
Orientation	N-S & E-W	_____	NW-SE & NE-SW
Conductivity	2000	1000	500

Jafari, A. and Babadagli, T.: "A Sensitivity Analysis for Effective Parameters on 2-D Fracture Network Permeability," June 2009 SPE Reservoir Evaluation & Engineering Journal.

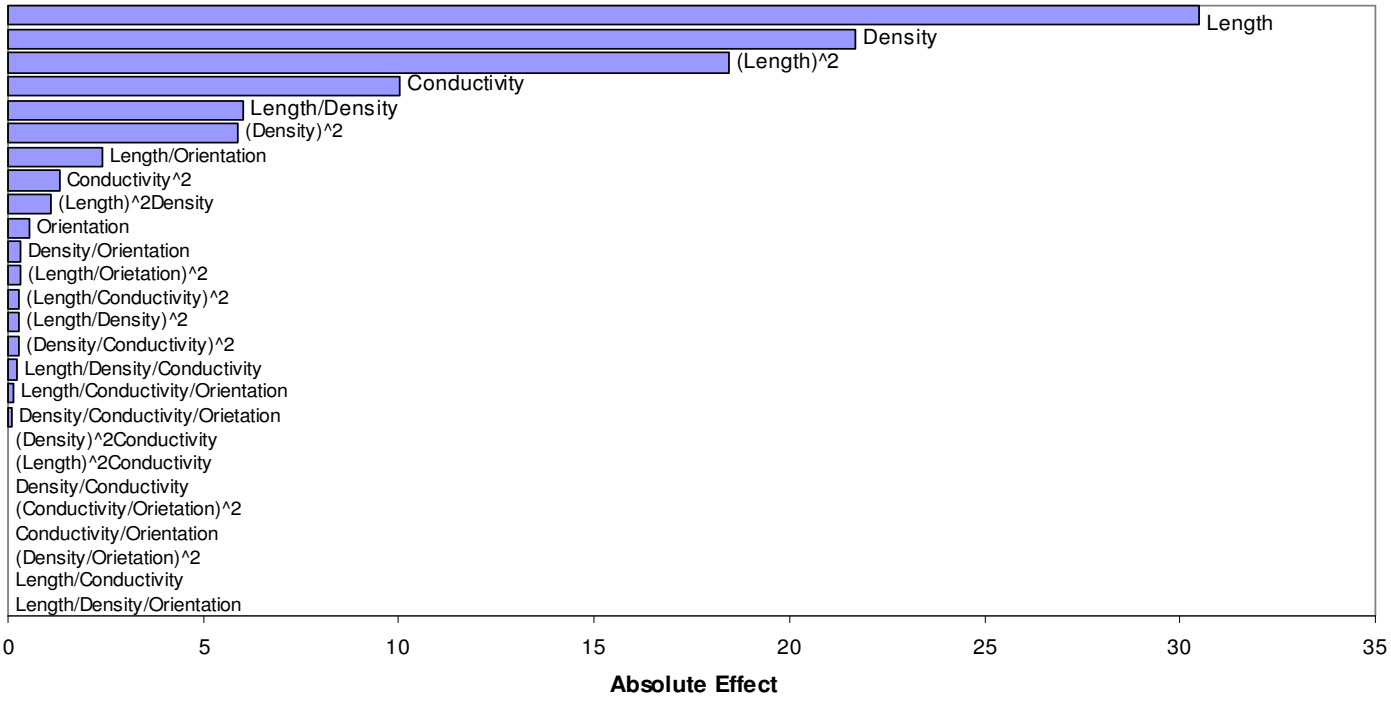

Figure 2.19 Pareto chart showing the results of the three-level factorial design.

As a next step, the high-order interactions were not considered (**Figure 2.20**), and the R-squared value became 0.988, which is very close to the previous one. Hence, **Figure 2.19** and **Figure 2.20** suggest that single (linear) factors such as fracture length and density are the most influential parameters on the response (FNP), which is similar to the two-level design given in **Figure 2.16**. This validates that our assumption on the linearity of relationship between different fracture network parameters and the FNP and also using the two-level full factorial design to minimize the number of runs without affecting the results.

Jafari, A. and Babadagli, T.: "A Sensitivity Analysis for Effective Parameters on 2-D Fracture Network Permeability," June 2009 SPE Reservoir Evaluation & Engineering Journal.

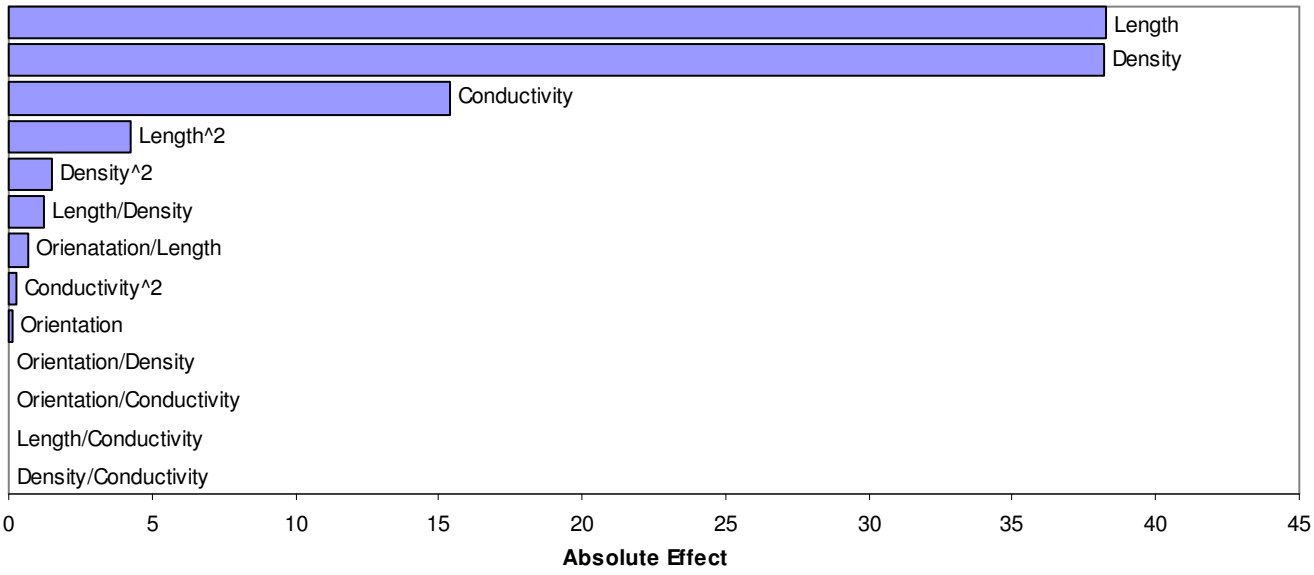

Figure 2.20 Pareto chart showing the results of the three-level factorial design.

It is necessary to mention that the second order interaction terms cannot be ignored in some cases and in this chapter, the second order terms often come on top three in the ranking, such as length/Density in **Figure 2.12**, **Figure 2.13**, **Figure 2.15**, **Figure 2.16** and **Figure 2.17**, Length/Conductivity in **Figure 2.14** and **Figure 2.18**, and Length^2 in **Figure 2.19**, etc.

The work presented in this chapter is based on 2-D fracture networks and the following conclusions apply to this assumption as well as others stated in the chapter.

Jafari, A. and Babadagli, T.: "A Sensitivity Analysis for Effective Parameters on 2-D Fracture Network Permeability," June 2009 SPE Reservoir Evaluation & Engineering Journal.

2.7 Conclusions

1. The effects of fracture network parameters, namely fracture density, length, connectivity, orientation, and aperture on the fracture network permeability (FNP) were studied. The most influential fracture network characteristics were identified to be the box-counting fractal dimension of intersection points and fracture lines, and maximum touch with scanline in x- and y-directions. A correlation between them and the FNP was obtained through a non-linear multivariable regression analysis and validated.

2. It was shown that among four parameters and their combinations, the fracture density and length, and their combination have the most important impact on the FNP since they are the parameters having direct impact on obtaining a percolating network. In general, the network properties dominate over single fracture conductivity to be effective parameters on the FNP.

3. The conductivity of individual fractures starts becoming the dominating term over the network properties as the density and length values decrease reaching certain -low- range and the conductivity is high enough (sensitivity analysis-3). This is also true for the cases of high fracture density and length but high single fracture conductivity (sensitivity analysis-7). The network properties dominate over single fracture conductivity in the case of low fracture density and length, and low single fracture conductivity.

Jafari, A. and Babadagli, T.: "A Sensitivity Analysis for Effective Parameters on 2-D Fracture Network Permeability," June 2009 SPE Reservoir Evaluation & Engineering Journal.

3 Artificial Neural Networks for Predicting the Equivalent Fracture Network Permeability

3.1 Overview

This chapter presents a new and practical approach to estimate the equivalent fracture network permeability (EFNP) using two different methods, i.e. multivariable regression analysis (MRA) and artificial neural networks (ANN). Different statistical and fractal characteristics of twenty natural fracture patterns collected from the outcrops of geothermal reservoirs were measured and then correlated to the EFNP using MRA and several empirical equations with different numbers of variables proposed. Next, synthetic fracture networks were generated and used for validation purposes. The EFNP of these synthetic fracture networks were predicted using the derived empirical equations. Also as a final effort, we took advantage of the capability of ANN to improve the correlations obtained through the MRA.

3.2 Derivation the empirical equation

Twenty different 2-D natural fracture patterns were selected representing characteristic fracture networks. Ten of them were collected from different

A version of this chapter has been published

Jafari, A. and Babadagli, T.: "Prediction the Equivalent Fracture Network Permeability using Multivariable Regression Analysis and Artificial Neural Networks," Proceedings World Geothermal Congress, Bali, Indonesia, 25-29 April 2010.

sources in the literature and a great portion of them were from the outcrops of geothermal reservoirs (**Table 3.1**).

Table 3.1 Sources of natural fracture patterns used in the chapter.

Pattern	Reference
1	Babadagli, 2000
2	Babadagli, 2000
3	Babadagli, 2001
4	Babadagli, 2001
5	Babadagli, 2001
6	Babadagli, 2001
7	Babadagli, 2001
8	Odling, 1992 (A)
9	Odling and Webman, 1991
10	Odling and Webman, 1991

The other ten patterns were acquired from the outcrops of the producing formations in the Kizildere, Germencik, and a few other smaller size geothermal fields in western Turkey. Some representative patterns are shown in **Figure 3.1**.

Jafari, A. and Babadagli, T.: "Prediction the Equivalent Fracture Network Permeability using Multivariable Regression Analysis and Artificial Neural Networks," Proceedings World Geothermal Congress, Bali, Indonesia, 25-29 April 2010.

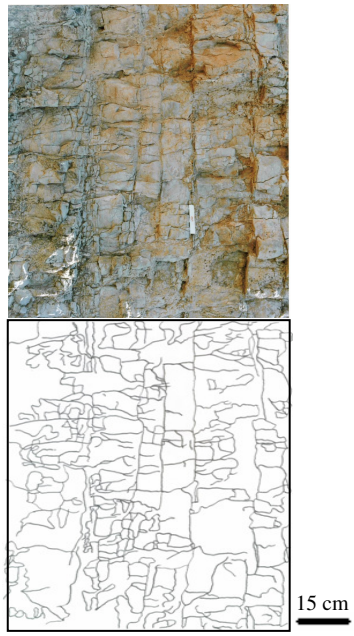

a. Outcrop of a producing formation (limestone) in the Kizildere field.

b. Outcrop of a producing formation (limestone) in the Karahayit-Pamukkale field.

Jafari, A. and Babadagli, T.: "Prediction the Equivalent Fracture Network Permeability using Multivariable Regression Analysis and Artificial Neural Networks," Proceedings World Geothermal Congress, Bali, Indonesia, 25-29 April 2010.

c. Outcrop of a producing formation (marble) in the Germencik field.

d. Outcrop of a producing formation (marble) in the Germencik field.

Figure 3.1(a, b, c and d) Typical natural (outcrop) fracture patterns from the geothermal fields in western Turkey used in the chapter.

Jafari, A. and Babadagli, T.: "Prediction the Equivalent Fracture Network Permeability using Multivariable Regression Analysis and Artificial Neural Networks," Proceedings World Geothermal Congress, Bali, Indonesia, 25-29 April 2010.

Although the images are at meter-scale, to be consistent with the previous chapter that used 100x100 m^2 synthetic network patterns (Jafari and Babadagli, 2008), the images were first digitized in a 100x100 m^2 square domain. The same process was repeated at the original scale, as will be explained later. For comparison, representative synthetic fracture patterns are given in **Figure 3.2**.

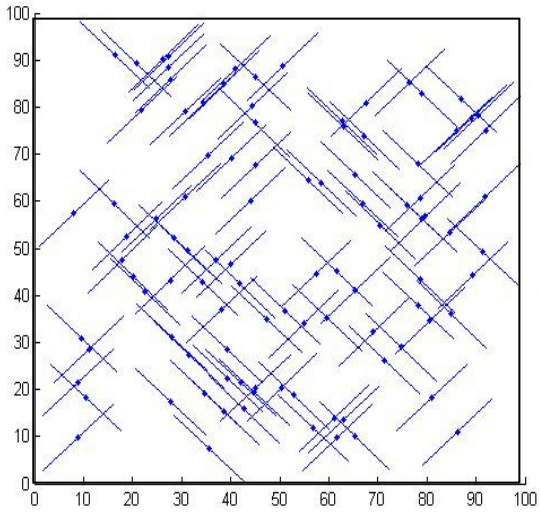

a. Two fracture sets oriented in NW-SE & NE-SW.

Jafari, A. and Babadagli, T.: "Prediction the Equivalent Fracture Network Permeability using Multivariable Regression Analysis and Artificial Neural Networks," Proceedings World Geothermal Congress, Bali, Indonesia, 25-29 April 2010.

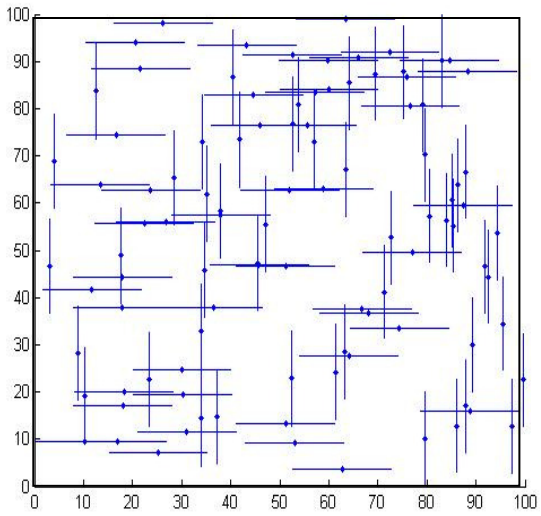

b. Two fracture sets oriented in N-S & E-W.

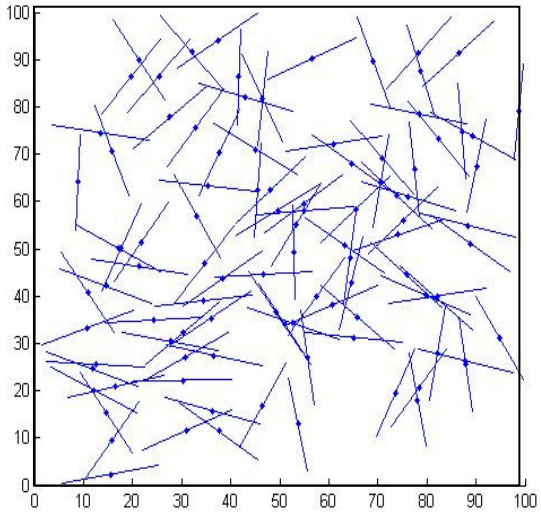

c. Fractures distributed randomly in all directions.

Figure 3.2(a, b and c) Typical synthetic of natural patterns representing different fracture network characteristics (density, length, orientation).

Jafari, A. and Babadagli, T.: "Prediction the Equivalent Fracture Network Permeability using Multivariable Regression Analysis and Artificial Neural Networks," Proceedings World Geothermal Congress, Bali, Indonesia, 25-29 April 2010.

Five statistical and fractal characteristics of the networks were measured as they showed the highest correlation with the EFNP in the previous chapter for synthetic networks (Jafari and Babadagli, 2008). They are given in **Table 3.2**. Different fractal features of fracture patterns using different fractal techniques were considered in addition to the statistical parameters shown in the previous chapter (Jafari and Babadagli, 2008). Using a commercial software package (FRACA), the equivalent permeability tensor of each fracture model with constant conductivity was calculated. In this exercise, the permeability in the Z and Y directions were not taken into account and only the permeability in the X direction of the equivalent permeability tensor was considered (**Table 3.2**).

Jafari, A. and Babadagli, T.: "Prediction the Equivalent Fracture Network Permeability using Multivariable Regression Analysis and Artificial Neural Networks," Proceedings World Geothermal Congress, Bali, Indonesia, 25-29 April 2010.

Table 3.2 Natural fracture patterns in the 100x100 m^2 square domain.

FD of Intersection Points using Box Counting Technique	Connectivity Index	Maximum Touch with X Scanning Lines	Maximum Touch with Y Scanning Lines	FD of Fracture Lines using Box Counting Technique	Conductivity mD.m	Permeability mD
1.867	1.064	15608	21143	1.557	1000	28.801
1.820	1.704	15396	17481	1.521	1000	85.936
1.892	1.516	19585	24571	1.598	1000	108.988
1.750	1.407	13331	15887	1.443	1000	56.751
1.774	1.465	15486	16721	1.487	1000	43.032
1.870	1.422	18933	24001	1.576	1000	104.354
1.872	1.275	15916	31323	1.630	1000	106.506
1.800	1.271	13364	16592	1.528	1000	49.509
1.769	1.745	16978	17563	1.567	1000	66.102
1.770	1.496	14366	18920	1.562	1000	70.835
1.298	1.500	489	317	1.270	1000	23.991
1.347	1.100	759	763	1.369	1000	10.387
0.797	1.091	114	266	1.264	1000	38.106
1.672	1.218	4720	5612	1.484	1000	11.863
1.660	1.149	4071	3094	1.493	1000	5.649
1.378	1.020	860	1210	1.481	1000	88.345
1.577	1.041	4697	2680	1.513	1000	9.085
1.893	2.611	4767	5473	1.682	1000	98.342
1.647	1.369	1687	1758	1.583	1000	21.625
1.653	1.558	996	1281	1.515	1000	29.411

FD: Fractal Dimension

The first and fifth columns in the table show the fractal dimension of fracture intersection points and fracture lines, respectively, in the domains using the box counting technique. The second one is the number of fracture line intersections divided by the number of fracture lines or density. The third and forth ones are defined as a result of the intersection between fracture lines and imaginary scanning lines in each X and Y direction.

Jafari, A. and Babadagli, T.: "Prediction the Equivalent Fracture Network Permeability using Multivariable Regression Analysis and Artificial Neural Networks," Proceedings World Geothermal Congress, Bali, Indonesia, 25-29 April 2010.

Then, the relationship between these parameters and EFNP was researched through multivariable regression analysis and three empirical equations were derived with 4, 5 and 6 independent variables (**Table 3.3**).

Table 3.3 Derived equations for EFNP (K) with different number of independent variables (Method: MRA).

Independent Variables	Derived Equation
4	$Ln(K) = a*exp(b*x_1)+c*ln(x_2)+d*ln(x_3)+ln(x_4)+f$
5	$Ln(K) = a*exp(b*x_1)+c*ln(x_2)+d*ln(x_3)+e*ln(x_4)+f*ln(x_5)+g$
6	$Ln(K) = a*exp(b*x_1)+c*ln(x_2)+d*ln(x_3)+e*ln(x_4)+f*ln(x_5)+g*ln(x_6)+h$

Jafari and Babadagli (2008) proposed an equation to predict the EFNP (the same as the first equation in **Table 3.3** but different constant coefficients). Initially, this equation was applied on natural fracture patterns. The comparison of the actual and calculated EFNPs is shown in **Figure 3.3**. Though the same scale (100x100 m^2) was used, the correlation is not very strong due to the fact that the equation was derived using synthetic (and random) patterns which show topologically different characters (poor connectivity, dead-end fractures, isolated fractures, etc. exist in the synthetic ones).

Jafari, A. and Babadagli, T.: "Prediction the Equivalent Fracture Network Permeability using Multivariable Regression Analysis and Artificial Neural Networks," Proceedings World Geothermal Congress, Bali, Indonesia, 25-29 April 2010.

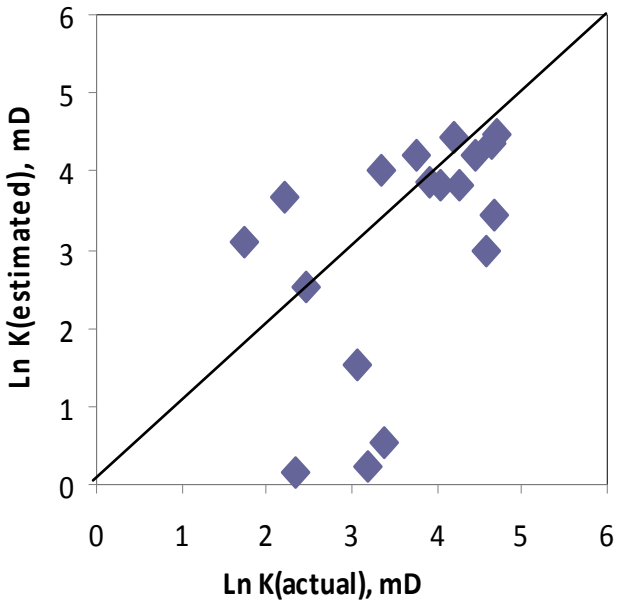

Figure 3.3 Actual EFNPs vs. estimated ones using the Jafari and Babadagli (2008) equation with 4 independent variables for natural patterns.

In **Table 3.3**, K stands for permeability in mD. In the first equation, x1, x2, x3 and x4 are the fractal dimension of fracture intersection points using the box counting technique, maximum intersection (touch) between fracture lines and the imaginary scanning line in X direction, maximum intersection (touch) between fracture lines and the imaginary scanning line in Y direction, and fractal dimension of fracture lines using the box counting technique, respectively. In the second equation, x1, x2, x3, x4 and x5 are the fractal dimension of fracture intersection points using the box counting technique, maximum intersection (touch) between fracture lines and the imaginary

Jafari, A. and Babadagli, T.: "Prediction the Equivalent Fracture Network Permeability using Multivariable Regression Analysis and Artificial Neural Networks," Proceedings World Geothermal Congress, Bali, Indonesia, 25-29 April 2010.

scanning line in X direction, maximum intersection (touch) between fracture lines and the imaginary scanning line in Y direction, fractal dimension of fracture lines using the box counting technique, and fracture conductivity respectively. In the third equation, x1, x2, x3, x4, x5 and x6 are the fractal dimension of fracture intersection points using the box counting technique, connectivity index, maximum intersection (touch) between fracture lines and the imaginary scanning line in X direction, maximum intersection (touch) between fracture lines and the imaginary scanning line in Y direction, fractal dimension of fracture lines using the box counting technique, and fracture conductivity, respectively. In all these equations, a, b, c, d, e, f, g and h are constant coefficients.

Having seen poor correlation with the existing correlation derived by Jafari and Babadagli (2008) using 800 synthetic patterns of different fracture network characteristics (**Figure 3.3**), new equations were generated by MRA using only 20 natural patterns from different geothermal reservoir outcrops patterns. The equations are the same types as given in **Table 3.3**. The comparisons of actual and calculated EFNP values are shown in **Figure 3.4**, **Figure 3.5** and **Figure 3.6**. These plots show the reliability of the equations and they slightly increase with increasing variables.

Jafari, A. and Babadagli, T.: "Prediction the Equivalent Fracture Network Permeability using Multivariable Regression Analysis and Artificial Neural Networks," Proceedings World Geothermal Congress, Bali, Indonesia, 25-29 April 2010.

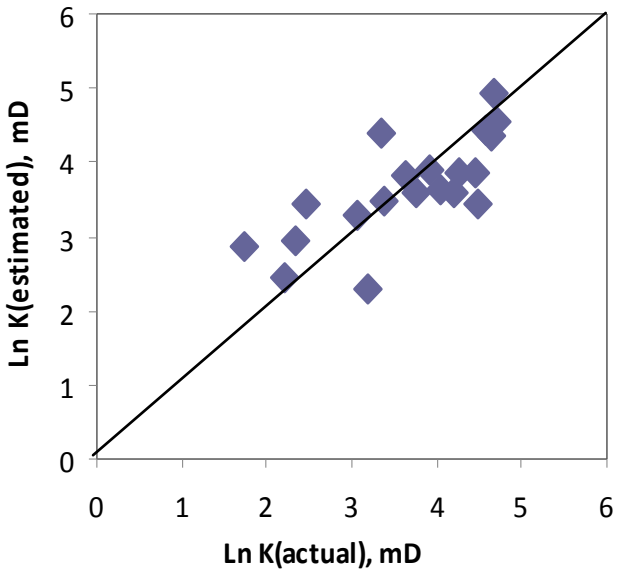

Figure 3.4 Actual EFNPs vs. estimated ones using the equation with 4 independent variables for natural patterns.

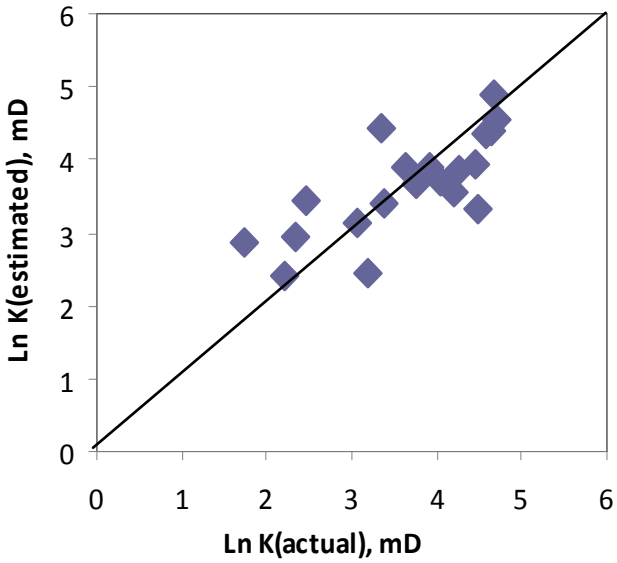

Figure 3.5 Actual EFNPs vs. estimated ones using the equation with 5 independent variables for natural patterns.

Jafari, A. and Babadagli, T.: "Prediction the Equivalent Fracture Network Permeability using Multivariable Regression Analysis and Artificial Neural Networks," Proceedings World Geothermal Congress, Bali, Indonesia, 25-29 April 2010.

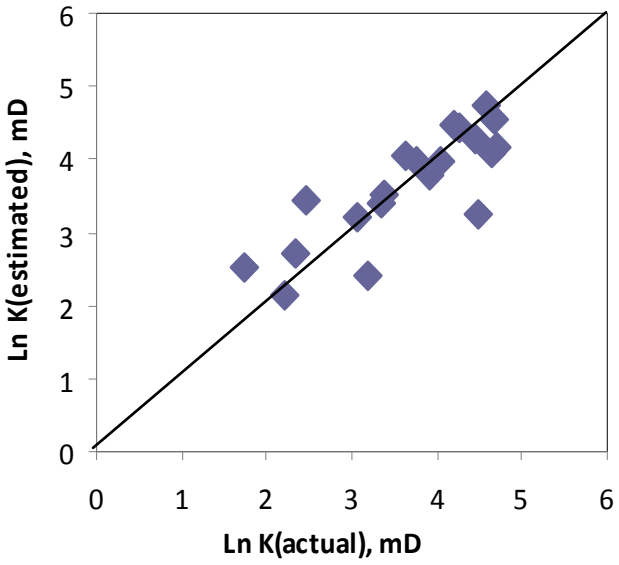

Figure 3.6 Actual EFNP vs. estimated ones using the equation with 6 independent variables for natural patterns.

To validate these equations, different synthetic patterns according to the following algorithms were generated. First, synthetic 2D fracture models within 100x100 m^2 square domains were generated (typical patterns are shown in **Figure 3.2**). A wide range of fracture lengths, densities, and orientations were considered in the patterns used for this validation process. In each model, fracture seeds are distributed according to a uniform distribution and each fracture is represented as a line in the fracture domain. The range of each fracture parameter in this algorithm is as follows:

Jafari, A. and Babadagli, T.: "Prediction the Equivalent Fracture Network Permeability using Multivariable Regression Analysis and Artificial Neural Networks," Proceedings World Geothermal Congress, Bali, Indonesia, 25-29 April 2010.

(1) Fracture length (in meters): (a) constant: 20, 40, 60, and 80 and (b) variable with a normal distribution and a mean value of 20, 40, 60, and 80,

(2) Density (# of fractures/domain): 50, 100, 150, 200 and 250 (domain is 100x100 m^2), and

(3) Orientation: Two fracture sets in the domain with the directions of (a) N-S & E-W, (b) NW-SE & NE-SW and (c) totally random.

It should be mentioned that instead of aperture, conductivity was used, which is related to aperture since the product of the intrinsic fracture permeability and the fracture aperture with parallel walls is defined as conductivity (Bourbiaux et al. 1998). Each data set had twenty different combinations of length and density. Also, five different realizations using different random number seeds for each combination were tried, to include the effect of randomness. Each of these models could represent one grid cell in the dual-porosity simulators. Then using the same software, their equivalent fracture permeability was measured. In order to validate the derived equations, these permeability values were estimated using these equations and plotted versus each other for comparison purposes (**Figure 3.7**, **Figure 3.8** and **Figure 3.9**).

Jafari, A. and Babadagli, T.: "Prediction the Equivalent Fracture Network Permeability using Multivariable Regression Analysis and Artificial Neural Networks," Proceedings World Geothermal Congress, Bali, Indonesia, 25-29 April 2010.

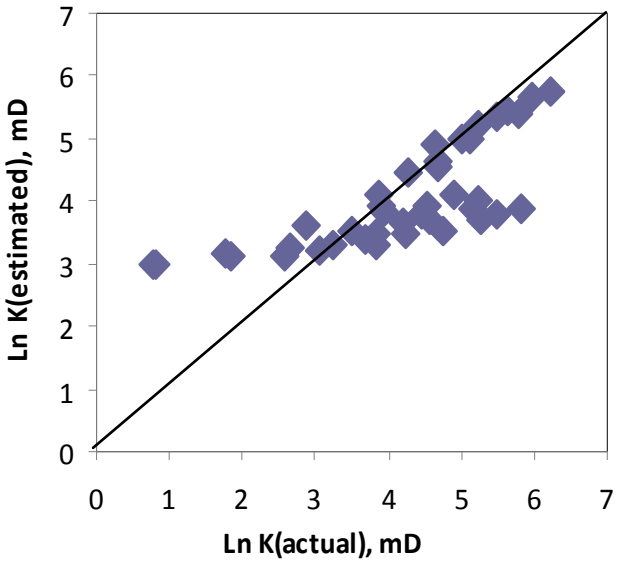

Figure 3.7 Actual EFNP vs. estimated ones using the equation with 4 independent variables. Validation of the equation derived for natural patterns using synthetic patterns.

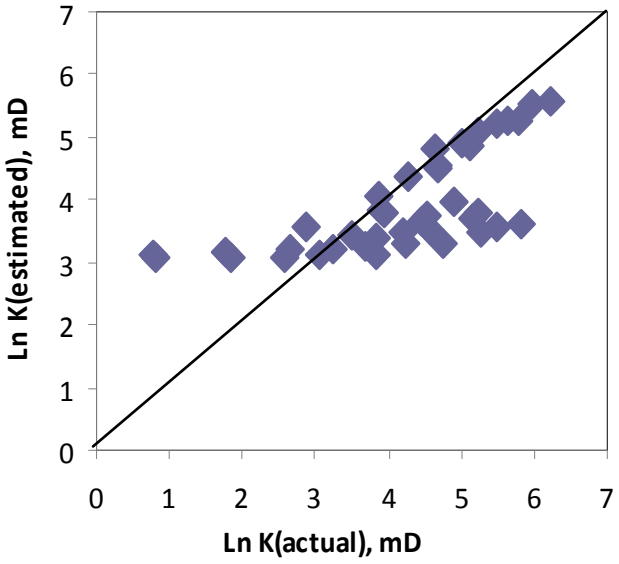

Figure 3.8 Actual EFNPs vs. estimated ones using the equation with 5 independent variables. Validation of the equation derived for natural patterns using synthetic patterns.

Jafari, A. and Babadagli, T.: "Prediction the Equivalent Fracture Network Permeability using Multivariable Regression Analysis and Artificial Neural Networks," Proceedings World Geothermal Congress, Bali, Indonesia, 25-29 April 2010.

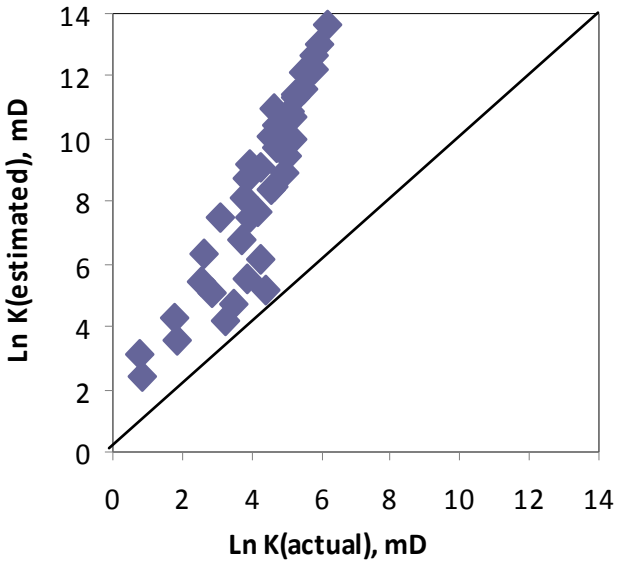

Figure 3.9 Actual EFNP vs. estimated ones using the equation with 6 independent variables. Validation of the equation derived for natural patterns using synthetic patterns.

The results show that the new equations with 4 and 5 variables derived using natural patterns showed reasonably good correlation for high permeability cases (higher density and longer fractures, i.e., well connectivity). The equation with 6 variables represented an opposite case and the deviation from the actual values was significantly higher for higher EFNP cases. Obviously, the nature of the synthetic fracture patterns is different and this difference is pronounced clearly through this analysis. For example, the additional parameter used in the 6-variable equation is the connectivity index and when this parameter is added in the MRA, the correlation becomes much weaker as seen in **Figure 3.9**. In fact, the density and length distributions of natural and synthetic (random) patterns can be approximated as they are statistical

Jafari, A. and Babadagli, T.: "Prediction the Equivalent Fracture Network Permeability using Multivariable Regression Analysis and Artificial Neural Networks," Proceedings World Geothermal Congress, Bali, Indonesia, 25-29 April 2010.

parameters but the connectivity characteristics depend on the nature of the fracturing process and may differ in natural and synthetic patterns. In other words, synthetic and natural fracture patterns may have the same density and fracture length distributions (statistically similar to each other) but connectivity is a topological parameter that has to do with the nature of the fracturing process (and other parameters like lithology) which may not be approximated as a random process. Also note that in generating synthetic patterns we assumed that fracture seeds are distributed according to a uniform distribution which may not be always the case in the field. This directly affects the connectivity rather than density and length as they are predefined parameters. These observations indicate that one has to pay attention when generating fracture networks through the discrete fracture network approach or similar techniques to represent the natural pattern, especially from an EFNP point of view.

The efforts made so far compared natural and synthetic pattern characteristics by generating 100x100 m^2 (typical numerical grid size scale) synthetic patterns and approximating the meter-scale natural patterns to the same size. The next step is to analyze the effect of the domain scale on the correlations and scale dependency of the EFNP. To achieve this, we focused on a much smaller fracture domain (meter-scale) using the same patterns at their original scale. The same natural patterns were digitized in a 1x1m square domain. Some patterns were larger than 1x1m^2 (at higher scales) and they were excluded in this analysis. Exactly the same procedure followed for the bigger scale was applied to derive new correlations based on the equations (with new coefficients this time) shown in **Table 3.3**. Then the equations were tested to

Jafari, A. and Babadagli, T.: "Prediction the Equivalent Fracture Network Permeability using Multivariable Regression Analysis and Artificial Neural Networks," Proceedings World Geothermal Congress, Bali, Indonesia, 25-29 April 2010.

predict the EFNPs. The correlations are good for 4 and 5 variable cases (**Figure 3.10** and **Figure 3.11**, respectively) except two patterns.

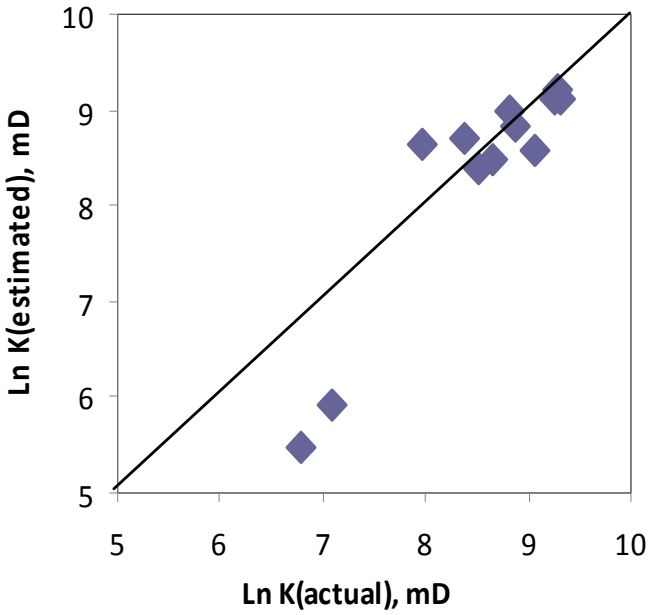

Figure 3.10 Actual EFNP vs. estimated ones using the equation with 4 independent variables for 1x1 m^2 square domain. Derived using only natural patterns.

Jafari, A. and Babadagli, T.: "Prediction the Equivalent Fracture Network Permeability using Multivariable Regression Analysis and Artificial Neural Networks," Proceedings World Geothermal Congress, Bali, Indonesia, 25-29 April 2010.

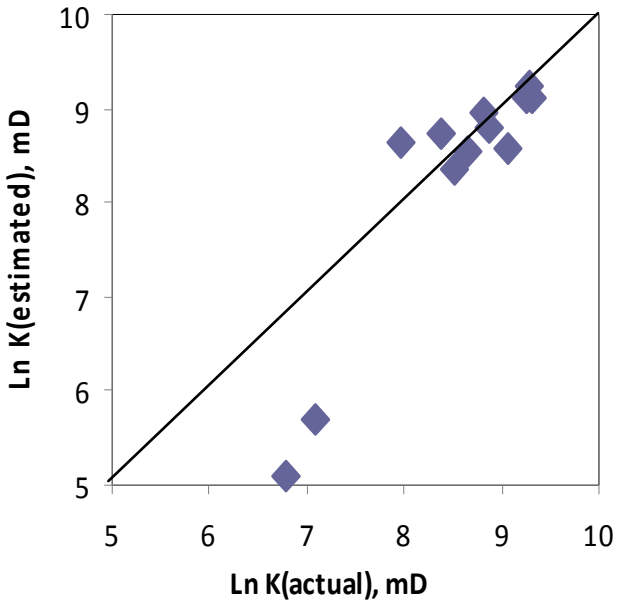

Figure 3.11 Actual EFNP vs. estimated ones using the equation with 5 independent variables for 1x1 m^2 square domain. Derived using only natural patterns.

These two patterns belong to a different lithology showing fracture patterns strongly oriented in one direction. When the 6-variable equation is used, one may observe additional two patterns showing deviation (**Figure 3.12**). They belong to much smaller size patterns than 1x1m^2 but are stretched out to this size while digitizing and are placed in a 1x1m^2 domain. Other than those exceptions, the patterns showed reasonably good correlations.

Jafari, A. and Babadagli, T.: "Prediction the Equivalent Fracture Network Permeability using Multivariable Regression Analysis and Artificial Neural Networks," Proceedings World Geothermal Congress, Bali, Indonesia, 25-29 April 2010.

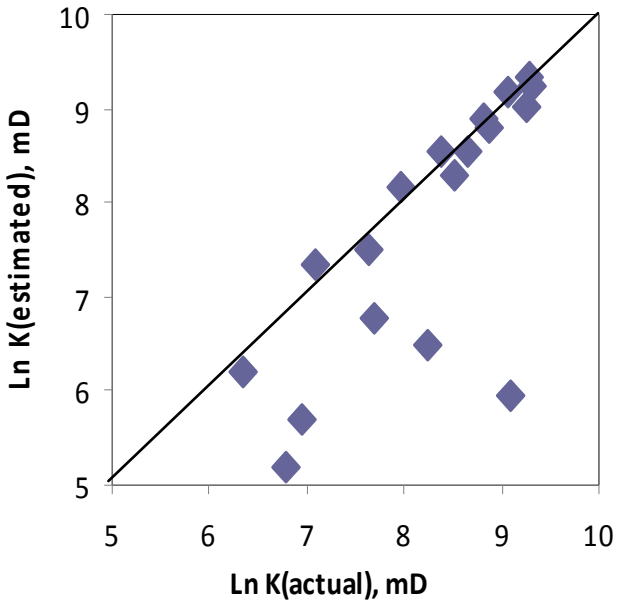

Figure 3.12 Actual EFNP vs. estimated ones using the equation with 6 independent variables for 1x1 m^2 square domain. Derived using only natural patterns.

In summary, the equations given in **Table 3.3** are useful in estimating the EFNP of not only the synthetic but also the natural fracture patterns. One has to pay attention, however, to the scale dependency and use proper coefficients at different scales.

3.3 Artificial neural networks

We also attempted to improve the accuracy of the equivalent fracture network prediction. It is believed that the relationships between the EFNP and different

Jafari, A. and Babadagli, T.: "Prediction the Equivalent Fracture Network Permeability using Multivariable Regression Analysis and Artificial Neural Networks," Proceedings World Geothermal Congress, Bali, Indonesia, 25-29 April 2010.

fracture networks parameters are nonlinear and very complicated; thus, multivariable regression analysis may be limited in capturing these complex relationships. Therefore, an ANN was selected to capture relationships between the EFNP and fracture network parameters, and was compared with the MRA analysis results.

A back propagation network with a supervised learning procedure was selected to model the problem, and different input variables and numbers in the input layer, different numbers of the hidden layers (between input and output layers), and neurons in each of these hidden layers were tested. In these structures, only one output in the output layer was defined (**Figure 3.13**).

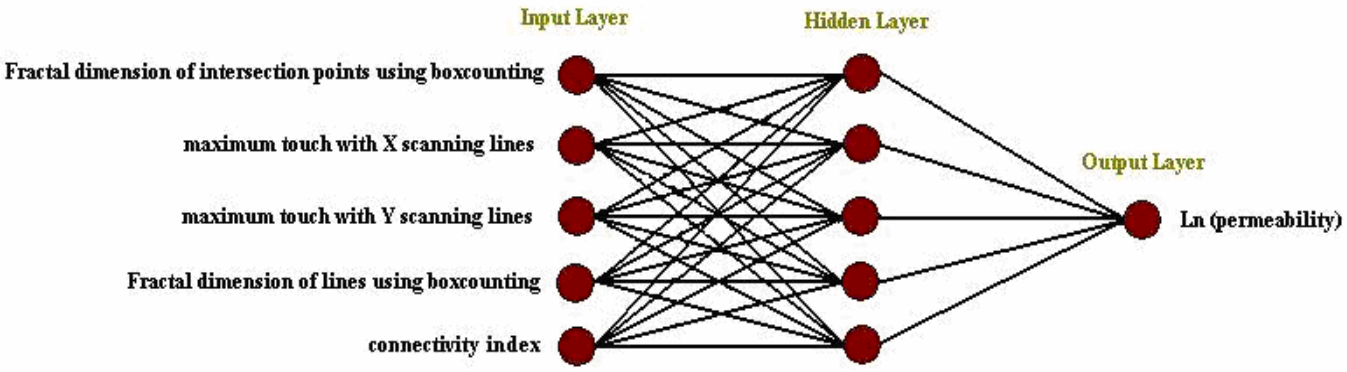

Figure 3.13 Topology of a back propagation network used in this chapter.

First, all natural fracture patterns data were put together and divided into three sets: 1) Training set 2) Validation set and 3) Test set. The "Training set" was used to train the network and capture the existing relationship. In the training

Jafari, A. and Babadagli, T.: "Prediction the Equivalent Fracture Network Permeability using Multivariable Regression Analysis and Artificial Neural Networks," Proceedings World Geothermal Congress, Bali, Indonesia, 25-29 April 2010.

process, inputs and the target are given and the network calculates its error, i.e. the difference between the target and response, and adjusts its weights on the connections between the different neurons. In order to prevent memorizing of the data set by the network, another set called the "Validation set" was fed during the training process. Thus, as soon as error for this set starts increasing, the training process stops. The last data set, i.e. the "Test set" was used to check the ability of the network to predict unseen or new data (MATLAB user's guide). The plot of the training, validation and test errors is shown in **Figure 3.14**. Note that in the training process, some synthetic patterns were also used in addition to the natural ones, to be able to have extreme values of EFNP (covering the whole range).

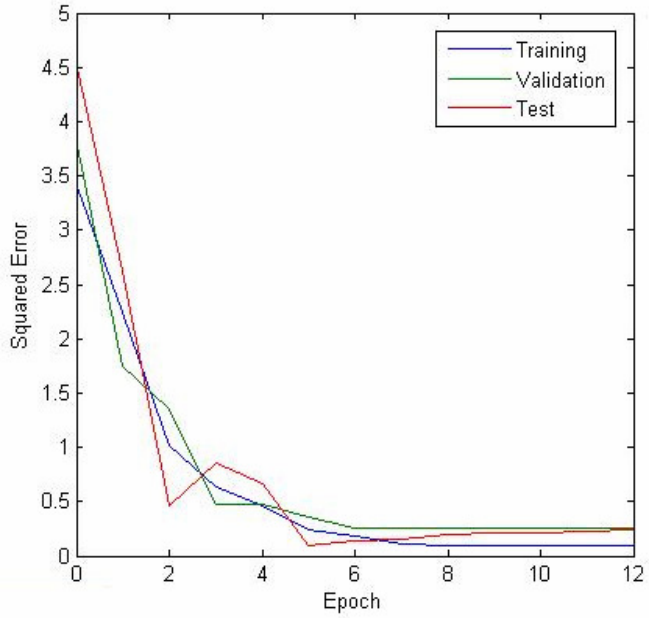

Figure 3.14 The error of three different data sets (training, validation and test) during the training process.

Jafari, A. and Babadagli, T.: "Prediction the Equivalent Fracture Network Permeability using Multivariable Regression Analysis and Artificial Neural Networks," Proceedings World Geothermal Congress, Bali, Indonesia, 25-29 April 2010.

Then, the real equivalent fracture permeability values of all these three data sets are plotted versus the estimated ones by the trained network, which shows a very promising correlation coefficient (**Figure 3.15**).

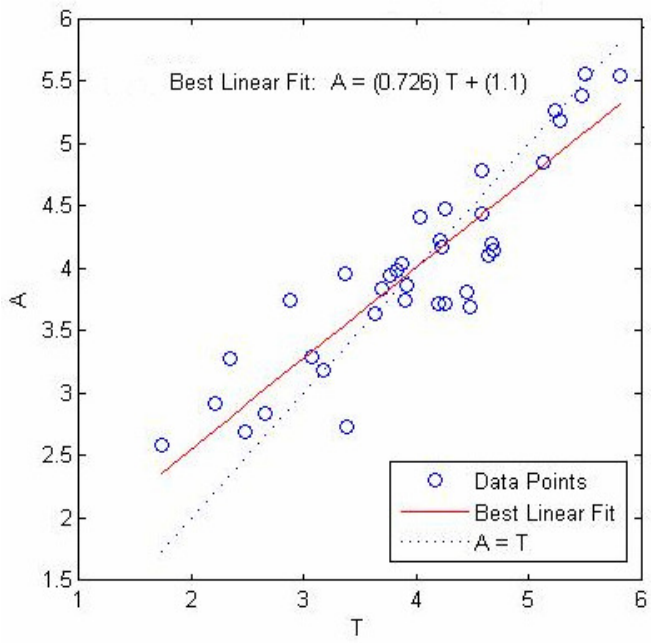

Figure 3.15 Cross plot of actual EFNP of the entire data set (training, validation and testing) versus the estimated ones. All natural patterns with some addition of synthetic patterns were used for training, validation, and testing.

Finally, only the input parameters of the synthetic fracture patterns are given to the trained network and it predicts the equivalent fracture network permeability values. The results are shown in **Figure 3.16**. Compared to the cases given in **Figure 3.7**, **Figure 3.8** and **Figure 3.9**, the reliability of the correlations improved significantly.

Jafari, A. and Babadagli, T.: "Prediction the Equivalent Fracture Network Permeability using Multivariable Regression Analysis and Artificial Neural Networks," Proceedings World Geothermal Congress, Bali, Indonesia, 25-29 April 2010.

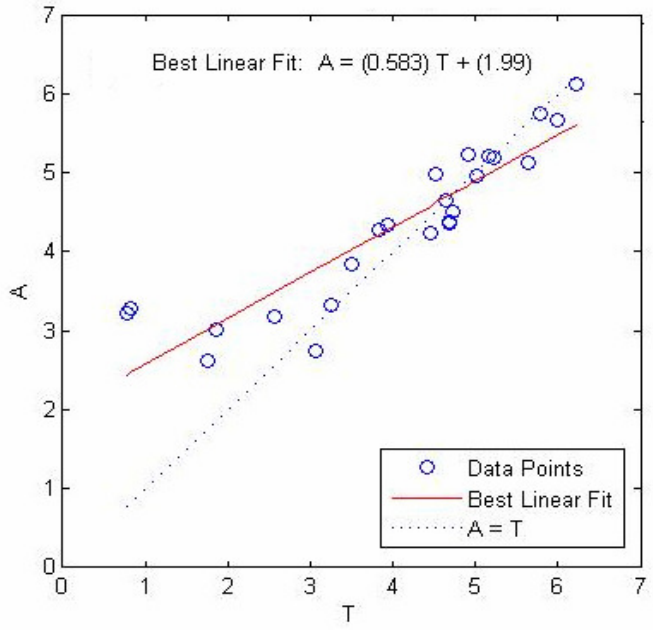

Figure 3.16 Cross plot of actual EFNP of synthetic fracture patterns versus the estimated ones.

3.4 Conclusions

1. The relationship between different statistical and fractal parameters of fracture networks and their equivalent fracture network permeability (EFNP) for natural patterns obtained from geothermal reservoir outcrops was studied. It was shown that the parameters that could be used for derivation of the empirical equations to predict EFNP are fractal dimension of fractures intersection points and fracture lines using box counting technique, connectivity index, maximum number of intersections between fractures and imaginary scanning lines in the X

Jafari, A. and Babadagli, T.: "Prediction the Equivalent Fracture Network Permeability using Multivariable Regression Analysis and Artificial Neural Networks," Proceedings World Geothermal Congress, Bali, Indonesia, 25-29 April 2010.

and Y directions, and conductivity.

2. The equations given in **Table 3.3** are useful in estimating the EFNP of not only the synthetic but also the natural fracture patterns. One has to pay attention, however, to the scale dependency and use proper coefficients at different scales.

3. The connectivity was found to be a critical parameter in using synthetic (or random) approaches in generating/representing natural fracture networks. The density and length distributions of natural and synthetic (random) patterns can be approximated as they are statistical parameters but the connectivity characteristics depend on the nature of the fracturing process and may differ in natural and synthetic patterns. In other words, synthetic and natural fracture patterns may have the same density and fracture length distribution (statistically similar to each other) but connectivity is a topological parameter that has to do with the nature of the fracturing process (and other parameters like lithology) which may not be approximated as a random process. These observations indicate that one has to pay attention when generating fracture networks through the discrete fracture network approach or similar techniques to represent the natural pattern, especially from an EFNP point of view.

4. It was found that a BPP network with one hidden layer containing 5 neurons is capable enough to capture the relationship between the fracture network parameters as inputs and the EFNP as an output. This

Jafari, A. and Babadagli, T.: "Prediction the Equivalent Fracture Network Permeability using Multivariable Regression Analysis and Artificial Neural Networks," Proceedings World Geothermal Congress, Bali, Indonesia, 25-29 April 2010.

type of ANN configuration yielded more reliable correlations compared to the ones obtained with the MRA.

Jafari, A. and Babadagli, T.: "Prediction the Equivalent Fracture Network Permeability using Multivariable Regression Analysis and Artificial Neural Networks," Proceedings World Geothermal Congress, Bali, Indonesia, 25-29 April 2010.

4 Effective Fracture Network Permeability of Geothermal Reservoirs

4.1 Overview

This chapter presents a new, simple, computationally efficient and practical method to accurately calculate effective fracture network permeability (EFNP) values for fracture dominated reservoirs. A set of fracture patterns from the outcrops of geothermal reservoirs in southwestern Turkey were chosen and their EFNP values were predicted using the new method; the computed permeability values are comparable to those obtained with a commercial software package and actual were tested. The proposed method is based on 2D fracture outcrop data, and is therefore limited to 2-D fracture networks.

4.2 Selection of data

In our previous work, only synthetic fracture patterns were used to derive empirical equations (Jafari and Babadagli, 2008, 2009a, and 2010a). However, the mechanism of fracturing and the stress-strain regimes of natural patterns caused by the matrix heterogeneity (and other lithological characteristics) are totally different for each natural pattern; synthetic generated patterns are not

Jafari, A. and Babadagli, T.: "Effective Fracture Network Permeability of Geothermal Reservoirs," Geothermics: International Journal of Geothermal Research and its Applications.

able to mimic these processes properly. As a result, the fracture connectivity of natural patterns may differ substantially from the synthetically generated ones. Therefore, it was decided to use natural fracture patterns from various reservoirs and formations with different characteristics for this work. To simplify analysis, the stress-strain regimes are not considered. However, many different fracture patterns were collected and classified based on reservoir type and lithology. The fracture patterns implicitly represent different fracture mechanisms due to variations in properties of reservoir rocks. Fracture patterns from six different regions/reservoirs (as indicated in **Figure 4.1**) and three different lithologies at several different scales are employed for the statistical representation of fracture network characteristics.

Jafari, A. and Babadagli, T.: "Effective Fracture Network Permeability of Geothermal Reservoirs," Geothermics: International Journal of Geothermal Research and its Applications.

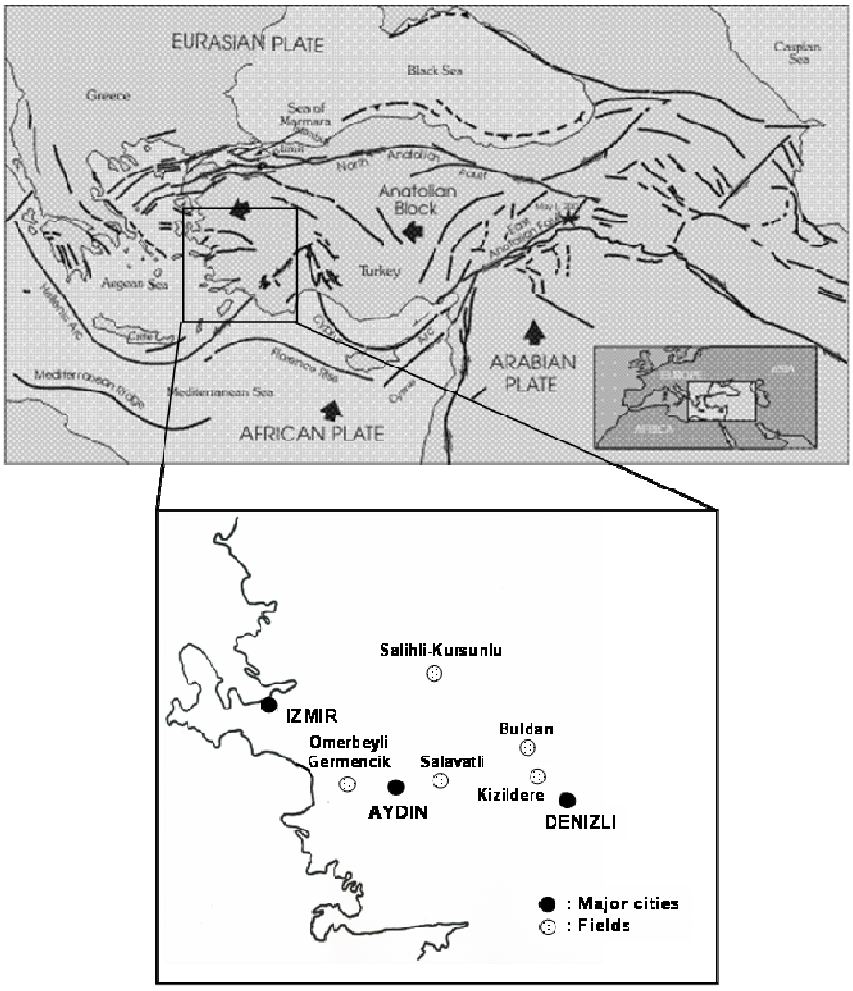

Figure 4.1 Plate tectonics map and location of geothermal fields in southwestern Turkey. Five points in the lower map indicate the field and outcrop locations where fracture patterns were photographed. (http://neic.usgs.gov/neis/eq_depot/2003/eq_030501/neic_tgac_anaflt1.gif)

A total of twenty two different fracture patterns at different scales were selected from different locations representing the geothermal reservoir formations in southwestern Turkey. Thus, seven different geothermal

Jafari, A. and Babadagli, T.: "Effective Fracture Network Permeability of Geothermal Reservoirs," Geothermics: International Journal of Geothermal Research and its Applications.

reservoirs in five different fields including the ones from two major fields, i.e. Kizildere and Germencik, were studied and the outcrop fracture patterns were mapped (Babadagli, 2001).

Figure 4.1 shows the tectonic map of Turkey and the locations of studied areas. The outcrops of geothermal reservoir rocks were mapped for multivariable regression analysis in order to derive empirical correlations which in turn could be used to calculate equivalent fracture network permeability (EFNP). Lithologies include marble, quartzite and limestone. **Table 4.1** presents the field names (or location of the outcrops) and the associated lithology.

Jafari, A. and Babadagli, T.: "Effective Fracture Network Permeability of Geothermal Reservoirs," Geothermics: International Journal of Geothermal Research and its Applications.

Table 4.1 The geothermal reservoirs with different lithologies in southwestern Turkey used in this chapter.

Fracture Pattern Number	Field Name		Lithology
1	Field 1	Omerbeyli - Germencik	Marble
2	Field 1	Omerbeyli – Germencik	Marble
3	Field 1	Omerbeyli – Germencik	Marble
4	Field 1	Omerbeyli – Germencik	Marble
5	Field 1	Omerbeyli – Germencik	Marble
6	Field 1	Omerbeyli - Germencik	Marble
7	Field 1	Omerbeyli – Germencik	Marble
8	Field 1	Omerbeyli – Germencik	Marble
9	Field 1	Omerbeyli - Germencik	Marble
10	Field 2	Salihi - Kursunlu	Marble
11	Field 2	Salihi - Kursunlu	Marble
12	Field 3	Buldan (Kizildere formation)	Limestone
13	Field 3	Buldan (Kizildere formation)	Limestone
14	Field 3	Buldan (Kizildere formation)	Limestone
15	Field 4	Salavatli	Marble
16	Field 5	Kizildere (upper formation)	Limestone
17	Field 5	Kizildere (upper formation)	Limestone
18	Field 5	Kizildere (upper formation)	Limestone
19	Field 5	Kizildere (upper formation)	Limestone
20	Field 5	Kizildere (upper formation)	Limestone
21	Field 5	Kizildere (lower formation)	Quartzite
22	Field 5	Kizildere (lower formation)	Quartzite

Representative fracture patterns are shown in **Figure 4.2** (**a**, **b**, **c** and **d**). As can be seen in the photos, most fractures are open to flow in the outcrop samples. In only one area, we observed fractures filled with minerals. In our analyses, all fractures are assumed to contribute to flow, i.e., they are not plugged by mineralization.

Jafari, A. and Babadagli, T.: "Effective Fracture Network Permeability of Geothermal Reservoirs," Geothermics: International Journal of Geothermal Research and its Applications.

(a) Outcrop: A producing formation (limestone) in Field 5 lower formation (photo and fracture trace map).

(b) Outcrop: A producing formation (limestone) in Field 5 upper formation (photo and fracture trace map).

(c) Outcrop: A producing formation (marble) in Field 1 (photo and fracture trace map).

Jafari, A. and Babadagli, T.: "Effective Fracture Network Permeability of Geothermal Reservoirs," Geothermics: International Journal of Geothermal Research and its Applications.

(d) Outcrop: A producing formation (marble) in Field 1 (photo and fracture trace map).

Figure 4.2 (a, b, c and d) Samples of natural fracture patterns (outcrop) from different geothermal fields in southwestern Turkey used in the chapter.

4.3 Data preparation

In accordance with the previous chapters, the 2D maps of natural fracture patterns were digitized using a 100x100 m^2 domain size and the fractal and statistical parameters of each fracture pattern were calculated. Image analyzer software ImageJ (Ferreira and Rasband, 2010) was employed to compute lacunarity. Lacunarity is a measure of gappiness (or hole or porosity) or visual texture of a fractal, and is useful for differentiating between two fractals having the same fractal dimension but different textures; it is defined as follows:

$$\Lambda_{\varepsilon} = \left(\frac{s}{M} \right)^2 \qquad \textbf{(1)}$$

Jafari, A. and Babadagli, T.: "Effective Fracture Network Permeability of Geothermal Reservoirs," Geothermics: International Journal of Geothermal Research and its Applications.

The lacunarity, Λ, is calculated as the variation in pixel density for different ε (grid size). Initially, the number of pixels within each grid box is counted using a standard non-overlapping box count. For each ε, a coefficient of variance is computed from the standard deviation (*s*) and the mean (*M*) of number of pixels per box. The open source software, Fraclac V.2 for ImageJ (Karperien, 2005, Rasband, -2010), computes the lacunarity based on the pixel density at different box sizes for an image. A homogeneous fractal has a low lacunarity whereas an increase in void space in the texture of a fractal leads to an increase in lacunarity (Hamida and Babadagli, 2005).

The digitized fracture patterns were exported to commercial fracture modeling software (FRACA) to calculate their equivalent fracture network permeability (EFNP). A 3D model with a grid block size of 100x100x10 m^3 was constructed and each digitized 2D fracture pattern (i.e. the digitized mapped fracture traces from outcrops) was imported into the 3D model in such a way that all fractures were considered to be vertically touching the top and the bottom of the layer. The EFNP was calculated for the 3D model using the software package (FRACA). The EFNP values for all patterns are tabulated in **Table 4.2**.

Jafari, A. and Babadagli, T.: "Effective Fracture Network Permeability of Geothermal Reservoirs," Geothermics: International Journal of Geothermal Research and its Applications.

Table 4.2 Statistical and fractal parameters of natural fracture patterns digitized using a 100x100 m^2 square box.

FD of Intersection Points using Box Counting Technique	Connectivity Index	Maximum Intersection Points with X Scanning Lines	Maximum Intersection Points with Y Scanning Lines	FD of Fracture Lines using Box Counting Technique	Lacunarity	Conductivity mD.m	Permeability mD
1.774	1.465	15486	16721	1.592	0.372	1000	43.032
1.786	1.303	15384	16494	1.583	0.404	1000	29.384
1.678	1.360	10582	17700	1.565	0.442	1000	79.516
1.870	1.422	18933	24001	1.625	0.360	1000	104.354
1.549	1.046	8782	9515	1.427	0.478	1000	33.702
1.769	1.745	16978	17563	1.596	0.355	1000	66.102
1.770	1.496	14366	18920	1.604	0.308	1000	70.835
1.869	1.152	15429	21813	1.626	0.296	1000	74.336
1.554	1.069	8972	9876	1.415	0.470	1000	15.964
1.771	1.016	11581	11543	1.522	0.370	1000	11.863
1.634	1.250	18745	6399	1.491	0.427	1000	5.649
1.745	1.066	14206	15393	1.567	0.426	1000	9.085
1.872	1.275	15916	31323	1.646	0.348	1000	106.506
1.820	1.395	17544	14811	1.581	0.393	1000	28.909
1.800	1.271	13364	16592	1.561	0.342	1000	49.509
1.704	1.447	8242	19627	1.597	0.301	1000	77.034
1.867	1.064	15608	21143	1.623	0.304	1000	28.801
1.820	1.704	15396	17481	1.582	0.474	1000	85.936
1.892	1.516	19585	24571	1.651	0.325	1000	108.988
1.750	1.407	13331	15887	1.580	0.389	1000	56.751
1.722	1.444	12047	16869	1.565	0.507	1000	66.149
1.690	1.352	10674	14886	1.501	0.499	1000	36.678

FD: Fractal Dimension

The fractal dimensions for different features of these 2D fracture networks (fracture intersection points and fracture network itself) are between 1 and 2 indicating that these fracture patterns are fractal. The fractal dimensions listed in **Table 4.2** are in line with the field observations of similar fracture patterns

Jafari, A. and Babadagli, T.: "Effective Fracture Network Permeability of Geothermal Reservoirs," Geothermics: International Journal of Geothermal Research and its Applications.

obtained for other geothermal reservoirs of similar lithology (Acuna et al., 1992 and 1995, Sammis et al., 1991 and 1992).

4.4 Multivariable regression analysis and derivation of correlations

An extensive multivariable regression analysis was performed to determine the type of relationship (linear or nonlinear –exponential, logarithmic) that might be present between the parameters given in columns 1 through 7 (inputs) and the EFNP listed in the last column (output) in **Table 4.2**. Seven parameters for deriving EFNP correlations were considered in the derivation process. These parameters are as follows:

(1) Fracture intersection points: This is the set of points representing the intersection of two fractures. It represents the connectivity and directly relates to the permeability. The fractal dimension of the distribution of these points was measured by the box-counting technique.

(2) Connectivity index: A ratio of the number of intersection points to the total number of fracture lines.

(3) Maximum intersections with X- and Y-scanning lines: The number of intersections (hits) of the imaginary scan lines with a fracture (obtained for the whole fracture network pattern in both X- and Y- directions). The scan line distances were selected as 1/10 of a grid-block in both the x- or y-directions. In other words, when a 100x100 m^2 grid is used, there are 1000 scan lines in each direction. Based on a sensitivity

Jafari, A. and Babadagli, T.: "Effective Fracture Network Permeability of Geothermal Reservoirs," Geothermics: International Journal of Geothermal Research and its Applications.

analysis, the latter number of scan lines was found to adequately characterize all the fractures with different sizes. The number of intersections (hits) obtained for the whole pattern represent the density and orientation of the fracture network and are related to the length of the fractures.

(4) Fractal dimension of fracture lines: Fractal dimension of fracture lines obtained by standard box counting techniques.

(5) Lacunarity: As defined in **Eq. 1**.

(6) Conductivity: Corresponds to the product of aperture and width of a single fracture.

The first and fifth columns in **Table 4.2** show the fractal dimension of fracture line intersection point and fracture lines in the domains using the box counting technique, respectively. An example of box-counting plot [log(r) vs. log n(r)] is given in **Figure 4.3**; it indicates the straight line behavior and upper and lower cut-offs of the fractal behavior.

Jafari, A. and Babadagli, T.: "Effective Fracture Network Permeability of Geothermal Reservoirs," Geothermics: International Journal of Geothermal Research and its Applications.

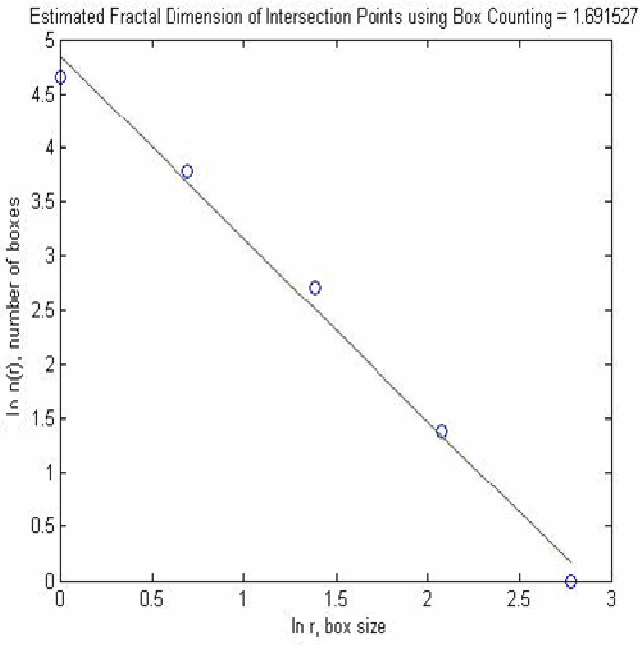

Figure 4.3 Log (r) vs. log n(r) plot showing the slope (box counting fractal dimension) and the upper and lower cut-offs (within the 1m – 16m range, the behavior is fractal as indicated by a straight line) of the fractal behavior. The box size (r) is in meters. Here *n* denotes the number of boxes filled with the feature (fractures).

In the second column, connectivity is defined as the number of fracture line intersections divided by the number of fracture lines or density. The third and fourth columns give the number of intersections between fracture lines and imaginary scanning lines in each X and Y direction, respectively. The sixth column shows lacunarity. The seventh column is the conductivity of each fracture which is used in lieu of aperture. Fracture conductivity is defined as the product of the intrinsic fracture permeability and the fracture aperture

Jafari, A. and Babadagli, T.: "Effective Fracture Network Permeability of Geothermal Reservoirs," Geothermics: International Journal of Geothermal Research and its Applications.

(parallel wall model; Bourbiaux et al. 1998). Note that all the fractures were assigned a constant conductivity value of 1000mD-m. It should be stressed that the conductivity (single fracture aperture) does not play a critical role as compared to the network properties such as fracture density and length above the percolation threshold (Jafari and Babadagli, 2009a). The only exception is very low density and short fracture networks, and even for this type of fracture system the single fracture conductivity and fracture network properties are of equal importance. Therefore the assumption of constant conductivity is justified. The last column in **Table 4.2** is the equivalent fracture network permeability calculated using the FRACA software.

Once the best correlation type, i.e., linear, logarithmic, exponential etc., between each input parameter (given in **Table 4.2**, columns 1 through 7) and the EFNP (**Table 4.2**, column 8) was determined, correlations (equations) with different numbers of the independent variables (inputs) were generated. In order to investigate the effect of the lithology, three different scenarios were considered that used: (1) all the available data points, (2) only fracture patterns in marble lithology, and (3) only fracture patterns in a specific reservoir with the same lithology (marble).

For all the three scenarios, the equations, given in **Table 4.3,** were applied. The constants in the correlations differ from scenario to scenario. In **Table 4.3**, R_n is the correlation coefficient for each scenario, n being the scenario number (n=1, 2, 3).

Jafari, A. and Babadagli, T.: "Effective Fracture Network Permeability of Geothermal Reservoirs," Geothermics: International Journal of Geothermal Research and its Applications.

Table 4.3 Equations for predicting EFNP with different numbers of independent variables and corresponding regression coefficients for three different scenarios (1: entire data set, 2: marbles only, 3: Field 1 only [see Table 4.1 for details]).

Independent Variables	Derived Equation	R_1	R_2	R_3
3	$Ln(K) = A.\exp(B.X_1)+C.Ln(X_2)+D.Ln(X_3)+E$	0.73	0.87	0.86
5	$Ln(K) = A.\exp(B.X_1)+C.Ln(X_2)+D.Ln(X_3)+E.Ln(X_4)+F.Ln(X_5)+G$	0.93	0.93	0.90
6	$Ln(K) = A.\exp(B.X_1)+C.Ln(X_2)+D.Ln(X_3)+E.Ln(X_4)+F.Ln(X_5)+G.Ln(X_6)+H$	0.93	0.94	1.0

In the first equation (**Table 4.3**), X1, X2 and X3 are the fractal dimensions of fracture intersection points, fractal dimensions of fracture lines and lacunarity, respectively. In the second equation, X1, X2, X3, X4 and X5 are the fractal dimensions of fracture intersection points, connectivity index, maximum number of intersection points between fracture lines and the imaginary scanning lines in X and Y directions, and fractal dimensions of fracture lines, respectively. Finally, in the third equation, X1, X2, X3, X4, X5 and X6 are the fractal dimensions of fracture intersection points, connectivity index, maximum number of intersection points between fracture lines and the imaginary scanning lines in X and Y directions, fractal dimensions of fracture lines, and lacunarity, respectively. In all these equations, A, B, C, D, E, F, G and H are constant coefficients, and *K* is the EFNP in the X direction in mD.

Jafari, A. and Babadagli, T.: "Effective Fracture Network Permeability of Geothermal Reservoirs," Geothermics: International Journal of Geothermal Research and its Applications.

4.5 Validation

To validate the derived correlations, a total of ten new fracture patterns were chosen from the same geothermal reservoirs in southwestern Turkey (but not used in the deriving the correlations) and two other sources (Odling 1992, Odling and Webman 1991) as tabulated in **Table 4.4**.

Table 4.4 Natural fracture patterns used for validation purposes.

Pattern	Reference
1	Babadagli, 2000 (Figure 4)
2	Babadagli, 2000 (Figure 3)
3	Babadagli, 2001 (Figure 4)
4	Babadagli, 2001 (Figure 2-o)
5	Babadagli, 2001 (Figure 2-n)
6	Babadagli, 2001 (Figure 3)
7	Babadagli, 2001 (Figure 2-p)
8	Odling, 1992a (Figure 1-a)
9	Odling and Webman, 1991 (Figure 2)
10	Odling and Webman, 1991 (Figure 7)

Using the correlations, and the fractal and statistical parameters of the latter fracture patterns, the EFNPs were obtained for each of the three scenarios. Then, the EFNPs were calculated using the FRACA, and the results are compared in **Figure 4.4**, **Figure 4.5** and **Figure 4.6**. In these figures, the FRACA permeability refers to a permeability value calculated by assuming that all the fractures have a constant conductivity (aperture) value. The calculation of EFNP using the proposed correlations was significantly faster than the computation with FRACA, which requires significant amount of computer time to perform a flow simulation and calculate the EFNP even for relatively simple fracture patterns.

Jafari, A. and Babadagli, T.: "Effective Fracture Network Permeability of Geothermal Reservoirs," Geothermics: International Journal of Geothermal Research and its Applications.

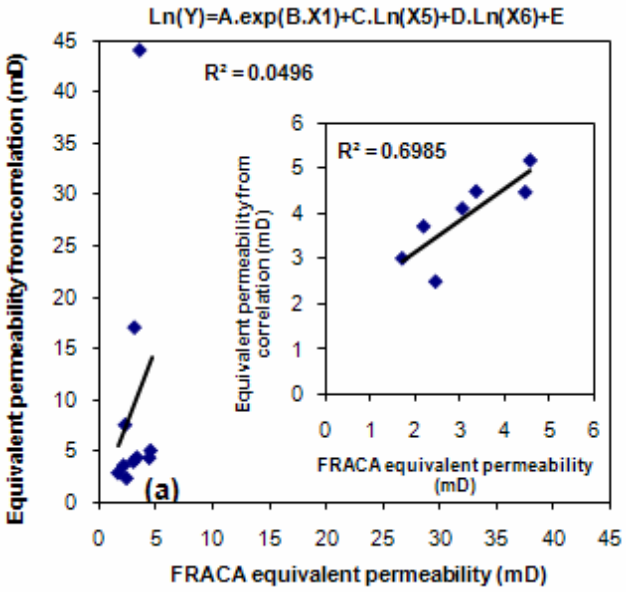

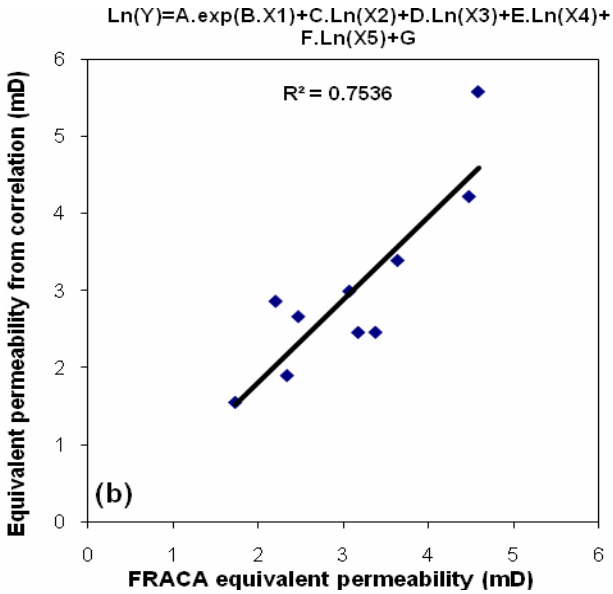

Jafari, A. and Babadagli, T.: "Effective Fracture Network Permeability of Geothermal Reservoirs," Geothermics: International Journal of Geothermal Research and its Applications.

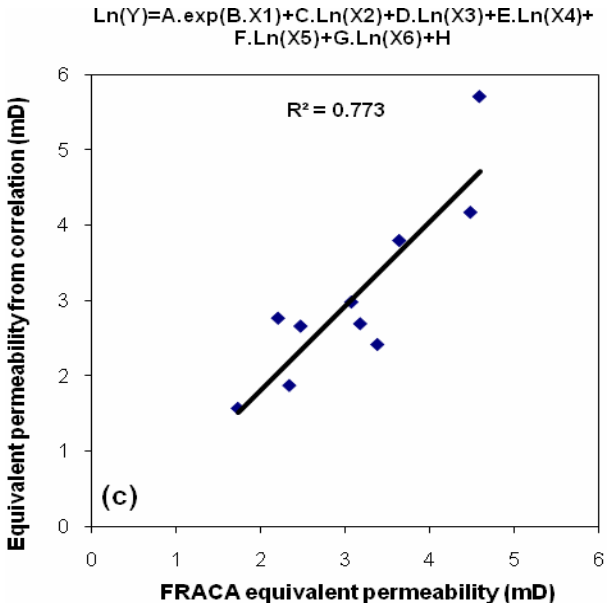

Figure 4.4(a, b and c) FRACA equivalent fracture network permeability values versus the predicted ones using correlations for all 22 fracture patterns. The graph given inside the plot in Figure 4.4a shows the correlation without the three patterns at mm (thin sections) and cm (rock pieces) scale (see Figure 4.7).

Jafari, A. and Babadagli, T.: "Effective Fracture Network Permeability of Geothermal Reservoirs," Geothermics: International Journal of Geothermal Research and its Applications.

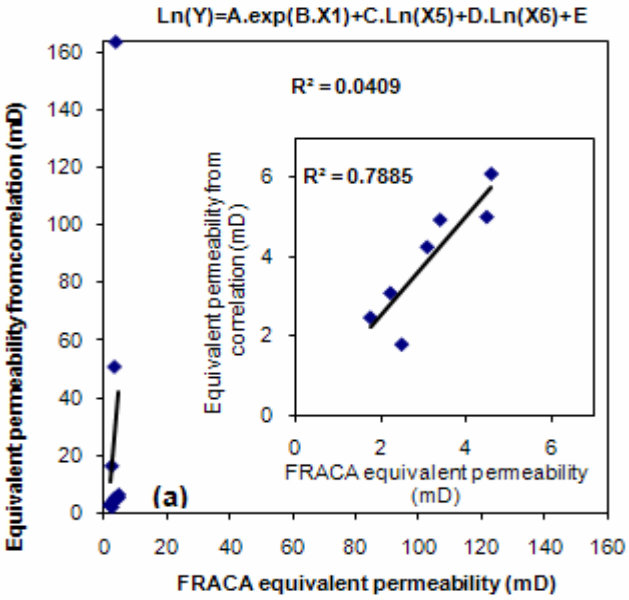

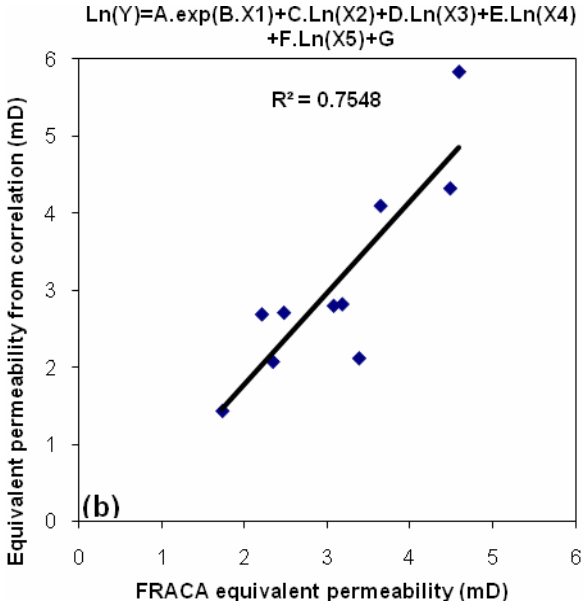

Jafari, A. and Babadagli, T.: "Effective Fracture Network Permeability of Geothermal Reservoirs," Geothermics: International Journal of Geothermal Research and its Applications.

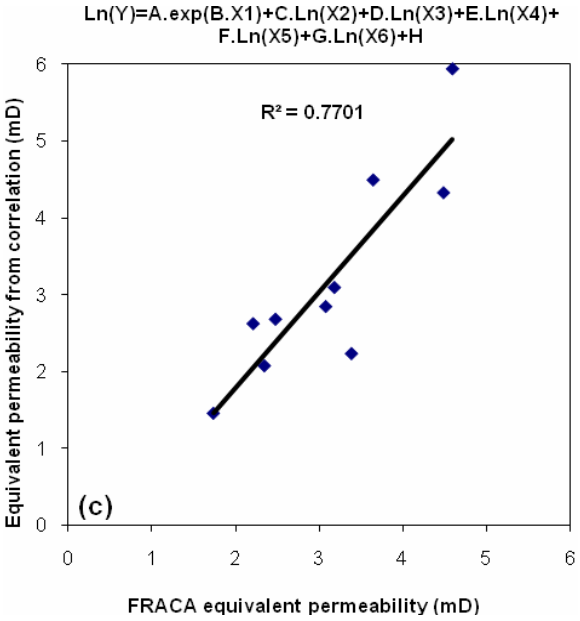

Figure 4.5(a, b and c) FRACA equivalent fracture network permeability values versus the predicted ones using correlations derived for only marble lithologies (first eleven data points in Table 4.1). The graph given inside the plot in Figure 4.5a shows the correlation without the three patterns at mm (thin sections) and cm (rock pieces) scale shown in Figure 4.7.

Jafari, A. and Babadagli, T.: "Effective Fracture Network Permeability of Geothermal Reservoirs," Geothermics: International Journal of Geothermal Research and its Applications.

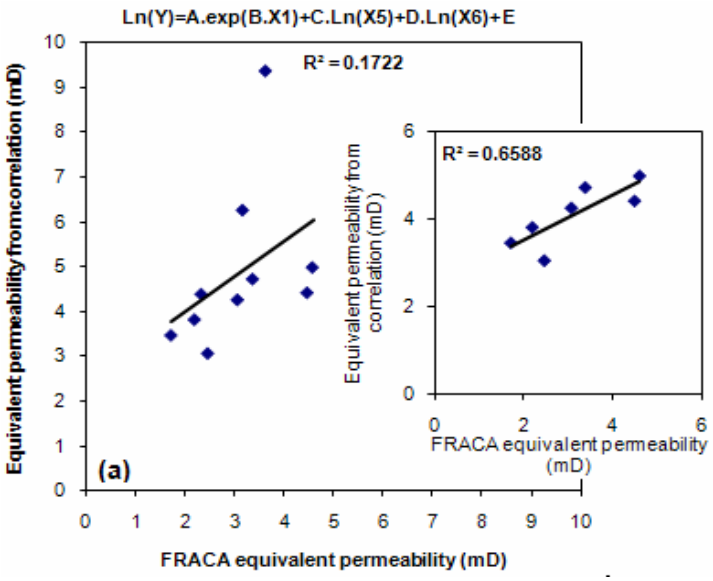

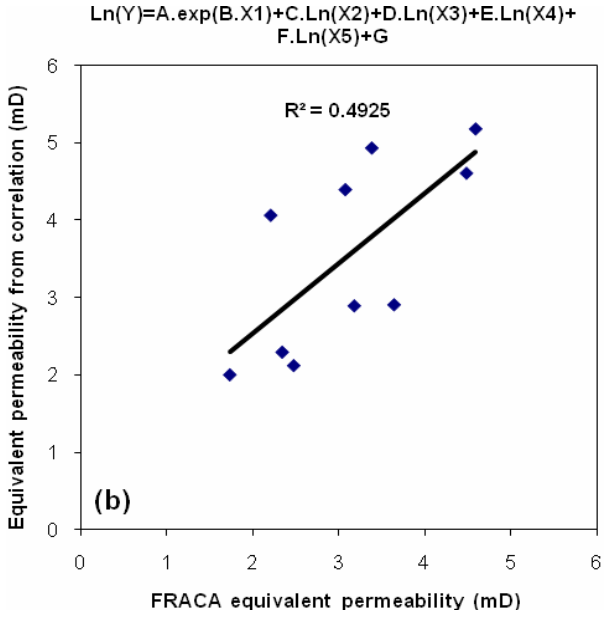

Jafari, A. and Babadagli, T.: "Effective Fracture Network Permeability of Geothermal Reservoirs," Geothermics: International Journal of Geothermal Research and its Applications.

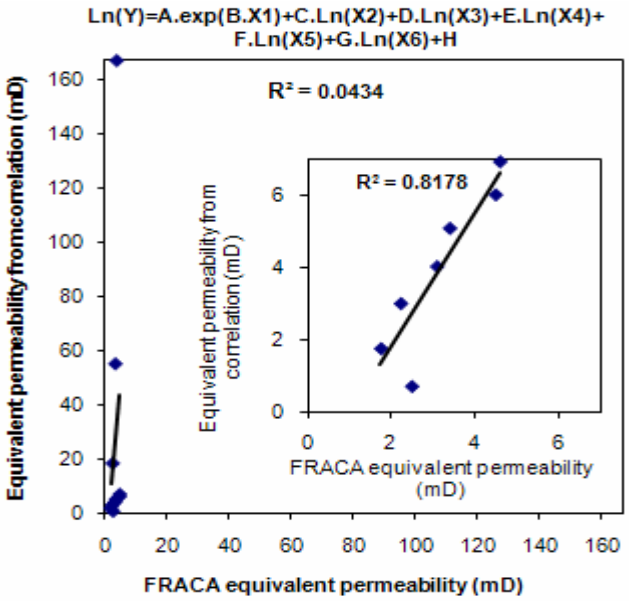

Figure 4.6(a, b and c) FRACA equivalent fracture network permeability values versus the predicted ones using correlations derived for only Field 1 (first nine data points in Table 4.1). The graphs given inside the plots in Figures 4.6a and 4.6c show the correlation without the three patterns at mm (thin sections) and cm (rock pieces) scale given in Figure 4.7.

Jafari, A. and Babadagli, T.: "Effective Fracture Network Permeability of Geothermal Reservoirs," Geothermics: International Journal of Geothermal Research and its Applications.

4.6 Analysis and discussion

Previously, we used synthetic patterns to generate correlations between the network properties and equivalent fracture network permeability (EFNP), and the correlations were validated using natural patterns (Jafari and Babadagli, 2008; 2010a). The present chapter utilizes natural fracture patterns that show topological differences from the commonly used synthetic random fracture networks. The synthetic patterns may not reflect certain network characteristics observed in natural patterns such as fracture connectivity and the presence of isolated and dead-end fractures. To overcome the limitations of synthetic patterns, only natural fracture patterns were used for the derivation and validation of the proposed correlations.

For the correlations with three independent variables, three patterns showed a large deviation from the correlation (**Figure 4.4a**, **Figure 4.5a** and **Figure 4.6a**). These are the patterns obtained at mm (Patterns - 1 and 3 obtained from thin sections shown in **Figure 4.7a** and **c**) and cm (Pattern 2 obtained from a rock piece shown in **Figure 4.7b**) scales (note that twenty two patterns obtained at mm, cm and meter scales were used at 100x100 m^2 box size in the correlation development exercise).

Jafari, A. and Babadagli, T.: "Effective Fracture Network Permeability of Geothermal Reservoirs," Geothermics: International Journal of Geothermal Research and its Applications.

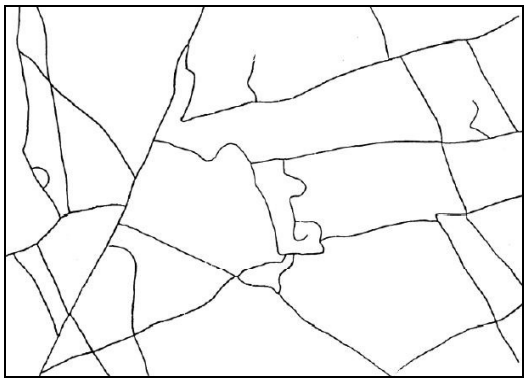

a. Pattern 1 1 mm

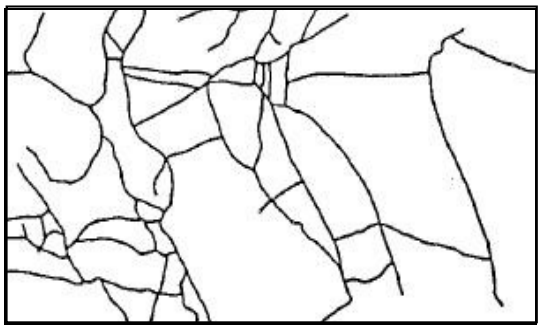

b. Pattern 2. 4 cm

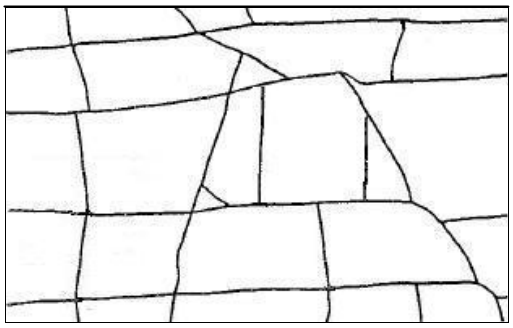

c. Pattern 3. 1mm

Jafari, A. and Babadagli, T.: "Effective Fracture Network Permeability of Geothermal Reservoirs," Geothermics: International Journal of Geothermal Research and its Applications.

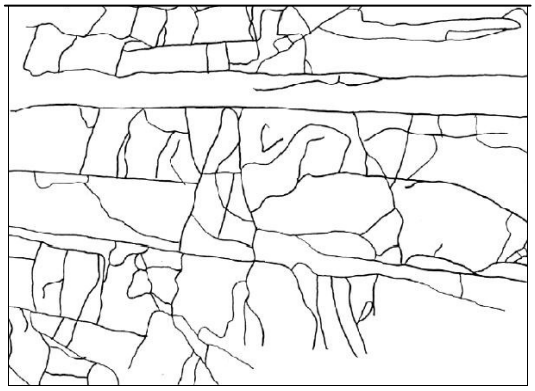

d. Pattern 4. 10 cm

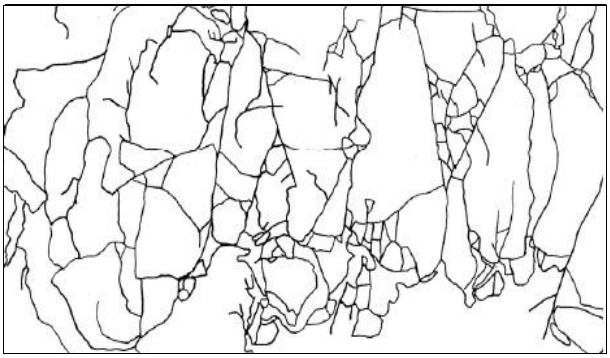

e. Pattern 5. 10 cm

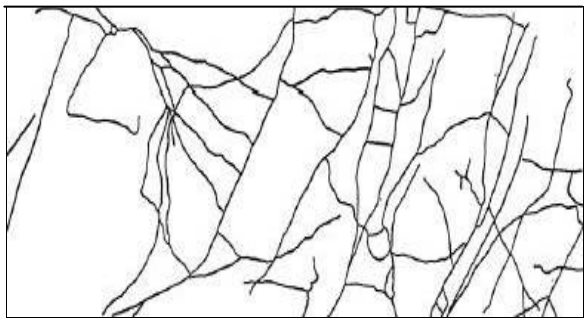

f. Pattern 6. 4 cm

Jafari, A. and Babadagli, T.: "Effective Fracture Network Permeability of Geothermal Reservoirs," Geothermics: International Journal of Geothermal Research and its Applications.

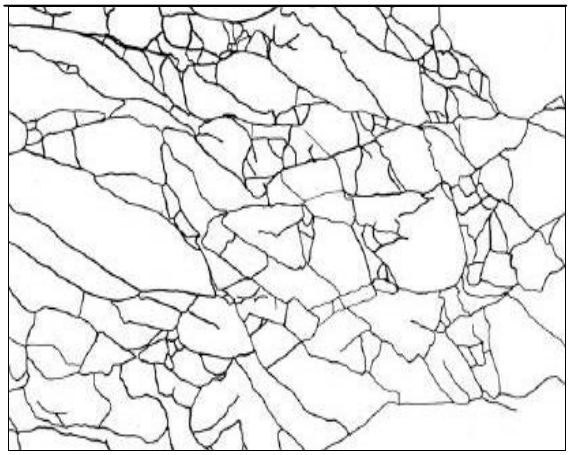

g. Pattern 7. 10 cm

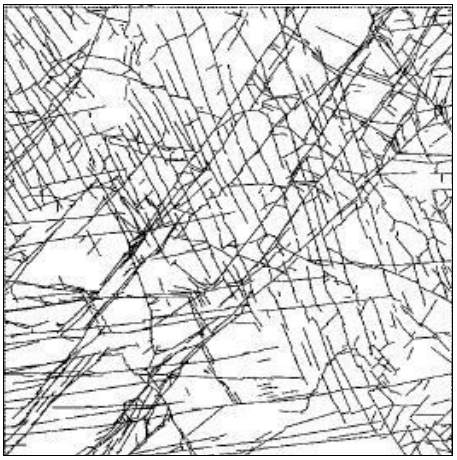

h. Pattern 8. 3 m

Jafari, A. and Babadagli, T.: "Effective Fracture Network Permeability of Geothermal Reservoirs," Geothermics: International Journal of Geothermal Research and its Applications.

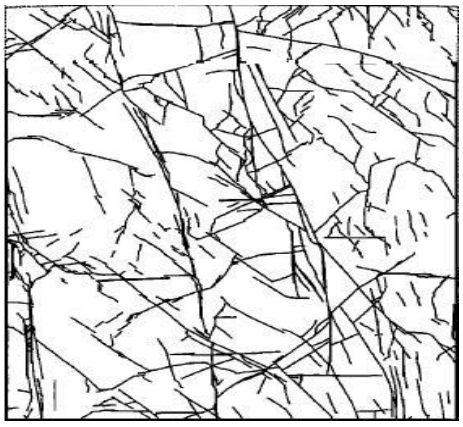

i. Pattern 9. 2 m

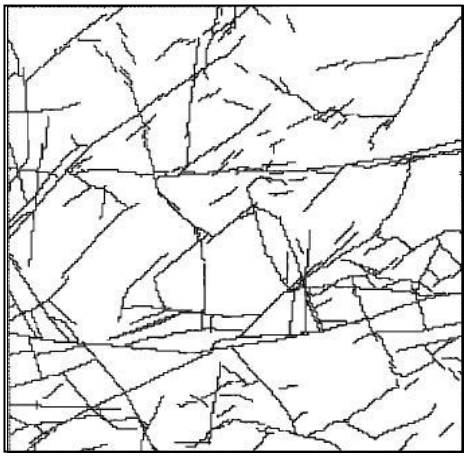

j. Pattern 10. 1.4 m

Figure 4.7(a, b, c, d, e, f, g, h, i and j) Fracture patterns used for validation of correlations.

Therefore, these three patterns represent relatively uniform characteristics of the network with a low fracture density. These types of characteristics are

Jafari, A. and Babadagli, T.: "Effective Fracture Network Permeability of Geothermal Reservoirs," Geothermics: International Journal of Geothermal Research and its Applications.

represented by the lowest fractal dimension of fracture intersection points, maximum intersection points between fracture lines and the imaginary scanning lines in X and Y directions and the fractal dimension of fracture lines. When these three patterns are excluded, much better correlations were observed even with only three independent variables. These plots are illustrated in **Figure 4.4a**, **Figure 4.5a** and **Figure 4.6a**. All the patterns shown in these figures are at meter scale similar to the ones displayed in **Figure 4.2** and represent more complex fracture patterns. The fracture patterns used in the validation process are given in **Figure 4.7**.

Regardless the type of the pattern and the scale, the five parameter correlation shows significant improvement as presented in **Figure 4.4b**, **Figure 4.5b** and **Figure 4.6b**. Addition of three new parameters and the exclusion of the lacunarity parameter results in a much better correlation for all types of patterns. The inclusion of lacunarity in the correlation is useful in reducing the number of other parameters if the fracture patterns show a complex structure, usually obtained at larger scales (meter-km).

Figure 4.4c, **Figure 4.5c** and **Figure 4.6c** show the results for six parameters. The first two cases (**Figure 4.4c** and **Figure 4.5c**) show a slight improvement when the lacunarity parameter is added to the 5-variable equation. The third case, however, presents significant deviations for the one small scale (mm-cm) pattern. In other words, the correlation developed for a single field did not yield a good agreement for a wide range of fracture network pattern types. The lacunarity parameter had a negative effect on the results as opposed to the other cases (the whole data and marble only scenarios) when only the patterns

Jafari, A. and Babadagli, T.: "Effective Fracture Network Permeability of Geothermal Reservoirs," Geothermics: International Journal of Geothermal Research and its Applications.

from a single field were considered. When the small scale patterns (Patterns 1, 2, and 3 in **Figure 4.7**) were excluded, the 6-variable case showed a remarkable improvement as can be observed through the comparison of **Figure 4.5b** and the small plot embedded inside the graph in **Figure 4.5c**.

For the third scenario (single field), the equation with a high correlation coefficient is the 5-variable equation. Generally speaking, the correlation coefficients for the third scenario are much smaller than those for the first two scenarios. The reason could be the different nature of the fracture patterns used for derivation and those employed for validation purposes. Only data from a particular location (Field 1) were used in deriving the correlations, and the resulting correlations were verified by using natural fracture patterns from different fields. The patterns from Field 1 were presumably exposed to the same tectonic history. Patterns used for validation, however, have different tectonic histories and represent different rock characteristics (**Table 4.3**). In other words, the fracture network topology, rock properties, and the tectonic history for Field 1 data set are different from the fracture patterns used in the validation process.

Above observations indicate that the 5-variable equation is the best correlation for predicting the EFNP regardless of the pattern complexity, type, and scale. The accuracy can be improved for complex patterns by the addition of lacunarity (6-variable equation in **Table 4.3**).

Jafari, A. and Babadagli, T.: "Effective Fracture Network Permeability of Geothermal Reservoirs," Geothermics: International Journal of Geothermal Research and its Applications.

4.7 Comparison of the results with numerical well test permeability values

In an attempt to demonstrate how 3-D data could be useful for the improvement of EFNP correlations, the numerical well test EFNP permeability was added to the correlations given in **Table 4.3**. Numerical pressure drawdown tests were performed on natural (Jafari and Babadagli, 2009b) and synthetic (Jafari and Babadagli, 2010b) fracture networks using FRACA software and observed that a single well test EFNP may not be sufficient to represent the nature of the fracture network. The previous chapter that used natural patterns (Jafari and Babadagli, 2009b) was applied in a single layer model with a single well, whereas the subsequent work (Jafari and Babadagli, 2010b) included non-uniform fracture network properties in the z-direction by forming the model with three different layers (assigning different fracture densities for each layer) with five wells.

Figure 4.8 presents a comparison of the EFNPs obtained through three different approaches:

(1) EFNPs (x-direction permeability, K_x) obtained from the FRACA software (2005) like the ones given in the last column of **Table 4.1**,

(2) EFNPs obtained from the pressure vs. time plot obtained from FRACA software (numerical drawdown test),

(3) EFNPs obtained from the correlations, which combines the equation with 5-independent values (given in **Table 4.3**) with the well test

Jafari, A. and Babadagli, T.: "Effective Fracture Network Permeability of Geothermal Reservoirs," Geothermics: International Journal of Geothermal Research and its Applications.

permeability obtained from the numerical well test exercise.

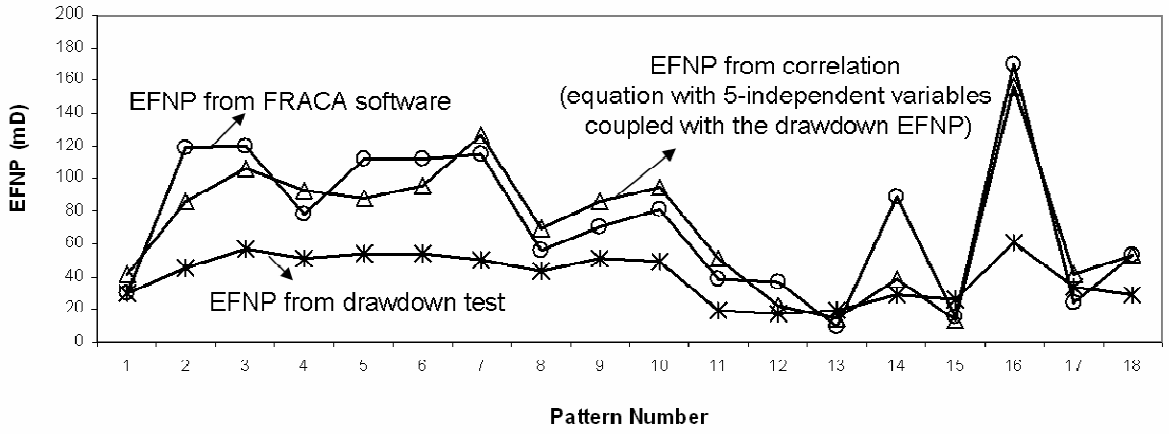

Figure 4.8 Comparison of the EFNP's obtained from three different approaches:
(1) EFNPs (x-direction permeability, K_x) obtained from the FRACA software (2005) like the ones given in the last column of Table 4.2,
(2) EFNPs obtained from the pressure vs. time plot obtained from FRACA software (numerical drawdown test),
(3) EFNPs obtained from the correlations, which combines the equation with 5-independent parameters (given in Table 4.3) with the welltest permeability obtained from the numerical well tests.

The cases include the ten validation patterns given in **Table 4.4** and eight additional patterns obtained from different parts of the outcrop regions of the fields shown in **Figure 4.1**. The EFNP from the numerical drawdown tests using the pressure vs. time data obtained from FRACA is considerably lower than the EFNP obtained directly from the FRACA. When an additional well test parameter is added to the correlation derived with 5-independent

Jafari, A. and Babadagli, T.: "Effective Fracture Network Permeability of Geothermal Reservoirs," Geothermics: International Journal of Geothermal Research and its Applications.

parameters (the second equation in **Table 4.3**), which makes it an equation with 6-independent variables (five 2-D fractal-statistical data and drawdown permeability), it yields a good agreement with the FRACA EFNPs. This exercise shows that well test EFNP does not adequately represent the entire network characteristics. This is mainly due to the fact that the well test derived permeability is dominated by major fracture networks and the drainage area and the location of the well. When we added 2-D fractal and statistical data to the well test permeability, the quality of the correlation is improved significantly as it considers not only 3-D well test permeability data but also fractures of any size (or scales) and all 2-D fracture network characteristics including density, length, orientation, and connectivity.

4.8 Comparison of the results with well test permeability values from the Kizildere geothermal field in Turkey

In a final attempt, the build-up measurements reported earlier (Arkan et al. 2002) for five wells (KD-6, KD-15, KD-16, KD-21 and KD-22) in the Kizildere geothermal field, Turkey, were selected to apply the derived equations in this work. The actual well test measurements in the literature were available only for this field and the comparative analysis was performed using this data. The locations of these wells are shown in **Figure 4.9**.

Jafari, A. and Babadagli, T.: "Effective Fracture Network Permeability of Geothermal Reservoirs," Geothermics: International Journal of Geothermal Research and its Applications.

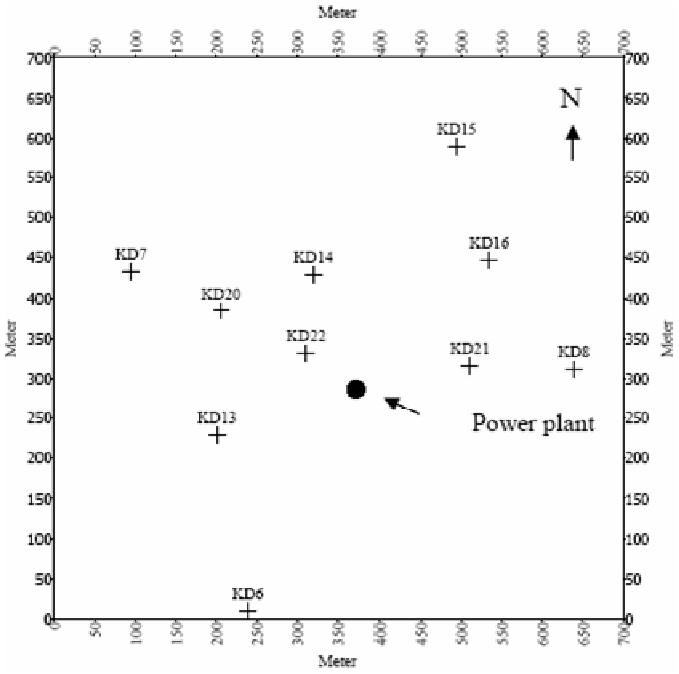

Figure 4.9 Location of the investigated wells (KD-6, KD-15, KD-16, KD-21 and KD-22) in the Kizildere geothermal field (Arkan et al. 2002).

The well tests were run and analyzed at different dates after mechanical reaming (DARMA), i.e. calcite cleaning. As Arkan et al (2002) concluded that the permeability generally decreases with days after mechanical reaming with some exceptions, we decided to use the well test permeability values for all five wells at the smallest DARMA, which has the least calcite deposition inside wellbore and, as a result, with minimal effects on the pressure behavior of the system. The well test data used in the comparison study are given in **Table 4.5**.

Jafari, A. and Babadagli, T.: "Effective Fracture Network Permeability of Geothermal Reservoirs," Geothermics: International Journal of Geothermal Research and its Applications.

Table 4.5 Well test permeability for five wells in the Kizildere geothermal field, Turkey (Arkan et al. 2002).

Well No.	Permeability, mD
KD-6	38.9
KD-15	126
KD-16	376
KD-21	173
KD-22	19.5

For this purpose, five 2-D outcrop fracture pattern images representing the producing formations were chosen. Each image was collected from different outcrop locations and they were illustrated in **Figure 4.10.**

a)

b)

c)

Jafari, A. and Babadagli, T.: "Effective Fracture Network Permeability of Geothermal Reservoirs," Geothermics: International Journal of Geothermal Research and its Applications.

d)

e)

Figure 4.10(a, b, c and e) Fracture outcrops from the Kizildere field used to test the equations given in Table 4.3 against the original well test results given in Table 4.5.

Jafari, A. and Babadagli, T.: "Effective Fracture Network Permeability of Geothermal Reservoirs," Geothermics: International Journal of Geothermal Research and its Applications.

Next, their permeability values were calculated using FRACA software and also through three derived equations given in **Table 4.3** based on three different scenarios: (1) all the available data points given in **Table 4.1**, (2) only fracture patterns in marble lithology, and (3) only fracture patterns in a specific reservoir with the same lithology (marble). The results were presented in the form of bar charts to compare the well test permeability values from five wells with computational ones (**Figure 4.11**, **Figure 4.12** and **Figure 4.13**).

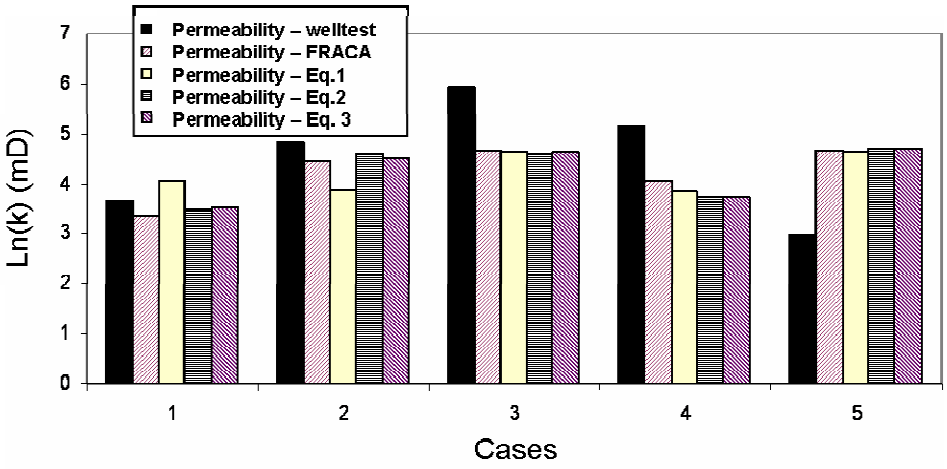

Figure 4.11 Comparison of the well test permeability values of the five wells (Cases 1 to 5: KD-6, KD-15, KD-16, KD-21 and KD-22 respectively) given in Table 4.5 with the predicted values obtained from the FRACA software as well as three derived equations (given in Table 4.3) for the first scenario.

Jafari, A. and Babadagli, T.: "Effective Fracture Network Permeability of Geothermal Reservoirs," Geothermics: International Journal of Geothermal Research and its Applications.

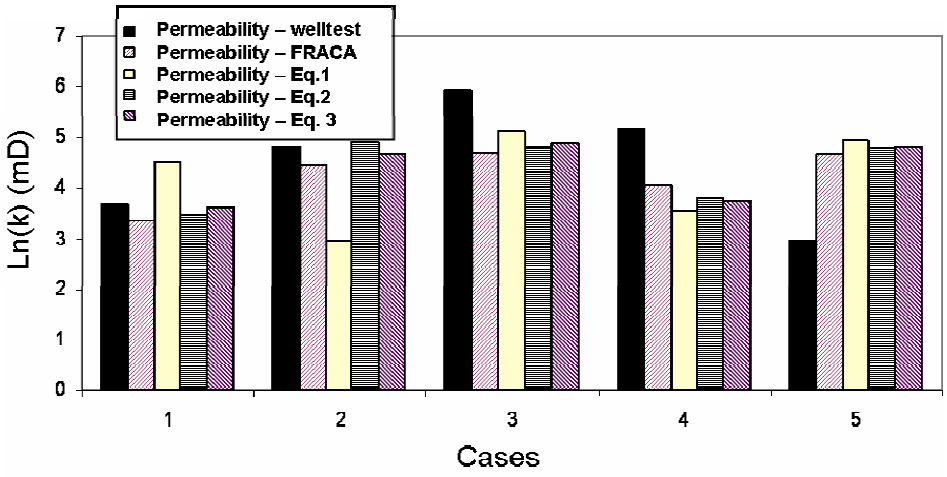

Figure 4.12 Comparison of the well test permeability values of the five wells (Cases 1 to 5: KD-6, KD-15, KD-16, KD-21 and KD-22 respectively) given in Table 4.5 with the predicted values obtained from the FRACA software as well as three derived equations (given in Table 4.3) for the second scenario.

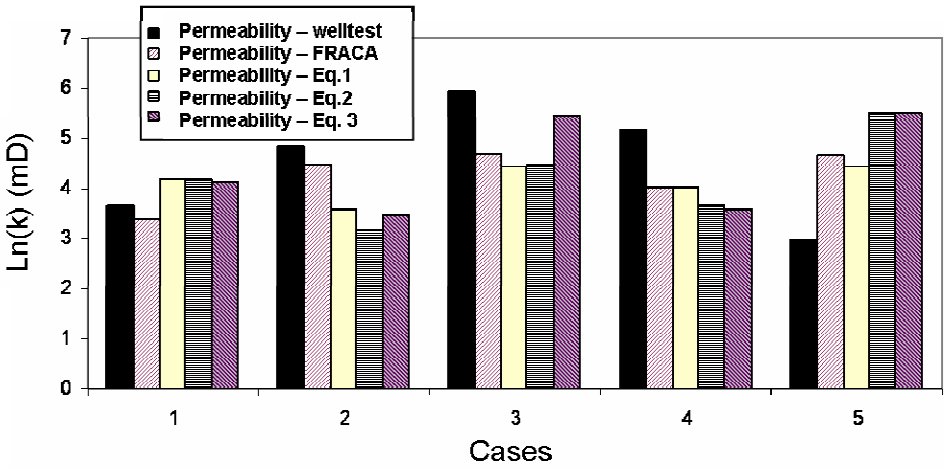

Figure 4.13 Comparison of the well test permeability values of the five wells (Cases 1 to 5: KD-6, KD-15, KD-16, KD-21 and KD-22 respectively) given in Table 4.5 with the predicted values obtained from the FRACA software as well as three derived equations (given in Table 4.3) for the third scenario.

Jafari, A. and Babadagli, T.: "Effective Fracture Network Permeability of Geothermal Reservoirs," Geothermics: International Journal of Geothermal Research and its Applications.

The following conclusions can be withdrawn from this exercise:

(1) Out of three scenarios of five cases, the best agreement between the four computational permeability values (three equations in **Table 4.3** and FRACA software) and actual well tests were obtained for the pattern given in **Figure 4.10a** (the first case in **Figure 4.11**) and scenario-1 (the equations generated using all data). This image was obtained from an outcrop area just by the field and represents the upper portion (limestone) of the two-layer producing formation in the reservoir (the bottom one is marble-quartzite –see Figure 3 of Onur et al. (2003) for the cross sectional map of the reservoir).

(2) The other scenarios (2 and 3 given in **Figure 4.12** and **Figure 4.13** respectively) also yielded a good agreement for the same image (case #1). The only exception is **Eq. 1** for the second scenario (**Figure 4.11**). This indicates that at least five-variable equation should be selected.

(3) The reasons why a good agreement was obtained for the third scenario (**Figure 4.13**) for this case (case #1), could be attributed to the nature of the fractures. The images used to derive equations in this scenario belong to a different the Omerbeyli-Germencik field and it is marble. However, these -marble- outcrop images represent a vertical fracture dominated systems (two examples are shown in **Figure 4.2c** and **d**), which are similar to the image we used in the comparison study (**Figure 4.10a**). Also, note that the bottom reservoir of the Kizildere is a marble-quartize system, which might show a similar fracture structure to that of the Omerbeyli-Germencik field, and it also affect the well test

Jafari, A. and Babadagli, T.: "Effective Fracture Network Permeability of Geothermal Reservoirs," Geothermics: International Journal of Geothermal Research and its Applications.

measurement along with the upper -limestone- formation.

(4) Another image that showed a good agreement was from the same outcrop area and lithology but different fracture configuration (**Figure 4.10b**). This case yielded a good agreement for scenarios 1 (**Figure 4.11**, case 2) and 2 (**Figure 4.12**, case 2) except **Eq. 1** for scenario 2 (equations developed using only the marble cases). Interestingly, scenario 3 gave a disagreement for case 2 for all equations. This can be attributed to the reasons explained in item (3) above. Note that the pattern in **Figure 4.10b** shows a fracture set predominantly oriented in horizontal direction unlike the pattern in **Figure 4.10a**.

Other three cases (cases 3, 4, and 5 that represent the patterns in **Figure 4.10c**, **d**, and **e**, respectively) did not show a good agreement for any scenario and image, and any method (FRACA and three derived equation given in **Table 4.3**). These images also represent a limestone lithology but were obtained from outcrop locations far from the field. Also, the fracture topology in these three patterns are remarkably different from the patterns shown in **Figure 4.10a** and **b**. No specific orientations of fractures are observed in **Figure 4.10c**, **d**, and **e** unlike the other two patterns. There is one set of fractures oriented in a specific direction in cases 1 and 2 (**Figure 4.10a** and **b**) containing almost parallel fractures and spanning two opposite sides of the patterns. However, in the other patterns (**Figure 4.10c**, **d**, and **e**), most fractures are like a disc (or circle) shape (**Figure 4.10c** and **d**) and have a high box-counting fractal dimension. It is obvious that this kind of

Jafari, A. and Babadagli, T.: "Effective Fracture Network Permeability of Geothermal Reservoirs," Geothermics: International Journal of Geothermal Research and its Applications.

fracture system has less tendency to span the entire system and, as a result, gives lower permeability. In fact, the computational permeability values for cases 3 and 4 were substantially lower than the actual one in all three scenarios. Other factors like weathering can be distinguished and could be a reason of inconsistent results with the actual well test data. The image in **Figure 4.10e** (case 5) is a good example of this situation.

(5) As a final point, one should mention that the field produces from two different reservoirs as explained in item (1) above. The lower reservoir is marble-quartzite and show a similar fracture patterns to the one in **Figure 4.10a**, which is vertical fracture dominated. Therefore, this particular pattern was able to represent the fracture pattern characteristics of both producing formations.

In conclusion, this exercise showed the applicability of the approach we proposed to estimate fracture network permeability values in geothermal reservoirs. It is important to distinguish appropriate fracture outcrop patterns that represent the actual fracture topology in the producing formations. Available geological, petrophysical, and even production data can be used at least to have a basic idea about fracture orientation, type density and topology in the selection of outcrop images as representative of the reservoir. Once the fracture outcrop patterns are selected, the equations generated in this chapter with five, or more variables, can be applied to estimate fracture network permeability values.

Jafari, A. and Babadagli, T.: "Effective Fracture Network Permeability of Geothermal Reservoirs," Geothermics: International Journal of Geothermal Research and its Applications.

4.9 Conclusions

1. Correlations for predicting equivalent fracture network permeability (EFNP) are developed using natural fracture patterns for both correlation development and validation. It is shown that the equation with only five independent variables is the best one for predicting equivalent fracture network permeability. In this equation, the independent variables are (1) the fractal dimension of fracture intersection points, (2) the connectivity index, (3) maximum intersection points between fracture lines and the imaginary scanning lines in X and (4) Y directions, and (5) the fractal dimension of fracture lines. Although increasing the number of the independent variables to six by including lacunarity improved the correlation slightly, the effort required to characterize another parameter and include it in the correlation is not justified.

2. The accuracy of predicted permeability mostly depends on the type of data that are used for the derivation of correlations. In other words, the fracture patterns being used for deriving a correlation must be similar to those present in the reservoir for which a production of EFNP is being made.

3. The results of our work also indicate that the addition of lacunarity is useful in reducing the number of other parameters if the fracture patterns show complex structure, usually obtained at larger scales (meter-km).

Jafari, A. and Babadagli, T.: "Effective Fracture Network Permeability of Geothermal Reservoirs," Geothermics: International Journal of Geothermal Research and its Applications.

4. The EFNPs obtained from numerical well (drawdown) tests did not match with the FRACA EFNPs. But, when the well test permeability is added to the equation with five independent variables (2-D fractal and statistical properties) given in **Table 4.2**, the quality of match with the FRACA EFNP's improved remarkably.

5. The three equations derived to estimate the EFNPs of geothermal reservoirs were also tested against the actual well test. This exercise showed the applicability of the approach we proposed to estimate fracture network permeability values in geothermal reservoirs. It was observed that it is important to distinguish appropriate fracture outcrop patterns that represent the actual fracture topology in the producing formations. Available geological, petrophysical, and even production data can be used at least to have a basic idea about fracture orientation, type density and topology. Once the fracture outcrop patterns are selected, the equations generated in this chapter with five, or more variables, can be applied to estimate fracture network permeability values.

Jafari, A. and Babadagli, T.: "Effective Fracture Network Permeability of Geothermal Reservoirs," Geothermics: International Journal of Geothermal Research and its Applications.

5 Incorporation of 1-D, 2-D and 3-D Data to Estimate Fracture Permeability

5.1 Overview

Well log and core information, seismic surveys, outcrop studies, and pressure transient tests are usually insufficient to generate representative 3-D fracture network maps individually. Any combination of these sources of data could potentially be used for accurate preparation of static models.

In the previous chapters, it was shown that there exists a strong correlation between the statistical and fractal parameters of 2-D fracture networks and their permeability. This chapter extends this work to fracture network permeability estimation using the statistical and fractal properties data conditioned to welltest information. For this purpose, 3-D fracture models of nineteen natural fracture patterns with all known fracture network parameters were generated initially. It is assumed that 2-D fracture traces on the top of these models and also 1-D data from imaginary wells which penetrated the whole thickness of the cubic models were available, as well as pressure

A version of this chapter has been accepted for publication

Jafari, A. and Babadagli, T.: "Generating 3-D Permeability Map of Fracture Networks Using Well, Outcrop and Pressure Transient Data," SPE 124077, SPE Resrvoir Evaluation and Engineering Journal.

transient tests. Next, the permeability of each 3-D fracture network model was measured and then used for drawdown well test simulations.

Finally, an extensive multivariable regression analysis using the statistical and fractal properties and welltest permeability as independent variables was performed to obtain a correlation for equivalent fracture network permeability.

5.2 Preparation of data for equivalent fracture network permeability (EFNP) correlation

This process consists of several steps. First, natural fracture network patterns from different sources representing different fracture network characteristics were selected. After measuring different statistical and fractal properties and obtaining well test permeability values by performing numerical well testing on the models generated from these patterns, a correlation between these properties and equivalent fracture network permeability was derived using multivariable regression analysis.

5.2.1 Fracture network patterns used

Nineteen different 2-D natural fracture patterns were selected in the correlation development process. Nine of them were taken from different sources in the literature which are shown in **Figure 5.1**.

Jafari, A. and Babadagli, T.: "Generating 3-D Permeability Map of Fracture Networks Using Well, Outcrop and Pressure Transient Data," SPE 124077, SPE Reservoir Evaluation and Engineering Journal.

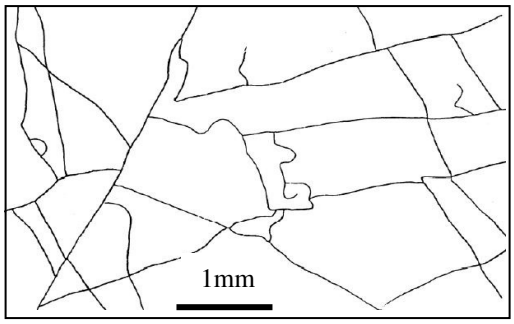

a (Figure 4 of Babadagli 2000).

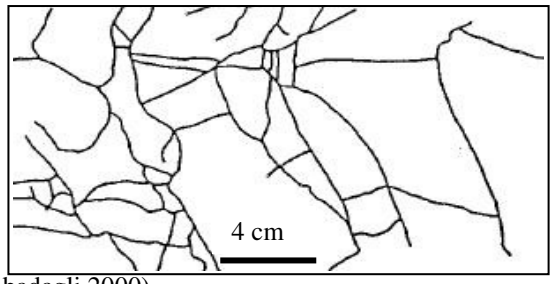

b (Figure 3 of Babadagli 2000).

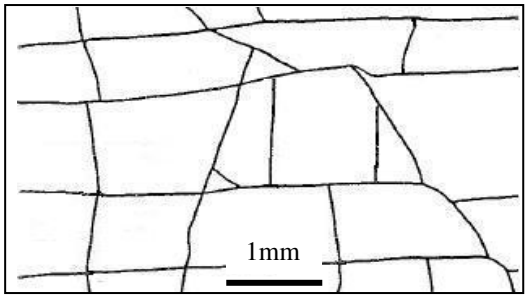

c (Figure 4 of Babadagli 2001).

Jafari, A. and Babadagli, T.: "Generating 3-D Permeability Map of Fracture Networks Using Well, Outcrop and Pressure Transient Data," SPE 124077, SPE Reservoir Evaluation and Engineering Journal.

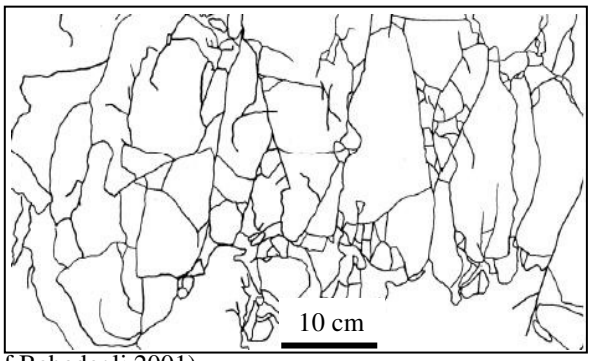

d (Figure 2n of Babadagli 2001).

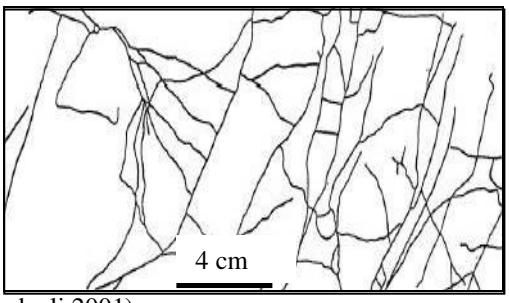

e (Figure 3 of Babadagli 2001).

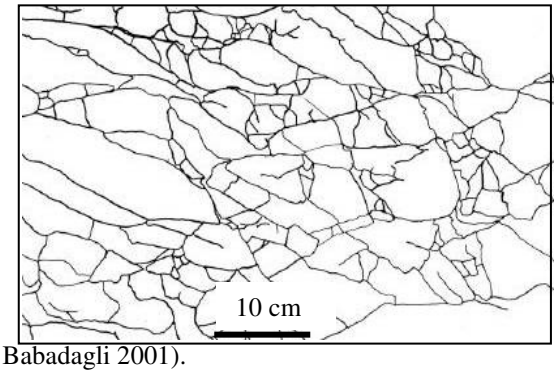

f (Figure 2p of Babadagli 2001).

Jafari, A. and Babadagli, T.: "Generating 3-D Permeability Map of Fracture Networks Using Well, Outcrop and Pressure Transient Data," SPE 124077, SPE Reservoir Evaluation and Engineering Journal.

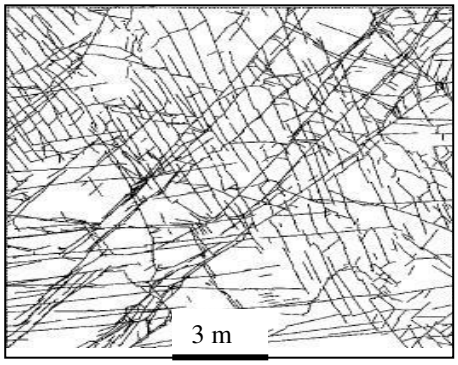

g (Figure 1a of Odling 1992 A).

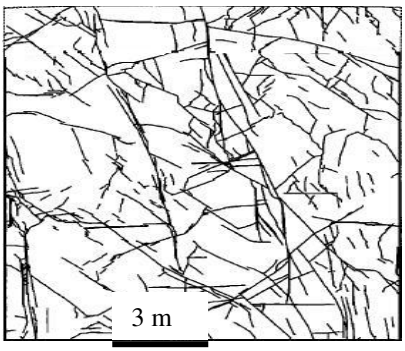

h (Figure 2 of Odling and Webman 1991).

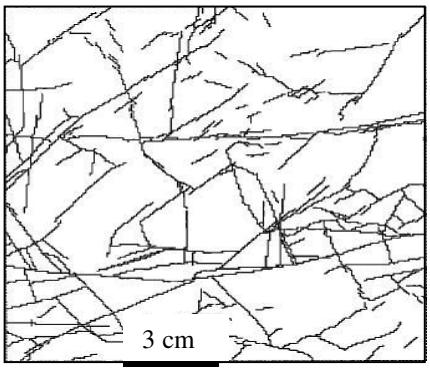

i (Figure 7 of Odling and Webman 1991).

Figure 5.1(a, b, c, d, e, f, g, h and i) Some of the natural fracture patterns and their sources used for derivation of the correlations.

Jafari, A. and Babadagli, T.: "Generating 3-D Permeability Map of Fracture Networks Using Well, Outcrop and Pressure Transient Data," SPE 124077, SPE Reservoir Evaluation and Engineering Journal.

The other ten patterns were collected from the outcrops of the producing formations of different geothermal fields in western Turkey. Although these nineteen patterns had different size scales, for the sake of consistency and based on the modeling approach adapted in the previous chapter (Jafari and Babadagli, 2008), the patterns were digitized in a cartesian coordinate with 100x100 m^2 square domain.

5.2.2 Measurement of statistical and fractal characteristics of the patterns

In order to describe complex geometries in the nature quantitatively, fractal geometry can be used (Mandelbrot, 1982). Fractal objects under different scales seem self-similar and have their own dimension which is a non-integer number and is known as the fractal dimension (Addison, 1997). It is proven by several researchers that natural fracture patterns show fractal characteristics (Barton and Larsen, 1985; La Pointe, 1988; Barton and Hseih, 1989) and fractal geometry is able to quantify the spatial distribution of these 2-D networks.

After digitizing the fracture patterns, they were exported and reconstructed in the MATLAB software's environment. Then, their statistical and fractal properties were measured applying different techniques.

First, the box counting technique was used to measure the fractal dimension of different fracture network properties including fracture intersection points, fracture mid points and fracture lines. The fractal dimension was obtained by

Jafari, A. and Babadagli, T.: "Generating 3-D Permeability Map of Fracture Networks Using Well, Outcrop and Pressure Transient Data," SPE 124077, SPE Reservoir Evaluation and Engineering Journal.

overlaying a set of different box sizes on the fracture network and counting the number of boxes contained different fracture features (fracture intersection points, fracture lines, etc) for each box size, and the plotting these numbers against the box sizes on a log-log scale. The slope of the straight line yields the fractal dimension of that specific feature of the fracture network (Barton and Larsen, 1985) according to the following relationship:

$$N(r) \alpha r^{-D} \qquad \textbf{(1)}$$

where $N(r)$ is the number of the boxes contained different fracture features and r is the box sizes and D is the fractal dimension. In the developed algorithm for this chapter, the box counting fractal dimension of fractures intersection points and fracture lines was measured.

Other different fracture network characteristics were quantified applying different statistical and fractal techniques. To consider the orientation effect, a square was overlaid on the fracture domain in such a way it covered the whole domain. Then, a set of imaginary scanning lines inside the square in X and Y directions were defined and the number of touches (intersections) between these scanning lines and fracture lines were counted. The effects of fracture orientation on the EFNP were taken into account through this method. To consider the intersection and connectivity of fractures in the domain, a new parameter called the connectivity index was defined as the total number of intersection point divided by total number of fracture lines. Four different fractal and statistical parameters were observed to show the strongest correlation to the EFNP (Jafari and Babadagli, 2008). The results of the

Jafari, A. and Babadagli, T.: "Generating 3-D Permeability Map of Fracture Networks Using Well, Outcrop and Pressure Transient Data," SPE 124077, SPE Reservoir Evaluation and Engineering Journal.

measurements of these parameters for nineteen natural fracture patterns are tabulated in **Table 5.1**. In this table, columns # 2 and 6 are fractal and # 3, 4 and 5 are statistical parameters. All the fractal dimensions in the tables lie between 1 and 2 which shows their fractal nature. The readers are referred to our previous publication for further details on the above listed fractal characteristics (Jafari and Babadagli, 2008).

Table 5.1 Different fractal and statistical characteristics and well test permeability values of the natural fracture patterns used in the derivation of the EFNP correlation. All cases have a constant single fracture conductivity value of 1000 mD.m.

Pattern	FD (Box-Counting) Intersection Point	Connectivity Index	Max Touch with X Scanning Line	Max Touch with Y Scanning Line	FD (Box-Counting) Lines	Welltest Permeability, mD	Kx, mD
1	1.867	1.064	15608	21143	1.557	34.289	28.801
2	1.820	1.704	15396	17481	1.521	46.252	85.936
3	1.892	1.516	19585	24571	1.598	54.276	108.988
4	1.750	1.407	13331	15887	1.443	48.682	56.751
5	1.774	1.465	15486	16721	1.487	41.501	43.032
6	1.870	1.422	18933	24001	1.576	52.291	104.354
7	1.872	1.275	15916	31323	1.630	39.673	106.506
8	1.800	1.271	13364	16592	1.528	42.223	49.509
9	1.769	1.745	16978	17563	1.567	48.857	66.102
10	1.770	1.496	14366	18920	1.562	48.498	70.835
11	1.298	1.500	489	317	1.270	31.532	23.991
12	1.347	1.100	759	763	1.369	19.762	10.387
13	0.797	1.091	114	266	1.264	34.483	38.106
14	1.660	1.149	4071	3094	1.493	8.303	5.649
15	1.378	1.020	860	1210	1.481	24.775	88.345
16	1.577	1.041	4697	2680	1.513	18.978	9.085
17	1.893	2.611	4767	5473	1.682	42.942	98.342
18	1.647	1.369	1687	1758	1.583	27.520	21.625
19	1.653	1.558	996	1281	1.515	12.836	29.411

FD: Fractal dimension

K_x : Equivalent Fracture Network Permeability obtained from the software (FRACA).

Jafari, A. and Babadagli, T.: "Generating 3-D Permeability Map of Fracture Networks Using Well, Outcrop and Pressure Transient Data," SPE 124077, SPE Reservoir Evaluation and Engineering Journal.

Next, they were exported to a commercial software package (FRACA) to measure their equivalent fracture network permeability (EFNP). Two assumptions were made in the measurement of the EFNP: (1) all fracture reservoirs consisted of only one layer, and (2) all fractures were entirely vertical.

Permeability is a vector quantity because its magnitude is dependent on the measurement direction (Nelson, 2001). For this chapter, conductivity instead of aperture was used for measuring permeability (Jafari and Babadagli, 2008). The conductivity is the product of the intrinsic fracture permeability and the fracture aperture (e) with parallel walls. The intrinsic fracture permeability and conductivity according to Poiseuille' law are expressed as $\frac{e^2}{12}$ and $\frac{e^3}{12}$ respectively (Bourbiaux et al., 1998).

In the FRACA package, first we imported the 2D fracture trace maps and a model with the above assumptions was built. The fracture network is discretized with a rectangular grid and then by applying a pressure varying linear boundary condition for each direction, mass balance equations are solved. Finally to derive the EFNP, flow rates across the block faces are computed (FRACA user manual). During this process, a constant fracture conductivity value (1000 mD.m) was entered for each single fracture for all patterns. We had showed in the previous chapter (SPE 113618 and SPEREE June 2009) that the conductivity does not play a critical role compared to the network properties such as fracture density and length (these two parameters are critical in order to be above the percolation threshold). The only exception

Jafari, A. and Babadagli, T.: "Generating 3-D Permeability Map of Fracture Networks Using Well, Outcrop and Pressure Transient Data," SPE 124077, SPE Reservoir Evaluation and Engineering Journal.

was low density and short fracture networks (however above the percolation threshold) and even this type of fracture system showed equivalent importance of the single fracture conductivity and fracture network properties (density and length).

5.2.3 Numerical well test simulations on the patterns

First, a 1x1x1 simulation grid cell with 100 m block size in X and Y and 10 m in Z directions (single-layer) for each fracture network pattern was defined in FRACA software and each fracture pattern was embedded in this model. Then, their equivalent fracture network permeability (EFNP) values were determined. In the next step, a 10x10x1 single porosity simulation grid cell with 1000 ft grid block size in the X and Y and 20 ft in the Z directions in a black oil simulator (ECLIPSE 100) was defined. Next, the EFNP for each fracture pattern exported from the FRACA software was placed in and repeated in all grid blocks. In other words, each grid contained the same EFNP of that fracture pattern). This was needed to be done to obtain a meaningful pressure transient period to measure the slope and the permeability. Then, one producer was placed in the middle of the model and the flow simulator was run. The reservoir PVT data of this model was taken from Odeh (1981). The principle components of EFNP matrix of each fracture pattern were used as directional permeability values in this black oil model and a drawdown test was run to obtain an average well test permeability using the pressure time relationship (**Figure 5.2**).

Jafari, A. and Babadagli, T.: "Generating 3-D Permeability Map of Fracture Networks Using Well, Outcrop and Pressure Transient Data," SPE 124077, SPE Reservoir Evaluation and Engineering Journal.

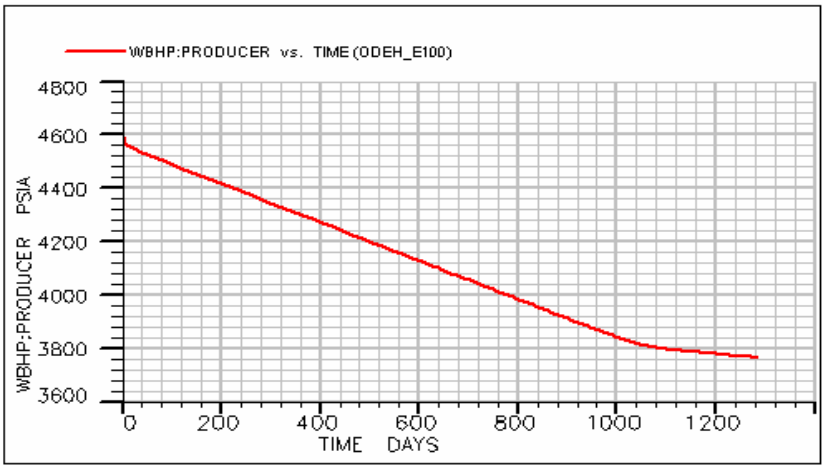

Figure 5.2 Pressure drawdown curve for the model with 10x10x1 gird cells in x, y and z direction respectively.

Then, the average permeability of the model using this pressure curve was calculated for each one. In the middle-time region (MTR) of a drawdown test, that represent the radial flow regime, a plot of P_{wf} vs. *log(t)* is a linear curve and using its slope, the reservoir permeability was calculated (Lee, 1982).

The results of well test permeability values for all patterns are given in **Table 5.1**. Only one of the principle components of the equivalent permeability tensor (K_x), of each 2D fracture pattern was considered throughout the chapter.

Jafari, A. and Babadagli, T.: "Generating 3-D Permeability Map of Fracture Networks Using Well, Outcrop and Pressure Transient Data," SPE 124077, SPE Reservoir Evaluation and Engineering Journal.

5.3 Analysis of the results and observations

In **Figure 5.2**, due to small size of the reservoir, an abrupt pressure drop can be seen. The actual Kx/Ky obtained using FRACA was plotted in **Figure 5.3**.

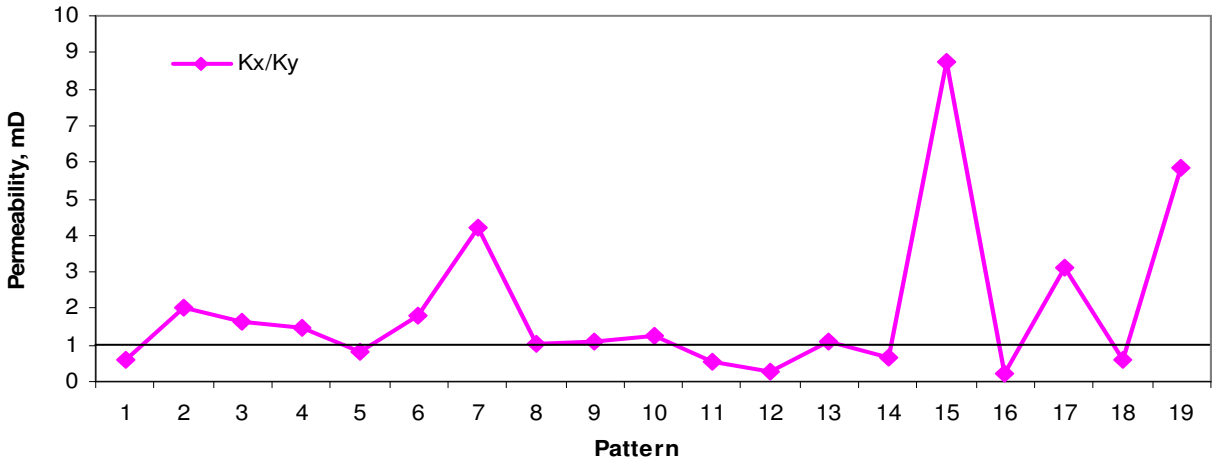

Figure 5.3 Actual Kx/Ky obtained using Fraca. Homogeneity line (Kx/Ky=1) is shown on the graph.

More increase in this parameter (Kx/Ky) means more permeability anisotropy in the x-y plane. Obviously, there is a huge difference between these two directional permeability values for pattern # 15 due to the fact that most of the fractures in this pattern are oriented in the x-direction. Mean permeability values (sqrt (Kx*Ky)) for all fracture patterns are plotted against welltest permeability (all values in mD) in **Figure 5.4**.

Jafari, A. and Babadagli, T.: "Generating 3-D Permeability Map of Fracture Networks Using Well, Outcrop and Pressure Transient Data," SPE 124077, SPE Reservoir Evaluation and Engineering Journal.

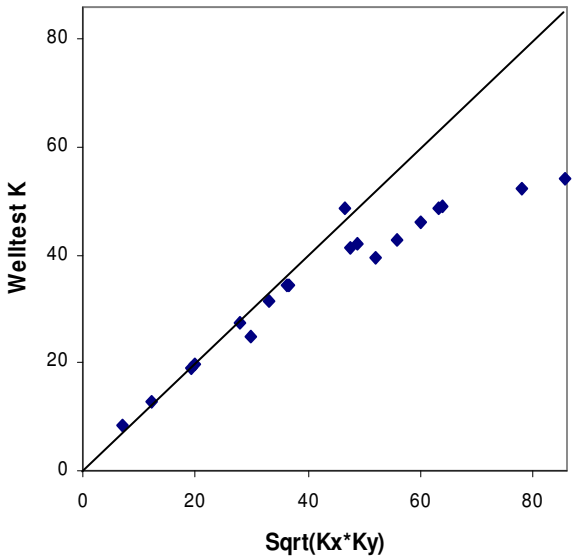

Figure 5.4 Sqrt(Kx*Ky) versus welltest average permeability.

A good correlation exists between these two variables; however at higher permeability values, there are some deviations from the main trend. **Figure 5.5** and **Figure 5.6** compare the welltest permeability values obtained from ECLIPSE simulations with the actual EFNP values obtained from the FRACA permeability for the X and Y directions, respectively.

Jafari, A. and Babadagli, T.: "Generating 3-D Permeability Map of Fracture Networks Using Well, Outcrop and Pressure Transient Data," SPE 124077, SPE Reservoir Evaluation and Engineering Journal.

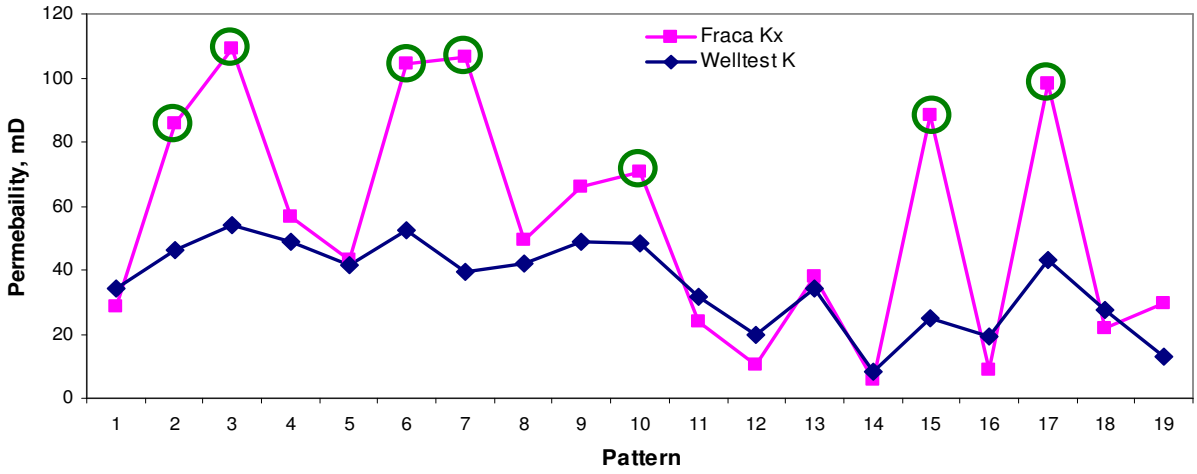

Figure 5.5 Comparison of actual EFNP (FRACA Kx) in the X-direction and average permeability obtained from drawdown welltest.

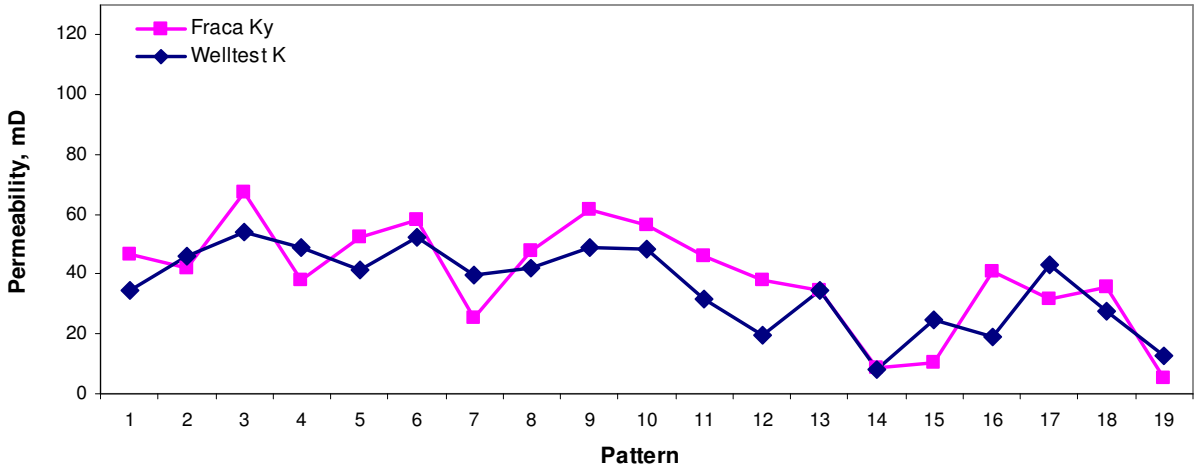

Figure 5.6 Comparison of actual EFNP (FRACA Ky) in the Y-direction and average permeability obtained from drawdown welltest.

Jafari, A. and Babadagli, T.: "Generating 3-D Permeability Map of Fracture Networks Using Well, Outcrop and Pressure Transient Data," SPE 124077, SPE Reservoir Evaluation and Engineering Journal.

In these figures, the separation between the welltest and actual EFNP from FRACA in the Y-direction is much less than that in the X-direction, which suggests that the impact of the permeability value in the Y-direction is dominant and has more weight on the average reservoir permeability and performance.

Seven cases in **Figure 5.5** (permeability in the X-direction) showed significant deviation from the actual permeability and is highlighted by circles. The actual permeability in the X-direction of these cases is much higher than their welltest (average) permeability. All the patterns showing significant deviation (the circled cases in **Figure 5.5**) are given in **Figure 5.7**.

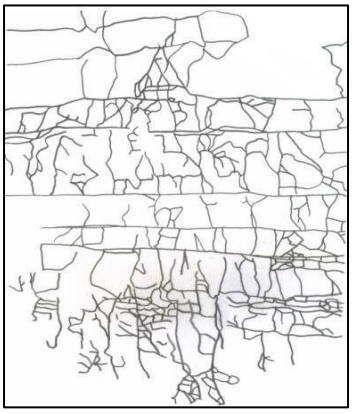

Pattern # 2 **15cm**

Jafari, A. and Babadagli, T.: "Generating 3-D Permeability Map of Fracture Networks Using Well, Outcrop and Pressure Transient Data," SPE 124077, SPE Reservoir Evaluation and Engineering Journal.

Pattern # 3 **15cm**

Pattern # 6 **15cm**

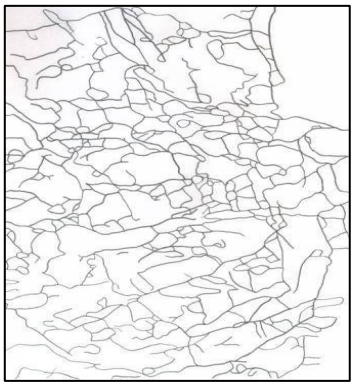

Pattern # 7 **15cm**

Jafari, A. and Babadagli, T.: "Generating 3-D Permeability Map of Fracture Networks Using Well, Outcrop and Pressure Transient Data," SPE 124077, SPE Reservoir Evaluation and Engineering Journal.

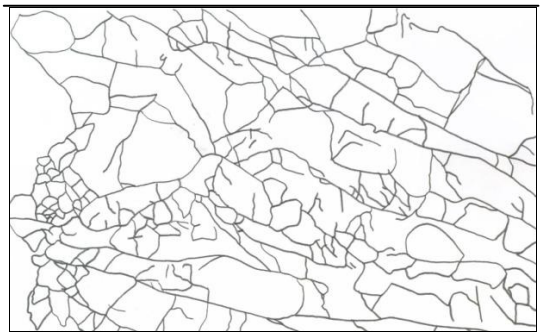

Pattern # 10 **15cm**

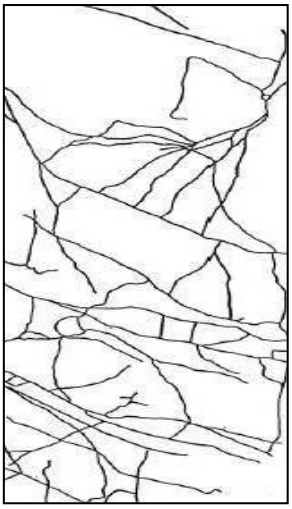

Pattern # 15 **4cm**

Jafari, A. and Babadagli, T.: "Generating 3-D Permeability Map of Fracture Networks Using Well, Outcrop and Pressure Transient Data," SPE 124077, SPE Reservoir Evaluation and Engineering Journal.

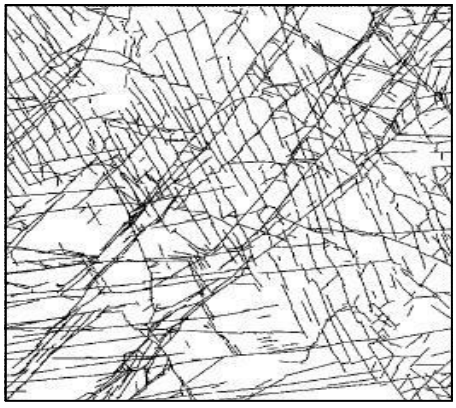

Pattern # 17 **3m**

Figure 5.7 Patterns showing significant deviation from the actual EFNP in Figure 5.5.

One can infer through the inspection of these patterns that they all show anisotropic behavior. In other words, long, well connected and continuous fractures spanning the whole domain in the X-direction of the patterns exist and they control the flow and make anisotropy behavior. Shorter and discontinuous fractures are obvious in the opposite direction (Y-direction). This yields a disagreement with the well test permeability obtained through a single porosity model of a black oil simulator and the one obtained from the solution of flow equation on the actual pattern.

After this extensive analysis, one has to emphasize several points regarding the mismatch for very high network permeability values as shown in **Figure 5.4**. The FRACA K_x permeability is by definition the average permeability between the two faces of the block perpendicular to the x-axis. As such, it represents

Jafari, A. and Babadagli, T.: "Generating 3-D Permeability Map of Fracture Networks Using Well, Outcrop and Pressure Transient Data," SPE 124077, SPE Reservoir Evaluation and Engineering Journal.

linear flow from one face to the next via the fracture network. All cases showing strong fracture continuity in the x-direction are therefore exhibit very high K_x permeability as expected. In this type of patterns, the nature of flow is essentially linear. By contrast, the well test would define a radial, or in case of strong heterogeneities elliptical flow regime. A mismatch between well test permeability and the square root of the K_x and K_x permeability values from FRACA at higher values of network permeability values (or more complex network structures) can be attributed to this. Modeling a well test based on the assumption of homogeneous permeability within each block may distort the well test pattern response, in fact forcing it to be radial while it would be fracture-dominated in reality when having large extent fractures spanning the entire grid block as observed in the cases showing deviations. Yet, however, visual characterization of fracture patterns is limited to 2-D images to implement any well test analysis on them using very limited commercial fracture network analysis software.

In summary, as we worked on hypothetical reservoir models in this chapter to introduce a new approach, the validation was possible only through commercial packages (black oil or DFN type models) in which certain limitations still exist. A final note should be made in this regard that, in the previous chapter (Jafari and Babadagli, 2010b), we applied correlations obtained through the methodology introduced here and observed a reasonably good match for well test data of a geothermal reservoir, even for complex fracture network structures.

Jafari, A. and Babadagli, T.: "Generating 3-D Permeability Map of Fracture Networks Using Well, Outcrop and Pressure Transient Data," SPE 124077, SPE Reservoir Evaluation and Engineering Journal.

5.4 Derivation of equivalent fracture network permeability (EFNP) correlation using 1-D (single well), 2-D (outcrop) and 3-D (well test) data

A practical approach in reservoir simulation is to utilize the available data to generate the permeability map of the fracture networks through an equation. Often times, data are limited to single well fracture information (1-D), outcrop analysis (2-D), or an average reservoir (or fracture network) permeability from well tests (3-D). In this section, we derive equations and then discuss their limitations and applicability conditions in terms of the availability of data related to fracture network characteristics.

In order to derive an equation, multivariable regression analysis (MRA) was performed. As mentioned earlier, we previously tested seven fractal (including the box-counting dimension of fracture intersection and mid-points, the sand-box dimension(mass dimension) of fracture intersection and mid-points, the fractal dimension of scanning lines in X- and Y- directions and the box-counting dimension of fracture lines) and five statistical parameters (including fracture length, fracture density, connectivity index and the maximum touch with scanning lines in the X- and Y-direction) of 2-D synthetic fracture networks against the EFNP and determined the correlation type for each parameter, i.e., linear, logarithmic, exponential, etc. This exercise was performed using 800 random fracture networks (Jafari and Babadagli, 2009). Later, we tested the reliability of this equation on natural patterns (Jafari and Babadagli, 2010a).

Jafari, A. and Babadagli, T.: "Generating 3-D Permeability Map of Fracture Networks Using Well, Outcrop and Pressure Transient Data," SPE 124077, SPE Reservoir Evaluation and Engineering Journal.

Four out of twelve parameters were found to present the highest correlation coefficient (as given below). We selected these four parameters and correlated them to the EFNP. Then, the following type of equation was found to be the most accurate with the highest correlation coefficient to predict the EFNP after testing several other types of equations with the same number of independent variables (Jafari and Babadagli, 2009):

$$Ln(Kx) = 25.008\exp(0.046X_1) + 2.895Ln(X_2) - 1.705Ln(X_3) + Ln(X_4) - 34.675 \quad \textbf{(2)}$$

where Kx denotes equivalent fracture network permeability in the X-direction, X_1 is the box-counting dimension of intersection points, X_2 is the maximum touch with scanning lines in the X-direction, X_3 is the maximum touch with scanning lines in Y-direction and X_4 is the box-counting dimension of fracture lines.

Here, unlike the previous chapter (Jafari and Babadagli, 2009), only natural patterns were used in deriving the equations. We performed the same procedure for the MRA analysis on natural fracture patterns (**Figure 5.1** lists and displays some of them) and added fracture connectivity index. The following equation was derived for the natural patterns:

$$Kx = 2.16\times10^{-10}\exp(13.720X_1) + 41.779Ln(X_2) - 37.779Ln(X_3) + 41.658Ln(X_4) - 1.262Ln(X_5) - 10.116 \quad \textbf{(3)}$$

Jafari, A. and Babadagli, T.: "Generating 3-D Permeability Map of Fracture Networks Using Well, Outcrop and Pressure Transient Data," SPE 124077, SPE Reservoir Evaluation and Engineering Journal.

where *Kx* denotes equivalent fracture network permeability in the X-direction, X_1 is the box-counting dimension of intersection points, X_2 the connectivity index, X_3 is the maximum touch with scanning lines in the X-direction, X_4 is the maximum touch with scanning lines in *Y*-direction and X_5 is the box-counting dimension of fracture lines.

Then due to wide distribution of permeability values, we again used logarithm of permeability to improve the correlation. Also we added the well test permeability to the independent variables. The following equation was obtained applying the same MRA analysis:

$$\begin{aligned} Ln(Kx) &= 18.867\exp(0.035X_1) + 0.626Ln(X_2) - 1.15Ln(X_3) \\ &\quad + 1.018Ln(X_4) + 1.754Ln(X_5) + 1.057Ln(X6) - 19.902 \end{aligned} \qquad \textbf{(4)}$$

where *Kx* denotes equivalent fracture network permeability in the X-direction, X_1 is the box-counting dimension of intersection points, X_2 is the fracture connectivity index, X_3 is the maximum touch with scanning lines in the X-direction, X_4 is the maximum touch with scanning lines in *Y*-direction, X_5 is the box-counting dimension of fracture lines and X_6 is the welltest permeability and other variables are the same as the variables in the previous equation.

5.5 Discussion

In the **Eq. 3** and **4**, X_1 and X_5 shows the spatial distribution of fracture intersection points and fracture lines respectively and an increase in these two

Jafari, A. and Babadagli, T.: "Generating 3-D Permeability Map of Fracture Networks Using Well, Outcrop and Pressure Transient Data," SPE 124077, SPE Reservoir Evaluation and Engineering Journal.

parameters shows a huge number of intersection points and fracture lines with a wide distribution through the domain. X_2 is defined as the total number of intersection points divided by the total number of fractures in the domain (fracture density). X_1 and X_2, in turn, can have some implications on the existence of a connected fracture path in the domain and as a result, higher permeability. X_3 and X_4 are used to take into account the orientation effect; since they quantify this property of the fracture network in both directions. If X_3 and X_4 are not roughly equal, it means that fractures in the domain are more oriented in one direction (anisotropic). If all fractures are oriented in one direction, the connectivity($X2$) decreases due to lack of fracture intersection and permeability will go down too. In this situation, the critical parameter would be fracture length; if fractures with regard to their lengths can span two opposite sides of the domain, only permeability in that specific direction would increase. Generally speaking, the independent variables with bigger constant coefficients have more influence on the result (dependent variable).

Figure 5.8 compares the EFNP values obtained through **Eqs. 2**, **3** and **4**. Here, the permeability measured using the FRACA package was considered as the actual permeability or the base case (represented by the square symbol and bolder line). As seen, an addition of well test permeability and fracture connectivity index in the correlation provided remarkable improvement. The permeability values obtained by **Eq. 4** (the circle symbol) yielded a much closer value to the actual one (the square symbol) except in one case (pattern #15). The only comment that can be made for this pattern is that it was obtained using a rectangular piece of rock (**Figure 5.3** of Babadagli, 2001) unlike all other patterns. Hence, its characteristics in terms of the scale and

Jafari, A. and Babadagli, T.: "Generating 3-D Permeability Map of Fracture Networks Using Well, Outcrop and Pressure Transient Data," SPE 124077, SPE Reservoir Evaluation and Engineering Journal.

being representative of a fracture system are expected to be different from the others shown in **Figure 5.7**. In other words, all other patterns are either at a meter scale (**Figure 5.1d**, **f**, **g**, **h**, and **i**) or at a smaller scale, but present a relatively more orthogonal (or uniform) pattern texture (**Figure 5.1a** and **c**).

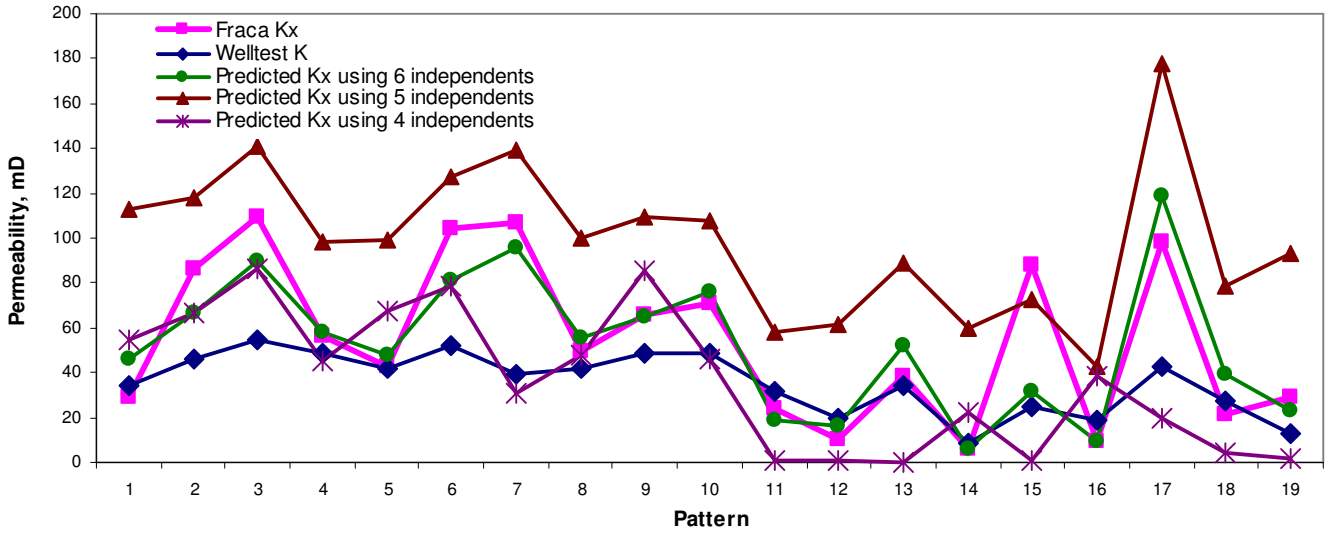

Figure 5.8 Five different equivalent fracture network permeability values using welltest, Fraca software and derived equations with 4 (Eq. 2 derived in Jafari and Babadagli, 2009) and 5 and 6 (Eq. 3 and 4 derived in this chapter) independent variables.

The EFNP values obtained by **Eq. 4** also showed a better agreement with the well test data (the diamond symbol in **Figure 5.8**) compared to the base case (the square symbol). One exception is pattern #17. This can be attributed again to the nature of the pattern. A set of long and continuous fracture groups

Jafari, A. and Babadagli, T.: "Generating 3-D Permeability Map of Fracture Networks Using Well, Outcrop and Pressure Transient Data," SPE 124077, SPE Reservoir Evaluation and Engineering Journal.

spanning the whole domain controls the flow and creates anisotropy. This could not easily be captured by well test simulation on a single porosity model converted from discrete fracture networks. But, this anisotropic nature of the pattern was captured through the fractal and statistical parameters used in **Eq. 4** as verified by a better match with the base case.

In another effort to improve the accuracy and universality of the derived equation, we added one more data set, i.e., 1-D well data. This type of data provides limited information about the fracture density obtained through core and log analysis but is more abundant compared to 2-D (outcrop) and 3-D (well test) data. Generally, fracture network maps are generated based on limited well (1-D) data. Therefore, we added this type of data and derived a new equation with two more independents.

We located an imaginary wellbore at the center of the models (listed in **Table 5.1**) in such a way to penetrate the whole reservoir thickness and with the same perforated thickness as equal as to the reservoir (i.e. 20ft) and then counted the number of the fractures intersecting the wellbore and the measured the fracture spacing in the vertical direction.

To do this, all fractures were extended in the Z-direction with a 45-degree inclination so that the imaginary well could intersect some number of fractures. Note that the correlations given above (**Eqs. 2**, **3** and **4**) were developed using the patterns with no inclination (extended 90 degrees) in the Z-direction. The fracture spacing and fracture wellbore intersection data are shown in **Table 5.2**.

Jafari, A. and Babadagli, T.: "Generating 3-D Permeability Map of Fracture Networks Using Well, Outcrop and Pressure Transient Data," SPE 124077, SPE Reservoir Evaluation and Engineering Journal.

Table 5.2 1-D, 2-D, and 3-D data used in the derivation of Eq. 6.

Pattern	FD (Box-Counting) Intersection Point	Connectivity Index	Max Touch with X Scanning Line	Max Touch with Y Scanning Line	FD (Box-Counting) Lines	Welltest Permeability, mD	Fracture spacing	Fracture-wellbore Intersection	Kx, mD
1	1.867	1.064	15608	21143	1.557	29.769	1.970	4	29.545
2	1.820	1.704	15396	17481	1.521	45.348	2.737	3	118.545
3	1.892	1.516	19585	24571	1.598	56.999	1.122	7	120.077
4	1.750	1.407	13331	15887	1.443	51.362	2.444	4	78.485
5	1.774	1.465	15486	16721	1.487	53.660	3.731	2	112.141
6	1.870	1.422	18933	24001	1.576	53.659	7.071	1	112.141
7	1.872	1.275	15916	31323	1.630	50.514	1.729	5	115.117
8	1.800	1.271	13364	16592	1.528	43.774	4.092	2	56.001
9	1.769	1.745	16978	17563	1.567	51.395	2.459	3	71.010
10	1.770	1.496	14366	18920	1.562	49.397	3.235	3	81.104
11	0.797	1.091	114	266	1.264	19.264	4.981	2	38.542
12	1.672	1.218	4720	5612	1.484	16.949	3.049	3	36.981
13	1.660	1.149	4071	3094	1.493	19.649	3.550	2	9.825
14	1.378	1.020	860	1210	1.481	28.733	7.071	1	88.872
15	1.577	1.041	4697	2680	1.513	26.524	2.538	3	15.212
16	1.893	2.611	4767	5473	1.682	60.970	2.088	4	169.827
17	1.647	1.369	1687	1758	1.583	33.349	2.739	3	23.733
18	1.653	1.558	996	1281	1.515	28.947	4.311	2	53.588

In addition to those, new well test permeability simulations were performed, as the fracture patterns in the Z-direction changed from the previous configuration given in **Table 5.1**. The 2-D fractal/statistical data are the same as before (columns 2 through 5) as the "surface" fracture patterns (X- and Y-directions) did not change.

Jafari, A. and Babadagli, T.: "Generating 3-D Permeability Map of Fracture Networks Using Well, Outcrop and Pressure Transient Data," SPE 124077, SPE Reservoir Evaluation and Engineering Journal.

The same procedure was followed to derive another correlation for these 45-degree inclined fracture patterns using MRA with 6 independent variables first.

$$\begin{aligned} Ln(Kx) &= 17.37\exp(0.011X_1) + 0.894Ln(X_2) - 1.111Ln(X_3) \\ &+ 1.112Ln(X_4) - 1.362Ln(X_5) + 1.132Ln(X6) - 17.64 \end{aligned} \quad \textbf{(5)}$$

The equation type is exactly the same as in **Eq. 4** but the constants are changed. Also using the new fracture patterns (with 45 degree inclination), the following correlation with 8 independent variables was obtained:

$$\begin{aligned} Ln(Kx) &= 15.858\exp(0.004X_1) + 1.182Ln(X_2) - 1.218Ln(X_3) + 1.280Ln(X_4) \\ &- 1.277Ln(X_5) + 0.979Ln(X6) - 0.555Ln(X7) - 0.763Ln(X8) - 14.677 \end{aligned} \quad \textbf{(6)}$$

where X_7 and X_8 are the fracture spacing in the wellbore and the number of the intersection between the fractures and the wellbore respectively, and other variables are exactly the same as the variables in the previous equation.

As a final attempt, we considered only 1-D (single well) and 3-D data (well test). This is the most encountered situation as the well data (cores and logs) are more abundant compared to the others and well test analysis is more common in reservoir development compared to outcrop analysis. The following equation was derived using the same approach and method but used only 3 independent variables, namely well test permeability, fracture spacing in the wellbore, and the number of the intersections between fractures and wellbore:

Jafari, A. and Babadagli, T.: "Generating 3-D Permeability Map of Fracture Networks Using Well, Outcrop and Pressure Transient Data," SPE 124077, SPE Reservoir Evaluation and Engineering Journal.

$$Ln(Kx) = 88.412Ln(X_1) + 28.884Ln(X_2) + 19.734Ln(X_3) - 297.435 \quad \textbf{(7)}$$

where *Kx* denotes equivalent fracture network permeability in the X-direction, X_1 is the welltest permeability, X_2 is the fracture spacing in the wellbore and X_3 is the number of the intersection between fractures and wellbore respectively.

Figure 5.9 compares the five EFNP values obtained using different equations (**Eqs. 5**, **6**, and **7**). The addition of single well data (**Eq. 6**) improved the predictive power and accuracy of the correlation derived to calculate the EFNP. Only, one case showed a better correlation with **Eq. 5** (pattern #3). Despite the minimal data used in the derivation, the EFNP value obtained from **Eq. 7** surprisingly yielded a reasonable match with the base case EFNP (FRACA Kx). For some patterns, it showed an even better match than with the EFNP values obtained through **Eq. 6** (Patterns # 3, 5, and 6). One may conclude from this exercise that, in general, with some support of 2-D fractal/statistical data, 1-D (single well) and 3-D (well test) data could be useful to accurately obtain the EFNP.

Jafari, A. and Babadagli, T.: "Generating 3-D Permeability Map of Fracture Networks Using Well, Outcrop and Pressure Transient Data," SPE 124077, SPE Reservoir Evaluation and Engineering Journal.

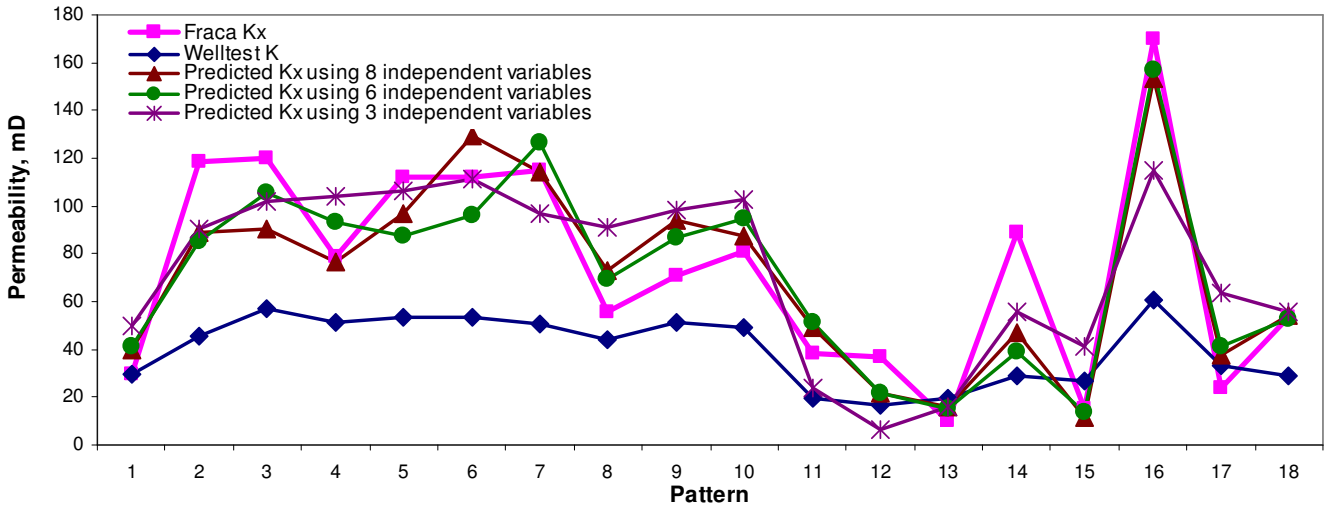

Figure 5.9 Five different EFNPs obtained using welltest, FRACA software (the base case), and Eqs. 5, 6 and 7.

It should be emphasized that only one well was used for the 1-D fracture density data (**Eqs. 6** and **7**) as the grid size selected in this analysis represents a typical one-well drainage area. More wells for larger areas can be used in the analysis and the accuracy of the correlations, in which 1-D data was honored, would be improved by increasing the number of wells. Obtaining the optimal number of wells to be cored and logged for the 1-D data provision is a critical issue and currently under research.

Jafari, A. and Babadagli, T.: "Generating 3-D Permeability Map of Fracture Networks Using Well, Outcrop and Pressure Transient Data," SPE 124077, SPE Reservoir Evaluation and Engineering Journal.

5.6 Conclusions

We proposed a practical approach to estimate equivalent fracture network permeability (EFNP) values. Four correlations were derived using nineteen 2-D natural patterns representing different fracture network types of different scales. Five statistical and fractal properties of the fracture patterns (2-D data), well test permeability obtained through a numerical well test simulation (3-D data), and fracture spacing and the number of fracture intersections obtained from a single well (1-D) were used as independent variables in these correlations.

Selection of the type of the correlations presented in this chapter for practical applications in the field totally depends on the availability of different types of data, i.e. 1-D, 2-D and 3-D. The eight-variable equation honors all these types of data and the best match to the actual EFNP obtained from single phase flow simulation on the fracture networks was observed for the correlation with eight independent variables (**Eq. 6**). The accuracy of the three-variable case (1-D well data and 3-D well test data) was surprisingly comparable to the six-variable correlation (five 2-D fractal and statistical parameters from outcrop studies and the permeability obtained from a single well pressure transient data). Hence, 1-D single well data could be useful when it is used along with the permeability obtained from a single well pressure transient test. For a better accuracy, this can be supported by additional fractal and statistical measurements on 2-D patterns obtained from outcrop studies.

Jafari, A. and Babadagli, T.: "Generating 3-D Permeability Map of Fracture Networks Using Well, Outcrop and Pressure Transient Data," SPE 124077, SPE Reservoir Evaluation and Engineering Journal.

6 Equivalent Fracture Permeability of Multilayered Naturally Fractured Reservoirs

6.1 Overview

Conventionally, logs, cores, seismic and pressure transient tests are used as a data base for modeling naturally fractured reservoirs (NFRs). In previous chapter it was shown that a strong correlation exists between the fractal parameters of 2-D fracture networks and their permeability and also this fact that 1-D well (cores-logs) and 3-D reservoir data (well test) may not be sufficient in fracture network permeability (FNP) mapping and that 2-D (outcrop) characteristics are needed. This chapter is an extension of those studies where only 2-D (single layer, uniform fracture characteristics in z-direction) representations were used.

In this chapter, we considered a more complex and realistic 3-D network system. 2-D random fractures with known fractal and statistical characteristics were distributed in the x- and y-directions. Variation of fracture network characteristics in the z-direction was presented by a multi layer system representing three different facieses with different fracture properties. Wells were placed in different locations of the model to collect 1-D fracture density and pressure transient data. In addition, five different

A version of this chapter was presented and also submitted for publication 157

Jafari, A. and Babadagli, T.: "Calculating Equivalent Fracture Network Permeability of Multi-Layer-Complex Naturally Fractured Reservoirs," SPE 132431, Western Regional Meeting, Anaheim, California, USA, 2010.

fractal and statistical properties of the network of each layer were measured.

Using available 1-D, 2-D, and 3-D data, multivariable regression analyses were performed to obtain equivalent FNP correlations and then the derived equations were validated against a new set of synthetic fracture networks and the conditions at which 1-D, 2-D and 3-D are sufficient to map fracture network permeability were determined. The importance of the inclusion of each data type, i.e., 1-D, 2-D and 3-D, in the correlations was discussed.

6.2 Building fracture network model

Initially, synthetic fracture networks with random orientation were generated in 100x100 m^2 domains. These fracture patterns had different length and density values (defined as the number of fractures per domain). To cover a wide range of these parameters, three different fracture lengths and densities (low, medium and high) spanning between very low (20m length 50 fracture/domain density) and very high (60m length 250 fracture/domain density) values were used (**Table 6.1**).

Table 6.1 Fracture length and density values used (with a random orientation) to generate the fracture network permeability correlations.

Fracture Length, (m)	Fracture density, (# / domain)	Fracture Orientation
20	50	Random
40	150	Random
60	250	Random

Jafari, A. and Babadagli, T.: "Calculating Equivalent Fracture Network Permeability of Multi-Layer-Complex Naturally Fractured Reservoirs," SPE 132431, Western Regional Meeting, Anaheim, California, USA, 2010.

Then, based on varying fracture length and density, different fracture patterns were generated and each of them was imbedded into a separate layer of a 3-D multilayer reservoir with three layers. In these cases, fracture conductivity was kept constant (1000 mD.m) and the orientations of the fractures in the x-y and z-directions were random. Each of these models in the above table was then built in a commercial software package (FRACA). **Figure 6.1a** shows a 2-D map of a fracture pattern with fracture length equal to 40m and a fracture density of 150. **Figure 6.1b** presents a side view of one these models with three layers. Each layer has a 10m thickness. In each model, five imaginary wells were placed penetrating the reservoir through the whole thickness, i.e., 30 m (**Figure 6.2**).

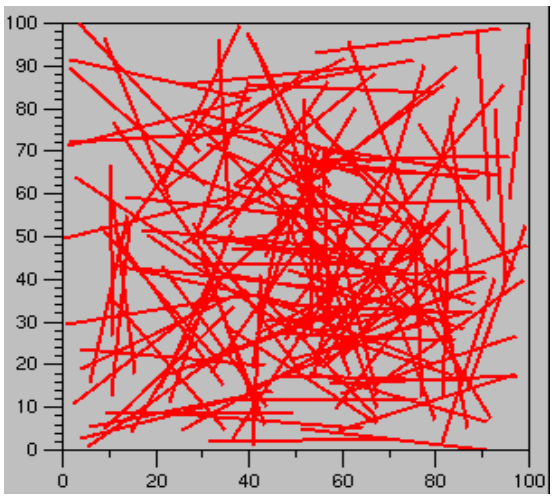

(a)

Jafari, A. and Babadagli, T.: "Calculating Equivalent Fracture Network Permeability of Multi-Layer-Complex Naturally Fractured Reservoirs," SPE 132431, Western Regional Meeting, Anaheim, California, USA, 2010.

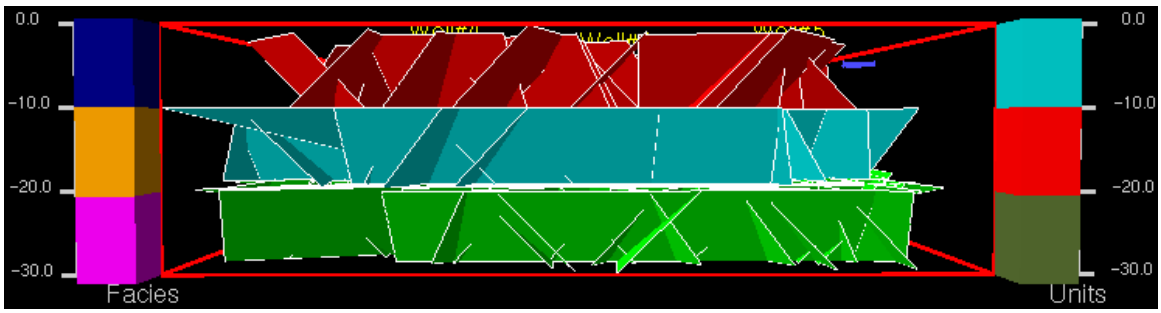

(b)

Figure 6.1 A Sample of (a) top view of the 2-D fracture map of a pattern with a fracture length=40 m and a fracture density=150 in a 100x100 m^2 domain, and (b) side view of a three layer fractured reservoir model.

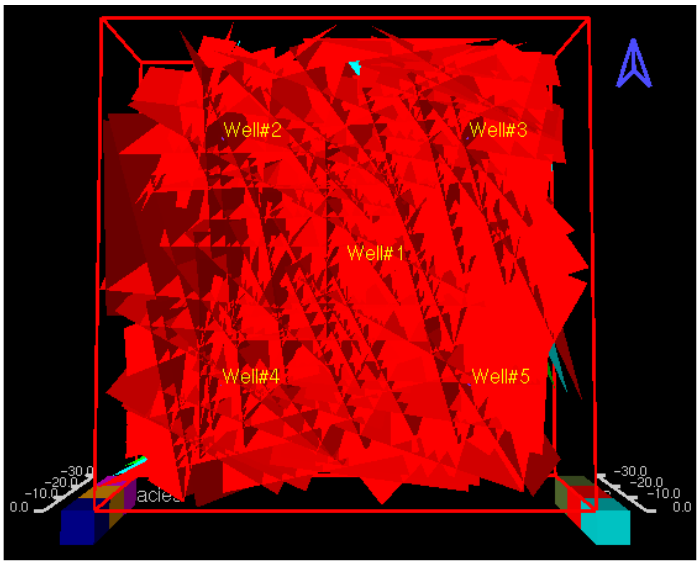

Figure 6.2 Plan view of a three layer fractured reservoir with five imaginary wells.

In total, ten different fractured reservoir realizations with three layers were defined for each case to include the random nature of the patterns. Hence, a total of 100 runs were performed in developing the correlations as will be

Jafari, A. and Babadagli, T.: "Calculating Equivalent Fracture Network Permeability of Multi-Layer-Complex Naturally Fractured Reservoirs," SPE 132431, Western Regional Meeting, Anaheim, California, USA, 2010.

explained in the next section. Each layer has a different fracture pattern even if the same density and length values were assigned. Note that, after applying an experimental analysis, the number of cases was reduced to an optimal value, which was found to be ten. These cases were represented in **Table 6.2**.

Once each 2-D fracture pattern was generated and before embedding it into the FRACA software for building the 3-D model, its 2-D properties were obtained using a code written in MATLAB. Also, 1-D data was provided through analyzing the imaginary wells (mainly fracture density related information). Then, the actual equivalent fracture network permeability of each model in **Table 6.2** was calculated using the software for the whole 3-D volume (100x100x30 m^3). Note that all possible combinations were covered as given in **Table 6.2**, i.e., lD-lL lD-lL lD-lL (Case 1, low-Density low-Length), hD-hL hD-hL hD-hL (Case 10, high-Density high-Length), mD-mL lD-lL mD-mL (Case 5, medium-Density medium-Length, low-Density low-Length), mD-mL mD-mL lD-lL (Case 6, medium-Density medium-Length, low-Density low-Length), and the number of cases was reduced to an optimum value of ten after applying an experimental analysis as mentioned above. Finally, a drawdown test was performed for each well in each model using the well test option of the software.

Jafari, A. and Babadagli, T.: "Calculating Equivalent Fracture Network Permeability of Multi-Layer-Complex Naturally Fractured Reservoirs," SPE 132431, Western Regional Meeting, Anaheim, California, USA, 2010.

Table 6.2 Ten different fracture reservoir configurations with three layers (L=Length, D= Density). l: low, m: medium, h: high.

Case No.	Density and length characteristics of each layer	Cases for three layers		
		Layer-1	Layer-2	Layer-3
1	lD-lL lD-lL lD-lL	L=20, D=50	L=20, D=50	L=20, D=50
2	lD-lL mD-mL lD-lL	L=20, D=50	L=40, D=150	L=20, D=50
3	lD-lL mD-mL hD-hL	L=20, D=50	L=40, D=150	L=60, D=250
4	lD-lL hD-hL lD-lL	L=20, D=50	L=60, D=250	L=20, D=50
5	mD-mL lD-lL mD-mL	L=40, D=150	L=20, D=50	L=40, D=150
6	mD-mL mD-mL mD-mL	L=40, D=150	L=40, D=150	L=40, D=150
7	mD-mL hD-hL mD-mL	L=40, D=150	L=60, D=250	L=40, D=150
8	hD-hL lD-lL hD-hL	L=60, D=250	L=20, D=50	L=60, D=250
9	hD-hL mD-mL hD-hL	L=60, D=250	L=40, D=150	L=60, D=250
10	hD-hL hD-hL hD-hL	L=60, D=250	L=60, D=250	L=60, D=250

Jafari, A. and Babadagli, T.: "Calculating Equivalent Fracture Network Permeability of Multi-Layer-Complex Naturally Fractured Reservoirs," SPE 132431, Western Regional Meeting, Anaheim, California, USA, 2010.

6.3 Fracture network permeability correlations

The actual fracture network permeability (FNP) values for each case obtained through the software are shown in **Table 6.3**. The last column in the table is the average permeability calculated using:

$$K_{ave} = \sqrt{(K_{max} \times K_{min})} \qquad (1)$$

Table 6.3 Different fractured reservoirs (models) with corresponding actual equivalent fracture network permeability obtained from the software (FRACA). Kave is as described in Eq. 1.

No.	Scenario	Cases for three layers			K_{max}, mD	K_{min}, mD	K_{ave}, mD
		Layer-1	Layer-2	Layer-3			
1	lDlL lDlL lDlL	L=20, D=50	L=20, D=50	L=20, D=50	29.69	4.186	11.148
2	lDlL mDmL lDlL	L=20, D=50	L=40, D=150	L=20, D=50	51.189	4.545	15.252
3	lDlL mDmL hDhL	L=20, D=50	L=40, D=150	L=60, D=250	82.155	4.769	19.793
4	lDlL hDhL lDlL	L=20, D=50	L=60, D=250	L=20, D=50	66.975	4.828	17.981
5	mDmL lDlL mDmL	L=40, D=150	L=20, D=50	L=40, D=150	69.972	4.661	18.06
6	mDmL mDmL mDmL	L=40, D=150	L=40, D=150	L=40, D=150	78.721	4.75	19.337
7	mDmL hDhL mDmL	L=40, D=150	L=60, D=250	L=40, D=150	90.804	4.853	20.992
8	hDhL lDlL hDhL	L=60, D=250	L=20, D=50	L=60, D=250	90.095	4.895	21
9	hDhL mDmL hDhL	L=60, D=250	L=40, D=150	L=60, D=250	108.57	4.858	22.967
10	hDhL hDhL hDhL	L=60, D=250	L=60, D=250	L=60, D=250	109.23	4.878	23.082

Jafari, A. and Babadagli, T.: "Calculating Equivalent Fracture Network Permeability of Multi-Layer-Complex Naturally Fractured Reservoirs," SPE 132431, Western Regional Meeting, Anaheim, California, USA, 2010.

Also, as mentioned earlier, five imaginary wells were embedded in each model penetrating the whole thickness of the reservoir. 1-D data was extracted for each well in the model and averaged for five wells resulting in a single number per model. These values are shown in **Table 6.4**.

Table 6.4 Different fractured reservoirs (models) with associated 1-D data.

No.	Scenario	Cases for three layers			Fracture intersection	Fracture spacing
		Layer-1	Layer-2	Layer-3		
1	lDlL lDlL lDlL	L=20, D=50	L=20, D=50	L=20, D=50	42	2.947
2	lDlL mDmL lDlL	L=20, D=50	L=40, D=150	L=20, D=50	38	3.24
3	lDlL mDmL hDhL	L=20, D=50	L=40, D=150	L=60, D=250	138	0.906
4	lDlL hDhL lDlL	L=20, D=50	L=60, D=250	L=20, D=50	118	1.092
5	mDmL lDlL mDmL	L=40, D=150	L=20, D=50	L=40, D=150	78	1.6
6	mDmL mDmL mDmL	L=40, D=150	L=40, D=150	L=40, D=150	143	0.909
7	mDmL hDhL mDmL	L=40, D=150	L=60, D=250	L=40, D=150	190	0.664
8	hDhL lDlL hDhL	L=60, D=250	L=20, D=50	L=60, D=250	186	0.676
9	hDhL mDmL hDhL	L=60, D=250	L=40, D=150	L=60, D=250	241	0.527
10	hDhL hDhL hDhL	L=60, D=250	L=60, D=250	L=60, D=250	327	0.395

Jafari, A. and Babadagli, T.: "Calculating Equivalent Fracture Network Permeability of Multi-Layer-Complex Naturally Fractured Reservoirs," SPE 132431, Western Regional Meeting, Anaheim, California, USA, 2010.

Fracture patterns in each layer were used separately to extract their 2-D data. Since each model has three layers with three different fracture patterns, three different sets of 2-D data exist for each model. Jafari and Babadagli (2008) correlated twelve statistical and fractal fracture networks properties to the FNP and observed that the following parameters showed the highest correlation:

(1) Fractal dimension of fracture intersecting points (Technique: Box counting),
(2) Fractal dimension of fracture lines (Technique: Box counting),
(3) Connectivity index (Jafari and Babadagli, 2009),
(4) Maximum touch with X scanning line (Jafari and Babadagli, 2009),
(5) Maximum touch with Y scanning line (Jafari and Babadagli, 2009).

The first two -fractal- properties were obtained through the classical box counting technique applied by Babadagli (2001) and Barton and Larsen (1985), respectively. The connectivity index was described by Jafari and Babadagli (2009a) as a ratio of the number of intersection points to the total number of lines. The maximum touch with scanning lines is the number of fractures touched by a scanline in a specific direction (X and Y) in the whole domain (Babadagli, 2001; Jafari and Babadagli, 2009a).

These five different statistical and fractal properties were calculated for the networks assigned to each layer and presented in **Table 6.5**, **Table 6.6** and **Table 6.7**. **Table 6.5** and **Table 6.6** show the 2-D statistical and fractal values for the least and the most conductive layers for each case, respectively. **Table 6.7** shows the average of these values. Each of these will be used individually in the correlation development to also test the relative contribution of the layers.

Jafari, A. and Babadagli, T.: "Calculating Equivalent Fracture Network Permeability of Multi-Layer-Complex Naturally Fractured Reservoirs," SPE 132431, Western Regional Meeting, Anaheim, California, USA, 2010.

Table 6.5 2-D fracture properties of the least conductive layer (short fractures with low density) in the three-layer model.

No.	Scenario	Cases for three layers			Fractal Dim.	Connectivity Index	Max. Touch with X Scanning Lines	Max. Touch with Y Scanning Lines	Fractal Dim.
		Layer-1	Layer-2	Layer-3	Intersec. Point				Lines
1	lDlL lDlL lDlL	L=20, D=50	L=20, D=50	L=20, D=50	1.234	0.780	6529	6269	1.348
2	lDlL mDmL lDlL	L=20, D=50	L=40, D=150	L=20, D=50	1.034	0.520	5736	6929	1.330
3	lDlL mDmL hDhL	L=20, D=50	L=40, D=150	L=60, D=250	1.234	0.860	6235	6213	1.332
4	lDlL hDhL lDlL	L=20, D=50	L=60, D=250	L=20, D=50	1.168	0.940	6401	6294	1.325
5	mDmL lDlL mDmL	L=40, D=150	L=20, D=50	L=40, D=150	1.186	0.720	6612	6136	1.335
6	mDmL mDmL mDmL	L=40, D=150	L=40, D=150	L=40, D=150	1.917	9.533	35618	39181	1.720
7	mDmL hDhL mDmL	L=40, D=150	L=60, D=250	L=40, D=150	1.902	8.913	37520	37241	1.721
8	hDhL lDlL hDhL	L=60, D=250	L=20, D=50	L=60, D=250	1.149	0.680	6345	6391	1.330
9	hDhL mDmL hDhL	L=60, D=250	L=40, D=150	L=60, D=250	1.910	9.480	36213	40121	1.725
10	hDhL hDhL hDhL	L=60, D=250	L=60, D=250	L=60, D=250	1.654	43.576	98187	93035	1.831

Jafari, A. and Babadagli, T.: "Calculating Equivalent Fracture Network Permeability of Multi-Layer-Complex Naturally Fractured Reservoirs," SPE 132431, Western Regional Meeting, Anaheim, California, USA, 2010.

Table 6.6 2-D fracture properties of the most conductive layer (long fractures-high density) in the three-layer model.

No.	Scenario	Cases for three layers			Fractal Dim.	Connectivity Index	Max. Touch with X Scanning Lines	Max. Touch with Y Scanning Lines	Fractal Dim.
		Layer-1	Layer-2	Layer-3	Intersec. Point				Lines
1	lDlL lDlL lDlL	L=20, D=50	L=20, D=50	L=20, D=50	1.234	0.78	6529	6269	1.348
2	lDlL mDmL lDlL	L=20, D=50	L=40, D=150	L=20, D=50	1.916	9.08	38336	38071	1.729
3	lDlL mDmL hDhL	L=20, D=50	L=40, D=150	L=60, D=250	1.955	43.164	95291	93902	1.835
4	lDlL hDhL lDlL	L=20, D=50	L=60, D=250	L=20, D=50	1.977	38.644	102500	88409	1.845
5	mDmL lDlL mDmL	L=40, D=150	L=20, D=50	L=40, D=150	1.936	8.753	36136	39398	1.728
6	mDmL mDmL mDmL	L=40, D=150	L=40, D=150	L=40, D=150	1.917	9.533	35618	39181	1.72
7	mDmL hDhL mDmL	L=40, D=150	L=60, D=250	L=40, D=150	1.966	40.404	97711	94150	1.836
8	hDhL lDlL hDhL	L=60, D=250	L=20, D=50	L=60, D=250	1.977	40.76	95095	97325	1.838
9	hDhL mDmL hDhL	L=60, D=250	L=40, D=150	L=60, D=250	1.985	38.948	99159	92893	1.842
10	hDhL hDhL hDhL	L=60, D=250	L=60, D=250	L=60, D=250	1.967	43.576	98187	93035	1.831

Jafari, A. and Babadagli, T.: "Calculating Equivalent Fracture Network Permeability of Multi-Layer-Complex Naturally Fractured Reservoirs," SPE 132431, Western Regional Meeting, Anaheim, California, USA, 2010.

Table 6.7 Average of 2-D fracture properties (arithmetic average of the least and most conductive layer values) in the three-layer model.

No.	Scenario	Cases for three layers			Fractal Dim.	Connectivity Index	Max. Touch with X Scanning Lines	Max. Touch with Y Scanning Lines	Fractal Dim.
		Layer-1	Layer-2	Layer-3	Intersec. Point				Lines
1	lDlL lDlL lDlL	L=20, D=50	L=20, D=50	L=20, D=50	1.234	0.78	6529	6269	1.348
2	lDlL mDmL lDlL	L=20, D=50	L=40, D=150	L=20, D=50	1.475	4.8	22036	22500	1.53
3	lDlL mDmL hDhL	L=20, D=50	L=40, D=150	L=60, D=250	1.594	22.012	50763	50058	1.583
4	lDlL hDhL lDlL	L=20, D=50	L=60, D=250	L=20, D=50	1.572	19.792	54451	47352	1.585
5	mDmL lDlL mDmL	L=40, D=150	L=20, D=50	L=40, D=150	1.561	4.737	21374	22767	1.532
6	mDmL mDmL mDmL	L=40, D=150	L=40, D=150	L=40, D=150	1.917	9.533	35618	39181	1.72
7	mDmL hDhL mDmL	L=40, D=150	L=60, D=250	L=40, D=150	1.934	24.659	67616	65696	1.778
8	hDhL lDlL hDhL	L=60, D=250	L=20, D=50	L=60, D=250	1.563	20.72	50720	51858	1.584
9	hDhL mDmL hDhL	L=60, D=250	L=40, D=150	L=60, D=250	1.947	24.214	67686	66507	1.783
10	hDhL hDhL hDhL	L=60, D=250	L=60, D=250	L=60, D=250	1.81	43.576	98187	93035	1.831

Finally, the pressure curves of drawdown test simulations for each well in different models were analyzed and the welltest permeability was calculated. Due to this fact that welltest analysis investigates the 3-D body of the reservoir, the resulted permeability values were considered as 3-D data. These welltest permeability values are shown in **Table 6.8**.

Jafari, A. and Babadagli, T.: "Calculating Equivalent Fracture Network Permeability of Multi-Layer-Complex Naturally Fractured Reservoirs," SPE 132431, Western Regional Meeting, Anaheim, California, USA, 2010.

Table 6.8 Different fractured reservoirs (models) with associated well test (3-D) permeability data.

No.	Scenario	Cases for three layers			Welltest K (Well#1), mD	Welltest K (Well#2), mD	Welltest K (Well#3), mD	Welltest K (Well#4), mD	Welltest K (Well#5), mD
		Layer-1	Layer-2	Layer-3					
1	lDlL lDlL lDlL	L=20, D=50	L=20, D=50	L=20, D=50	31.044	22.827	22.245	11.136	20.042
2	lDlL mDmL lDlL	L=20, D=50	L=40, D=150	L=20, D=50	22.45	22.477	14.871	23.453	15.011
3	lDlL mDmL hDhL	L=20, D=50	L=40, D=150	L=60, D=250	383.325	67.254	98.799	57.535	75.037
4	lDlL hDhL lDlL	L=20, D=50	L=60, D=250	L=20, D=50	232.061	112.143	69.96	25.699	88.365
5	mDmL lDlL mDmL	L=40, D=150	L=20, D=50	L=40, D=150	41.429	63.798	33.057	37.506	69.227
6	mDmL mDmL mDmL	L=40, D=150	L=40, D=150	L=40, D=150	263.35	93.235	94.081	139.798	76.149
7	mDmL hDhL mDmL	L=40, D=150	L=60, D=250	L=40, D=150	369.72	171.514	69	65.118	107.993
8	hDhL lDlL hDhL	L=60, D=250	L=20, D=50	L=60, D=250	524.337	191.93	166.854	107.378	137.726
9	hDhL mDmL hDhL	L=60, D=250	L=40, D=150	L=60, D=250	1029.615	155.385	272.733	232.177	154.372
10	hDhL hDhL hDhL	L=60, D=250	L=60, D=250	L=60, D=250	2220.827	141.403	454.835	194.503	180

The next step after compiling the data was to apply a multivariable regression analysis to correlate these data to the equivalent FNP. In this exercise, different possible scenarios in terms of the availability of the 1-D, 2-D and 3-D data were considered and for each case, a different equation was derived as described below.

Jafari, A. and Babadagli, T.: "Calculating Equivalent Fracture Network Permeability of Multi-Layer-Complex Naturally Fractured Reservoirs," SPE 132431, Western Regional Meeting, Anaheim, California, USA, 2010.

6.3.1 Only 1-D Data

The first possible scenario is based on the availability of only 1-D data, i.e., fracture data from image logs and cores. Two parameters were measured in each wellbore: (1) the number of the fracture intersection, and (2) the distance between intersecting fractures inside the well (**Table 6.4**). Then, the following equation was derived using these two dependent parameters:

$$Ln(K_{ave}) = -1.063\,Ln(X_1) - 1.367\,Ln(X_2) + 8.076 \qquad \textbf{(2)}$$

where K_{ave} denotes the actual average FNP obtained using the software, X_1 is the number of fracture intersections and X_2 is fracture spacing. As the software used does not provide individual well properties, an average value of all the properties from the five wells were used in this equation.

6.3.2 Only 3-D Data

In this case, all five wells in each model were independently considered and the following equation was obtained:

$$\begin{aligned} Ln(K_{ave}) = {} & 0.142\,Ln(X_1) - 0.098\,Ln(X_2) - 0.301\,Ln(X_3) \\ & + 0.168\,Ln(X_4) + 0.278\,Ln(X_5) + 2.026 \end{aligned} \qquad \textbf{(3)}$$

where K_{ave} denotes the actual average FNP, and X_1, X_2, X_3, X_4 and X_5 are the average welltest permeability values from wells 1, 2, 3, 4 and 5, respectively.

Jafari, A. and Babadagli, T.: "Calculating Equivalent Fracture Network Permeability of Multi-Layer-Complex Naturally Fractured Reservoirs," SPE 132431, Western Regional Meeting, Anaheim, California, USA, 2010.

6.3.3 1-D and 3-D Data

By combining available 1-D and 3-D data, the following equation was derived:

$$Ln(K_{ave}) = 0.41Ln(X_1) - 0.143Ln(X_2) - 0.5Ln(X_3) + 0.26Ln(X_4) + 0.59Ln(X_5) - 1.69Ln(X_6) - 1.02Ln(X_7) + 8.12 \quad \textbf{(4)}$$

where K_{ave} denotes the actual average equivalent fracture network permeability, X_1, X_2, X_3, X_4 and X_5 are the average well test permeability from wells 1, 2, 3, 4 and 5, respectively, X_6 is the number of fracture intersections in the well and finally X_7 is fracture spacing.

6.3.4 2-D and 3-D Data

In this case, three different equations using both 2-D and 3-D data which took into account the 2-D properties of the least conductive, most conductive layers, and the average of these two layers (the arithmetic average of the least and most conductive layer values) were derived, respectively:

$$Ln(K_{ave}) = 0.2Ln(X_1) - 0.153Ln(X_2) - 0.37Ln(X_3) + 0.208Ln(X_4) + 0.312Ln(X_5) - 0.035Ln(X_6) + 1.97 \quad \textbf{(5)}$$

$$Ln(K_{ave}) = 0.012Ln(X_1) - 0.09Ln(X_2) - 0.113Ln(X_3) + 0.14Ln(X_4) + 0.187Ln(X_5) - 0.0856Ln(X_6) + 2.12 \quad \textbf{(6)}$$

$$Ln(K_{ave}) = -0.042Ln(X_1) - 0.067Ln(X_2) - 0.068Ln(X_3) + 0.124Ln(X_4) + 0.172Ln(X_5) + 0.126Ln(X_6) + 2.187 \quad \textbf{(7)}$$

where K_{ave} denotes the actual average equivalent fracture network permeability, X_1, X_2, X_3, X_4 and X_5 are the average well test permeability

Jafari, A. and Babadagli, T.: "Calculating Equivalent Fracture Network Permeability of Multi-Layer-Complex Naturally Fractured Reservoirs," SPE 132431, Western Regional Meeting, Anaheim, California, USA, 2010.

from wells 1, 2, 3, 4 and 5, respectively, and X_6 *is* the connectivity index in the 2-D plane of the least conductive, most conductive and average of these two layers (the arithmetic average of the least and most conductive layer values) in **Eqs. 5**, **6** and **7**, respectively.

6.3.5 1-D, 2-D and 3-D Data

At this stage, with the assumption of the availability of all three types of data, three equations honoring all 1-D, 2-D and 3-D data were derived. 2-D properties of the least conductive, most conductive and the average of the most and least conductive layer values were taken into account, respectively:

$$Ln(K_{ave}) = 0.32Ln(X_1) - 0.15Ln(X_2) - 0.44Ln(X_3) + 0.24Ln(X_4) + 0.5Ln(X_5) - 0.8Ln(X_6) - 0.4Ln(X_7) - 0.018Ln(X_8) + 4.7 \quad \textbf{(8)}$$

$$Ln(K_{ave}) = -0.14Ln(X_1) - 0.06Ln(X_2) + 0.02Ln(X_3) + 0.09Ln(X_4) + 0.02Ln(X_5) + 0.4Ln(X_6) + 0.1Ln(X_7) - 0.1Ln(X_8) + 1.07 \quad \textbf{(9)}$$

$$Ln(K_{ave}) = -0.05Ln(X_1) - 0.06Ln(X_2) - 0.06Ln(X_3) + 0.12Ln(X_4) + 0.16Ln(X_5) - 0.8Ln(X_6) - 0.8Ln(X_7) - 0.125Ln(X_8) + 6.08 \quad \textbf{(10)}$$

where K_{ave} denotes the actual average equivalent FNP, X_1, X_2, X_3, X_4 and X_5 are the average well test permeability values from wells 1, 2, 3, 4 and 5 respectively, X_6 is the number of fracture intersection points, X_7 is fracture spacing in the well and X_8 is the connectivity index of the 2-D plane (of the least conductive, most conductive and an average of these values, respectively in **Eqs. 8**, **9** and **10**).

Jafari, A. and Babadagli, T.: "Calculating Equivalent Fracture Network Permeability of Multi-Layer-Complex Naturally Fractured Reservoirs," SPE 132431, Western Regional Meeting, Anaheim, California, USA, 2010.

The regression coefficients representing the reliability of the derived equations listed above are given in **Table 6.9**.

Table 6.9 The regression coefficients of each derived equation listed above.

Equation	Regression Coefficients (R^2)
2	0.8287
3	0.9291
4	0.9516
5	0.9515
6	0.9976
7	0.9974
8	0.9529
9	0.9999
10	0.9999

6.4 Validation

To validate the derived equations (**Eqs. 3** through **10**), five new synthetic fracture sets were generated with different properties and random representations being totally independent of the cases used for correlation development. The five cases used for validation are presented in **Table 6.10**.

Jafari, A. and Babadagli, T.: "Calculating Equivalent Fracture Network Permeability of Multi-Layer-Complex Naturally Fractured Reservoirs," SPE 132431, Western Regional Meeting, Anaheim, California, USA, 2010.

Table 6.10 New data set used to validate the derived equations.

No.	Scenario	Cases for three layers			Kmax, mD	Kmin, mD	Kave, mD
		Layer-1	Layer-2	Layer-3			
1	lDlL mDmL hDhL	L=20, D=50	L=40, D=149	L=60, D=250	82.982	4.748	19.85
2	lDlL hDhL lDlL	L=20, D=50	L=60, D=250	L=20, D=50	62.585	4.854	17.429
3	mDmL lDlL mDmL	L=40, D=149	L=20, D=50	L=40, D=149	69.089	4.733	18.084
4	hDhL mDmL hDhL	L=60, D=250	L=40, D=149	L=60, D=250	96.489	4.855	21.644
5	hDhL hDhL hDhL	L=60, D=250	L=60, D=250	L=60, D=250	124.615	4.846	24.575

Figure 6.3 through **Figure 6.11** show the actual permeability values against the predicted ones for each equation given in **Eqs. 3** through **10** respectively. In each plot, a 45^{o} line was drawn to indicate the deviations from the actual data.

As seen in **Figure 6.3**, the correlation is relatively high. This means that if the well data from five wells are fully available, one may obtain the FNP using only well data with a reasonably high correlation coefficient. Note, however, that this requires logging and coring five wells throughout the entire production zone within a 100x100 m^2 area, which may not be a common practice in reality due to its high cost.

Jafari, A. and Babadagli, T.: "Calculating Equivalent Fracture Network Permeability of Multi-Layer-Complex Naturally Fractured Reservoirs," SPE 132431, Western Regional Meeting, Anaheim, California, USA, 2010.

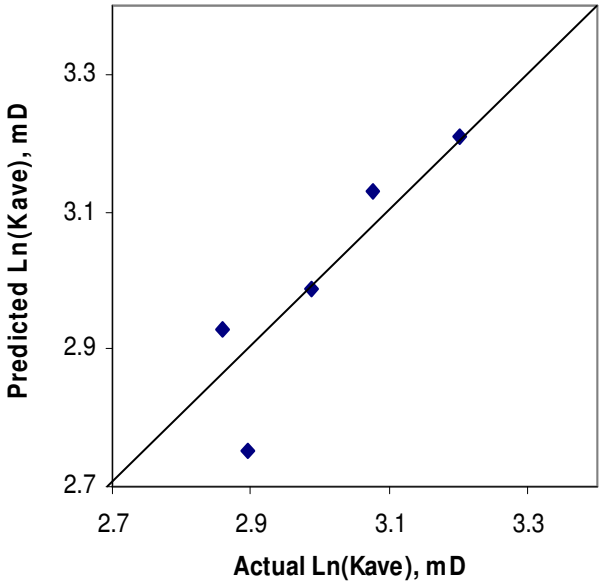

Figure 6.3 Actual average permeability against the predicted one using Eq. 2.

The next question was whether single (or more) well test data can provide good correlations with the FNP with similar accuracy. To answer this question, only 3-D (well test) data and then the combination of 1-D and 3-D data were tested. It was observed that the prediction accuracy is not in an acceptable range even if all drawdown tests from all (five) wells are included (**Figure 6.4** and **Figure 6.5**). The reason behind this could be the high degree of the heterogeneity of fracture distribution. Hence, the well test data may not be sufficient to capture local changes in the fracture network characteristic and might have been dominated only by the most conductive layer.

Jafari, A. and Babadagli, T.: "Calculating Equivalent Fracture Network Permeability of Multi-Layer-Complex Naturally Fractured Reservoirs," SPE 132431, Western Regional Meeting, Anaheim, California, USA, 2010.

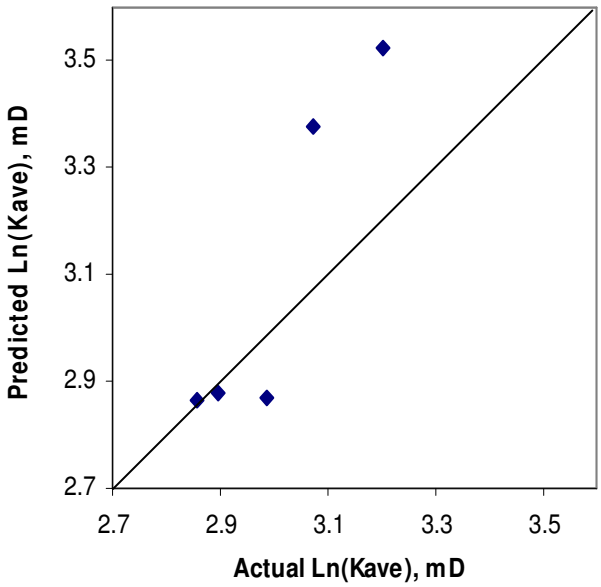

Figure 6.4 Actual average permeability against the predicted one using Eq. 3.

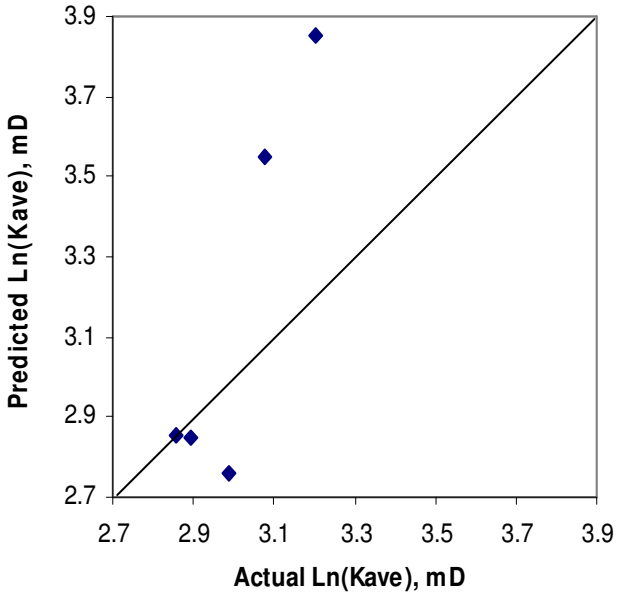

Figure 6.5 Actual average permeability against the predicted one using Eq. 4.

Jafari, A. and Babadagli, T.: "Calculating Equivalent Fracture Network Permeability of Multi-Layer-Complex Naturally Fractured Reservoirs," SPE 132431, Western Regional Meeting, Anaheim, California, USA, 2010.

Improvements can be obtained when 2-D data are combined with 3-D data (**Figure 6.6**, **Figure 6.7** and **Figure 6.8**). One may notice that adding 2-D data to 3-D data improved the permeability prediction, especially when the 2-D properties of the most conductive layer (**Figure 6.7**) were used. Although the average of the most and least conductive layer values yielded a better correlation for the FNP (**Figure 6.8**), the contribution of the data from the least conductive layer data was not as significant as the other two cases. This, in turn, shows that the layer with longer and higher number (density) fracture dominates the total fluid flow in the system and one has to pay attention to this layer in outcrop (2-D) data collection.

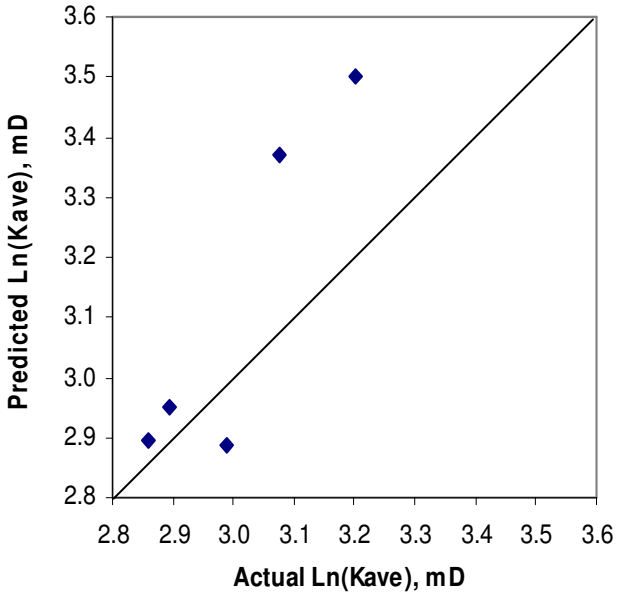

Figure 6.6 Actual average permeability against the predicted one using Eq. 5.

Jafari, A. and Babadagli, T.: "Calculating Equivalent Fracture Network Permeability of Multi-Layer-Complex Naturally Fractured Reservoirs," SPE 132431, Western Regional Meeting, Anaheim, California, USA, 2010.

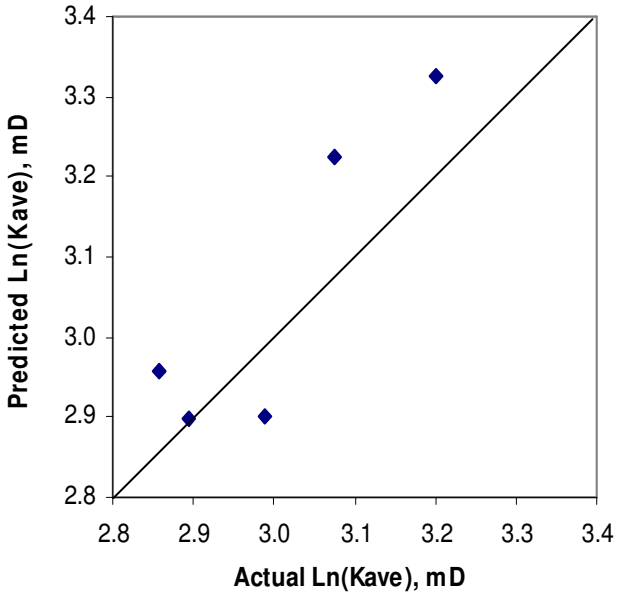

Figure 6.7 Actual average permeability against the predicted one using Eq. 6.

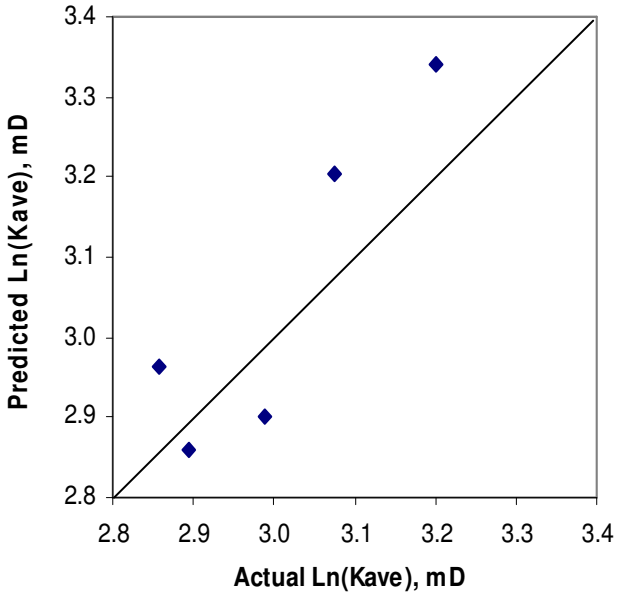

Figure 6.8 Actual average permeability against the predicted one using Eq. 7.

Jafari, A. and Babadagli, T.: "Calculating Equivalent Fracture Network Permeability of Multi-Layer-Complex Naturally Fractured Reservoirs," SPE 132431, Western Regional Meeting, Anaheim, California, USA, 2010.

Figure 6.9, **Figure 6.10** and **Figure 6.11** show the result of combining all three data types including 1-D, 2-D and 3-D data. Once again, the prediction power of the derived equations improved, especially when the 2-D properties of the most conductive layer (**Figure 6.10**) or the average value of the most and least conductive layer properties (**Figure 6.11**) were considered. Note that the deviations are typically due to the high FNP cases as seen in **Figure 6.4** through **Figure 6.9**. The addition of 2-D data of the most conductive layer resulted in a better agreement with the actual data as seen in **Figure 6.10** and **Figure 6.11**.

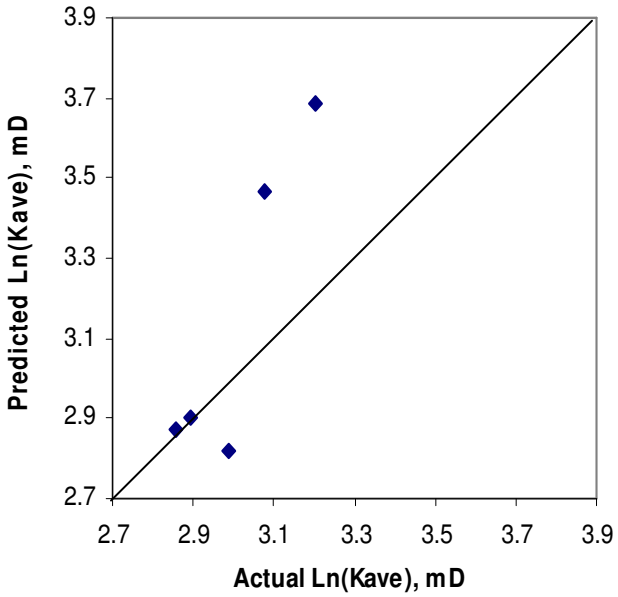

Figure 6.9 Actual average permeability against the predicted one using Eq. 8.

Jafari, A. and Babadagli, T.: "Calculating Equivalent Fracture Network Permeability of Multi-Layer-Complex Naturally Fractured Reservoirs," SPE 132431, Western Regional Meeting, Anaheim, California, USA, 2010.

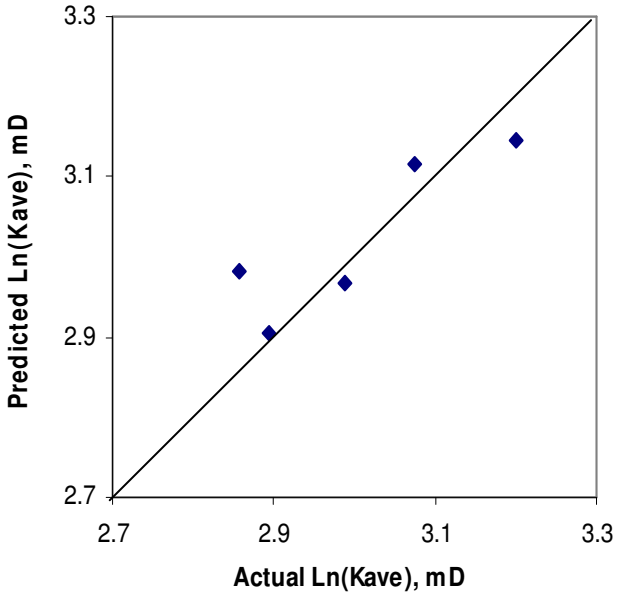

Figure 6.10 Actual average permeability against the predicted one using Eq. 9.

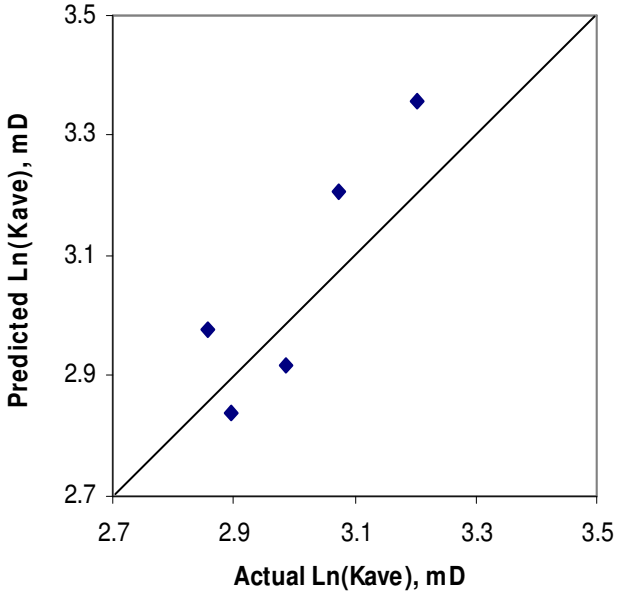

Figure 6.11 Actual average permeability against the predicted one using Eq. 10.

Jafari, A. and Babadagli, T.: "Calculating Equivalent Fracture Network Permeability of Multi-Layer-Complex Naturally Fractured Reservoirs," SPE 132431, Western Regional Meeting, Anaheim, California, USA, 2010.

6.5 Conclusions

This chapter reports an approach to estimate the fracture network permeability (FNP) of complex, multi-layer fracture network patterns. Different data sets (1-D wellbore, 2-D outcrop, and 3-D well test data) were considered for different configurations such as low, high or medium fracture density-length combinations. Different scenarios were tested considering the availability of the data, i.e., 1-D or 3-D data only, their combinations, and 1-D, 2-D, and 3-D data altogether, and eight different equations were derived to estimate the FNP and the results were validated.

The validation results revealed that using only 3-D data from different wells to predict the FNP would not yield good correlations due to wide spatial heterogeneity of the fracture properties in the reservoir, which cannot be captured from single-well tests. However, it was shown that having a combination of 1-D, 2-D and 3-D data would result in a more reliable equation. Also, it is recommended that the 2-D data of the most conductive layer in reservoir which has longer fractures with a higher density should be incorporated in the correlations. This type of layer dominates the total fluid flow regime in the whole system and hence needs to be weighed more than the other layers with lower conductivity. 1-D data from well logs and cores (the number of the fracture intersections and the distance between intersecting fractures) also yields a good correlation if enough wells representing the different parts of the reservoirs are logged and cored (5 wells in a 100x100 m^2 area in our particular example). This, however, is an expensive practice compared to the well tests and outcrop analysis.

A version of this chapter was presented and also submitted for publication

Jafari, A. and Babadagli, T.: "Calculating Equivalent Fracture Network Permeability of Multi-Layer-Complex Naturally Fractured Reservoirs," SPE 132431, Western Regional Meeting, Anaheim, California, USA, 2010.

7 Percolation-Fractal Properties and Fracture Network Permeability

7.1 Overview

In practice, all available data including 1-D (cores, logs, drilling), 2-D (outcrop) and 3-D (pressure transient tests) and even seismic data are incorporated to build a fracture network and corresponding permeability model to perform simulation. Often times, however, only a limited amount of these data are available and alternative approaches are needed. One of the options is statistical techniques based on the percolation theory as the correct characterization of fracture network topology is a critical parameter to analyze the connectivity of opposite boundaries and to eventually estimate the permeability -percolating- of the system, and this can be achieved with this theory. In this chapter, the concepts of percolation theory and fractal geometry are combined to define the connectivity characteristics of 2-D fracture networks and a new approach to estimate the equivalent fracture network permeability (EFNP) is introduced.

A version of this chapter has been submitted for publication

Jafari, A. and Babadagli, T.: "Relationship between Percolation-Fractal Properties and Fracture Network Permeability of 2-D Fracture Networks," 2010.

7.2 Synthetic fracture patterns

Using a developed algorithm, twenty different fracture patterns which cover all possible combinations of varying fracture parameters were generated. The randomly oriented fractures were distributed within a 100x100 m^2 sized domain according to a uniform distribution. In these patterns, the number of fractures per domain (density) and fracture length were of varying parameters. The number of fractures per domain varied between 50 and 250. Also, fracture length had a range of 20 to 80 meters (**Table 7.1**). Properties of each fracture pattern were defined as an average of ten different random realizations as given in **Table 7.1**. Then, using a commercial software package (FRACA), the equivalent fracture network permeability (EFNP) of each of these patterns was calculated. In this software, fracture conductivity is used instead of aperture for measuring permeability (FRACA, 2005) which is defined as the product of the intrinsic fracture permeability and the fracture aperture (e) with parallel walls. Also, the intrinsic fracture permeability and conductivity according to Poiseuille' law are expressed as $\frac{e^2}{12}$ and $\frac{e^3}{12}$ respectively (Bourbiaux et al., 1998). In all of the patterns, constant fracture conductivity, i.e., 1000 mD.m, was assigned to all fractures in the domain. Two assumptions were made for the measurement of the EFNP: (1) all fracture reservoirs consisted of only one layer, and (2) all fractures were entirely vertical.

Each 2-D fracture pattern (in the form of trace map) was imported and then a model with the above assumptions was built. The fracture network in the FRACA software was discretized with a rectangular grid and then the mass balance equations were solved by applying a pressure varying linear boundary condition for each direction. Finally, the flow rates across the

Jafari, A. and Babadagli, T.: "Relationship between Percolation-Fractal Properties and Fracture Network Permeability of 2-D Fracture Networks," 2010.

block faces were computed to calculate the EFNP (FRACA, 2005). The EFNP values for each pattern are shown in **Table 7.1**. Because only very limited number of fracture clusters in each pattern at very low fracture length and density could span the two opposite faces of the domain, the average value of EFNP over ten different realizations for these patterns was fairly low.

Table 7.1 Generated synthetic fracture patterns used in this chapter.

Pattern	Fracture Length, m	Number of Fractures	Permebaility mD
1	20	50	5.609
2	40	50	27.343
3	60	50	74.672
4	80	50	124.025
5	20	100	161.214
6	40	100	77.643
7	60	100	155.048
8	80	100	266.795
9	20	150	395.592
10	40	150	459.049
11	60	150	120.310
12	80	150	274.240
13	20	200	424.930
14	40	200	583.337
15	60	200	696.129
16	80	200	185.112
17	20	250	384.561
18	40	250	621.084
19	60	250	825.885
20	80	250	1018.037

7.3 Fractal properties of the fracture networks

Shortly after Mandelbrot's well known book on fractals (Mandelbrot, 1982) in which many different synthetic and natural fractal objects were

Jafari, A. and Babadagli, T.: "Relationship between Percolation-Fractal Properties and Fracture Network Permeability of 2-D Fracture Networks," 2010.

introduced, fractality of natural fracture patterns were tested and reported (Barton and Larsen, 1985; La Pointe, 1988; Barton and Hseih, 1989).

In this chapter, we took advantage of the usefulness of fractal geometry in the quantification of many different properties of fracture networks and developed an algorithm to calculate the fractal characteristic of generated fracture patterns (total number is 200, the different realizations of twenty different configurations is given in **Table 7.1**).

We begin with the classical box counting dimension as first tested by Barton and Larsen (1985) for fracture networks according to the following relationship:

$$N(r) \alpha r^{-D} \tag{1}$$

where $N(r)$ is the number of the boxes (grids) containing different fracture features, r is the box sizes and D is the fractal dimension. In this commonly used technique, the fractal dimension is obtained by overlaying a set of different boxes (grids) with different sizes on the fracture network and counting the number of boxes containing different fracture features (fracture intersection points, fracture lines, etc) for each box size. A plot of the number of occupied boxes versus the size of those boxes is developed and then the slope of the straight line fitted to the points gives the fractal dimension of that specific feature of the fracture network. The fractal dimension of fracture intersection points and fracture lines was measured using this technique.

Other fracture network characteristics were quantified by applying different statistical and fractal techniques. To consider the orientation effect, a

Jafari, A. and Babadagli, T.: "Relationship between Percolation-Fractal Properties and Fracture Network Permeability of 2-D Fracture Networks," 2010.

square was overlaid on the fracture domain. Then, a number of imaginary scanning lines in the X and Y directions (horizontal and vertical) inside the square were defined. Next, the number of intersections between these scanning lines and fracture lines were counted. This process was repeated with different square sizes and at the end, the number of intersections was plotted against the square size and the slope of the best fitted line was calculated (Babadagli, 2001). The effects of fracture orientation on the EFNP were taken into account with this method. If all fractures are either in the X (horizontal) or Y (vertical) directions, the fractal dimension using the X and Y-direction scanning lines would be different from each other; but in randomly uniform distributed fractures, these two fractal dimensions are expected to be close to each other.

A new parameter called the connectivity index was defined as the total number of intersection point divided by the total number of fracture lines to take into account the connectivity (intersection). The results are presented in **Table 7.2**. One may notice that all the fractal dimensions lie between 1 and 2 which indicates the fractal nature of a 2-D system and there is meaningful relation between the fractal dimensions and fracture length as well as number of fractures. Note that twelve different fractal and statistical characteristics of fracture networks were tested against permeability and five of them listed in **Table 7.2** were observed to show the strongest correlation (Jafari and Babadagli, 2008). For further details about the measurement of these fractal properties, readers are referred to previous publications (Jafari and Babadagli, 2008 and 2009).

Jafari, A. and Babadagli, T.: "Relationship between Percolation-Fractal Properties and Fracture Network Permeability of 2-D Fracture Networks," 2010.

Table 7.2 Fractal dimension of different features of the synthetics fracture networks.

Length	Number of Fractures	FD of intersection points	FD of X-scanning lines	FD of Y-scanning lines	Connectivity Index	FD of fracture lines	Permeability mD
20	50	1.162	1.565	1.592	0.732	1.336	5.609
40	50	1.605	1.180	1.204	3.478	1.501	77.643
60	50	1.747	1.038	1.029	8.096	1.588	120.310
80	50	1.839	0.979	0.969	13.702	1.641	185.112
20	100	1.577	1.424	1.522	1.435	1.504	27.343
40	100	1.843	1.223	1.223	6.530	1.647	155.048
60	100	1.912	1.052	1.059	15.968	1.714	274.240
80	100	1.941	0.993	0.984	27.270	1.761	384.561
20	150	1.778	1.746	1.692	2.225	1.594	74.672
40	150	1.913	1.236	1.237	9.439	1.722	266.795
60	150	1.940	1.039	1.044	24.705	1.774	424.930
80	150	1.967	0.980	0.982	41.930	1.816	621.084
20	200	1.868	1.546	1.530	2.853	1.657	124.025
40	200	1.941	1.220	1.225	13.395	1.769	395.592
60	200	1.963	1.039	1.041	32.229	1.814	583.337
80	200	1.980	0.980	0.980	56.216	1.847	825.885
20	250	1.905	1.444	1.405	3.640	1.701	161.214
40	250	1.957	1.177	1.167	16.858	1.798	459.049
60	250	1.970	1.041	1.029	40.944	1.838	696.129
80	250	1.984	0.986	0.981	70.622	1.866	1018.037

7.4 Percolation theory and fracture network permeability

Percolation theory is a general mathematical theory which can be used to describe the connectivity and conductivity (permeability) of systems with complex geometry (Stauffer and Aharony, 1992). The advantage of using this theory is that many results can be expressed through simple algebraic relationships known as scaling law (power laws) (King et al., 2002). Density of the objects placed randomly in space is directly related to the overall properties of the system of interest (Masihi et al.; 2005, 2007). The easiest model for understanding what the percolation theory is all about is an infinite lattice consisting of sites and bonds. Now, suppose some of

Jafari, A. and Babadagli, T.: "Relationship between Percolation-Fractal Properties and Fracture Network Permeability of 2-D Fracture Networks," 2010.

these either sites or bonds are occupied (open to flow) with a probability "*p*". For small values of this "*p*", most of the occupied sites (or bonds) form isolated clusters (connected occupied sites). As this probability increases, number of these clusters increase and also, some of those grow or merge into others and at a particular value known as percolation threshold, one of these clusters spans the entire domain and connects the opposite faces together. This critical value depends on the detail and dimensionality of the lattice or grid. Around this critical threshold, the following simple analytical term known as scaling law or power law exists (King et al., 2002; Masihi et al., 2005, 2007):

$$P(p) \alpha (p - p_c)^{\beta} \qquad p > p_c \tag{2}$$

where $P(p)$ is the probability that a site or bond connected to the spanning cluster in the domain. The exponent β is known as the universal exponent and it is independent of the lattice characteristics, and only depends on the dimensionality of space. Hence, whether the system is lattice or continuum percolation, its value would be the same being 0.139 and 0.4 for 2D and 3D spaces, respectively.

The above percolation analysis using lattice is called lattice percolation. However, in fracture analyses using this theory, fractures need to be placed randomly and independently within a continuum space. This is called continuum percolation and interestingly, the same scaling (power) laws with the same critical exponents as in lattice percolation apply to the continuum percolation (King et al., 2002).

The major advantage of continuum percolation against the lattice

percolation in the analysis of fracture networks is that fractures can be placed at any location in the domain and are not limited to any specific points on the lattice. Also, the number of fracture intersections (connectivity) is not limited to any specific (maximal) number (Masihi, 2005). It has been postulated that there is a relationship between the effective permeability of a system and its percolation properties presented by the following scaling law (Stauffer and Aharony, 1992):

$$K_{eff}\ \alpha(p - p_c)^{\mu} \tag{3}$$

where K_{eff} is the effective permeability, p and p_c are occupancy probability and percolation threshold respectively, and μ is a universal exponent.

The main focus of this chapter was to improve the relationship given in **Eq. 3** to further develop a methodology to obtain equivalent (effective) fracture network permeability. The readily available 2-D fractal and statistical properties of fracture networks were used in this exercise.

The most difficult part of using percolation theory in a continuum system is to define an equivalent term to the occupancy probability in lattice percolation. As suggested by Adler and Thovert (1999), this could be done by using the excluded volume concept. Thus, using the excluded volume (3-D objects) concept introduced by Balberg et al. (1984), the excluded area (2-D) of fractures was calculated using the following equation:

$$A_{ex} = \frac{2}{\pi} l^2 \tag{4}$$

Jafari, A. and Babadagli, T.: "Relationship between Percolation-Fractal Properties and Fracture Network Permeability of 2-D Fracture Networks," 2010.

where A_{ex} is the excluded area and l is the length of the fractures in the pattern. This equation is valid for isotropic (randomly and uniformly) oriented fracture patterns (Adler and Thovert, 1999).

Next, the fracture density of each fracture pattern, which is defined as the number of fractures per domain area, was calculated using the following relationship suggested by Khamforoush et al. (2008):

$$\rho = \frac{N_{fr}}{L^2} \quad \textbf{(5)}$$

where ρ is fracture density, N_{fr} is the number of fractures in the domain and L^2 is the area of the domain, which was taken as 100x100 m^2 in this chapter.

Then, the dimensionless density of each fracture pattern was calculated as follows (Khamforoush et al., 2008; Adler and Thovert, 1999):

$$\rho' = \rho . A_{ex} \quad \textbf{(6)}$$

It is necessary to mention that by using an excluded area to dimensionless the fracture density, macroscopic properties of fracture networks become independent of fracture shape as shown earlier (Adler, 1992; Huseby et al., 1997; Koudina et al., 1998; Whitaker, 1998; Mardia and Jupp, 2000; Huseby et al., 2001; Bogdanov et al., 2003a; Bogdanov et al., 2003b; Mourzenko et al., 2004; Vaentini et al., 2007; Khamforoush et al., 2008).

For 2-D randomly oriented fracture sticks, the continuum percolation threshold in terms of dimensionless density (ρ'_c) has been determined to

be 3.6 (Adler and Thovert, 1999). Since the purpose of this chapter was to show any possible correlation between fractal-percolation properties and equivalent fracture network permeability (EFNP) and not specifically the percolation threshold for these finite-sized fracture patterns, to eventually propose a practical method to estimate EFNPs, this number was adopted and used throughout this chapter for the evaluation of the percolation properties of different fracture patterns. The results of the percolation analysis of different patterns are presented in **Table 7.3**. In this table, two fracture patterns ended up with a negative ($\rho'-\rho'_c$) value and these permeability values were ignored. This can be attributed to the finite size effect of the fracture patterns as explained by King et al. (2002), i.e., it is possible to have connectivity and hence permeability, at much lower values than the percolation threshold due to the random nature of the process.

Table 7.3 Percolation proeprties of different fracture patterns.

Length	Number of Fractures	Excluded Area (Aex)	Fracture Density (ρ)	Dimensionless Density (ρ')	(ρ'-ρ'c)	Permeability mD
20	50	254.777	0.005	1.274	-2.326	5.609
40	50	1019.108	0.005	5.096	1.496	77.643
60	50	2292.994	0.005	11.465	7.865	120.310
80	50	4076.433	0.005	20.382	16.782	185.112
20	100	254.777	0.01	2.548	-1.052	27.343
40	100	1019.108	0.01	10.191	6.591	155.048
60	100	2292.994	0.01	22.930	19.330	274.240
80	100	4076.433	0.01	40.764	37.164	384.561
20	150	254.777	0.015	3.822	0.222	74.672
40	150	1019.108	0.015	15.287	11.687	266.795
60	150	2292.994	0.015	34.395	30.795	424.930
80	150	4076.433	0.015	61.146	57.546	621.084
20	200	254.777	0.02	5.096	1.496	124.025
40	200	1019.108	0.02	20.382	16.782	395.592
60	200	2292.994	0.02	45.860	42.260	583.337
80	200	4076.433	0.02	81.529	77.929	825.885
20	250	254.777	0.025	6.369	2.769	161.214
40	250	1019.108	0.025	25.478	21.878	459.049
60	250	2292.994	0.025	57.325	53.725	696.129
80	250	4076.433	0.025	101.911	98.311	1018.037

Jafari, A. and Babadagli, T.: "Relationship between Percolation-Fractal Properties and Fracture Network Permeability of 2-D Fracture Networks," 2010.

7.5 Analysis of the results and discussion

To estimate equivalent fracture network permeability through **Eq. 3**, we begin with the relationship between fractal and percolation properties of generated fracture patterns. **Figure 7.1** shows that as the fractal dimension of fracture intersection points increases, the dimensionless density (**Eq. 6**) increases for all fracture densities. The relationship is not linear and all the curves converge as the fractal dimension value approaches a fractal dimension value of two. Note that the dimensionless density is dependent on the number of fractures, fracture length, and also the shape and size of the domain. As expected, the fracture patterns with a higher number of fractures have higher fractal dimensions and after a critical value of the dimensionless density, the fractal dimension of the intersection points do not change regardless of the fracture density.

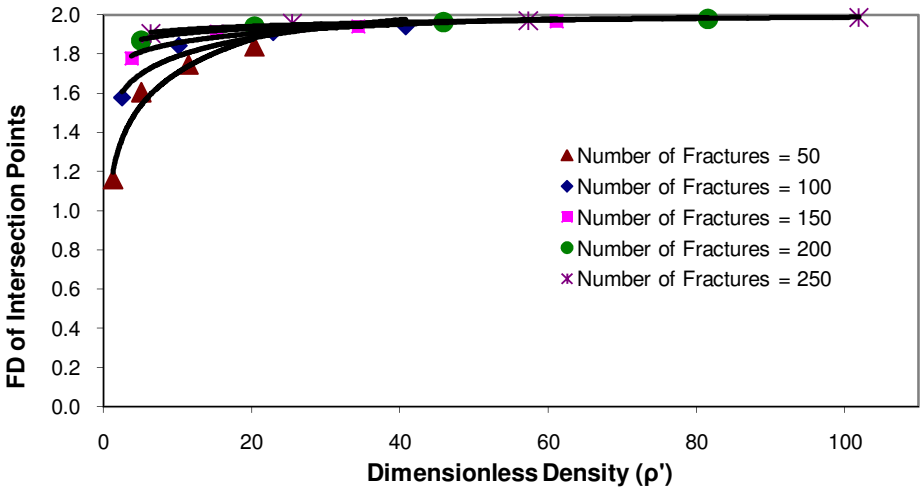

Figure 7.1 Fractal dimension (FD) of fracture intersection points vs. dimensionless density for different fracture densities and lengths.

Jafari, A. and Babadagli, T.: "Relationship between Percolation-Fractal Properties and Fracture Network Permeability of 2-D Fracture Networks," 2010.

In **Figure 7.2** and **Figure 7.3**, the fractal dimension obtained through the scanning lines technique in both the X- and Y-directions is plotted against the difference between dimensionless density and the dimensionless percolation threshold ($\rho'-\rho'_c$). The curves in these plots show the same trend as in **Figure 7.1**, because fractures were placed and oriented within the domain randomly and according to a uniform distribution and there is not any bias in their orientation. As can also be inferred from these figures, an inverse relationship exists between the fractal dimension of scanning lines in the X- and Y-directions and ($\rho'-\rho'_c$). If fact, the more uniformly and randomly oriented the fractures were in the domain, the more similar the fractal dimensions of scanning lines in X and Y-directions. In other words, if fractures were oriented mostly in one direction, the fractal dimension of scanning lines in the X- and Y-directions would be different and as a result, they show a different trend against ($\rho'-\rho'_c$).

One may note that for a given number of fractures in the domain, as the fracture length increases, the fractal dimension of the scanning lines in the X- and Y-directions decreases, especially near the percolation threshold at which ($\rho'-\rho'_c$) will experience a continuous increase.

Jafari, A. and Babadagli, T.: "Relationship between Percolation-Fractal Properties and Fracture Network Permeability of 2-D Fracture Networks," 2010.

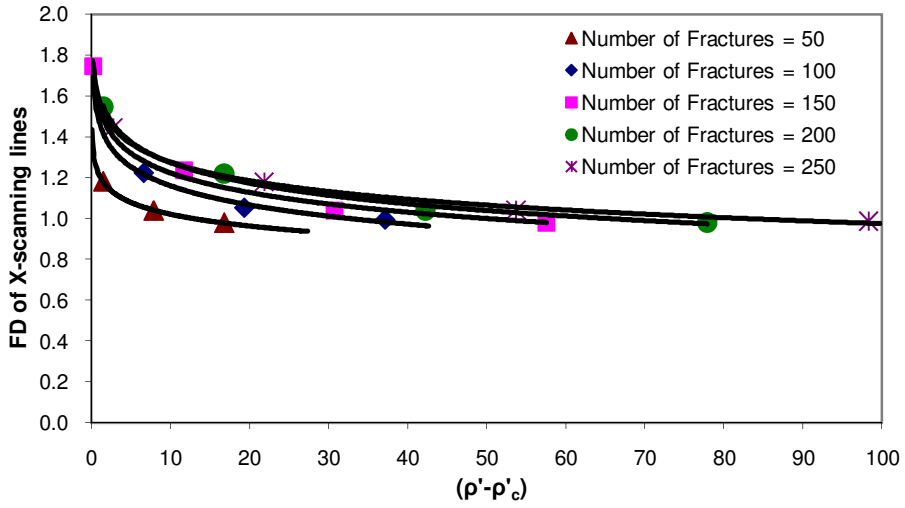

Figure 7.2 Fractal dimension of X-scanning lines (in X-direction) vs. the difference between dimensionless density and dimensionless percolation threshold ($\rho'-\rho'_c$) for different fracture densities and lengths.

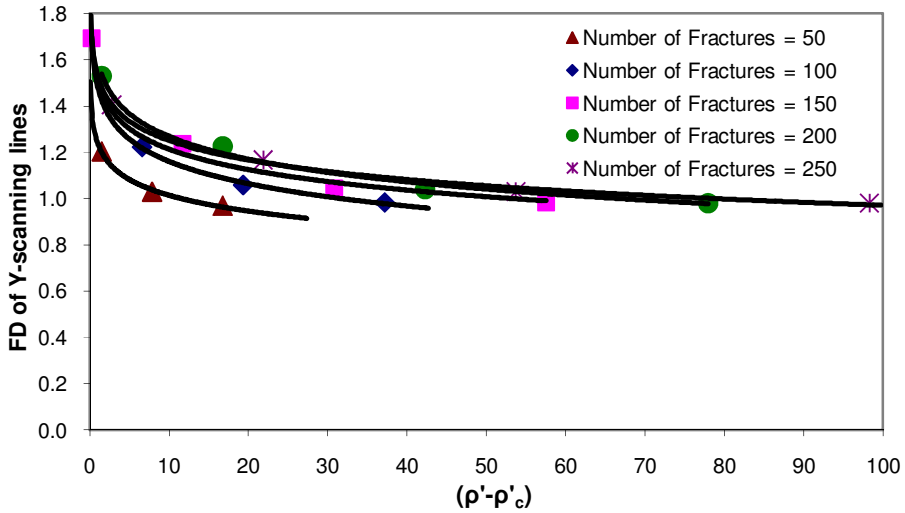

Figure 7.3 Fractal dimension of Y-scanning lines (in Y direction) vs. the difference between dimensionless density and dimensionless percolation threshold ($\rho'-\rho'_c$) for different fracture densities and lengths.

.

Jafari, A. and Babadagli, T.: "Relationship between Percolation-Fractal Properties and Fracture Network Permeability of 2-D Fracture Networks," 2010.

The connectivity index was plotted against $(\rho'-\rho'_c)$ in **Figure 7.4**. A linear relationship is obvious. Both connectivity index and $(\rho'-\rho'_c)$ primarily depend on the number of fractures and fracture length as well as the domain size. For instance, for a given number of fractures in the domain, connectivity index and $(\rho'-\rho'_c)$ both increase by an increase in fracture length. It can also be noticed that fracture patterns with a higher number of fractures have higher $(\rho'-\rho'_c)$ values.

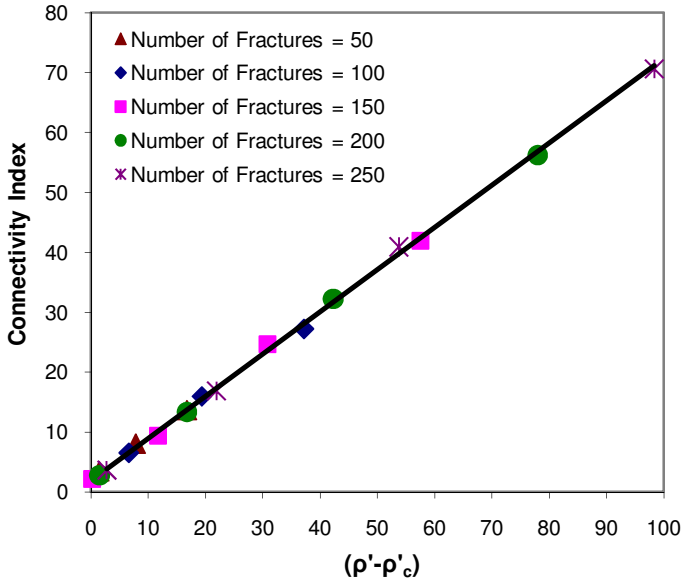

Figure 7.4 Connectivity index vs. the difference between dimensionless density and dimensionless percolation threshold $(\rho'-\rho'_c)$ for different fracture densities and lengths.

Figure 7.5 illustrates the change of the fractal dimension of fracture lines with the dimensionless density. The behavior is not linear, especially close to the percolation threshold. One may infer from this plot that as the fractal dimension becomes bigger and approaches the value of two (this means that spatially the fractures are uniformly located within the entire domain),

Jafari, A. and Babadagli, T.: "Relationship between Percolation-Fractal Properties and Fracture Network Permeability of 2-D Fracture Networks," 2010.

the chances of having a percolating network increases. As a result of this, the dimensionless density increases accordingly. Finally, at higher dimensionless densities, the curves converge, representing a case of very well developed fracture networks in the system.

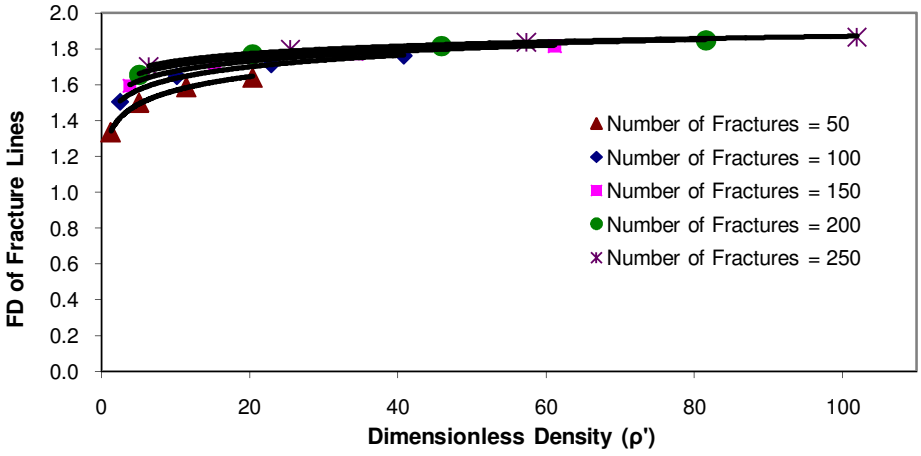

Figure 7.5 Fractal dimension of fracture lines vs. dimensionless density for different fracture densities and lengths.

Finally, the equivalent fracture network permeability was plotted against $(\rho'-\rho'_c)$ in **Figure 7.6**. There is a non linear-direct relationship between these two parameters but an obvious trend is observed. Also, the higher the number of fractures in the domain, the higher the equivalent fracture network permeability (EFNP), especially around the percolation threshold [low values of $(\rho'-\rho'_c)$]. For a given number of fractures, as fracture length increases, the $(\rho'-\rho'_c)$ and EFNP increase. At higher values of $(\rho'-\rho'_c)$, all curves converge and follow the same trend. To show this converging trend the points were connected, which is represented by solid lines.

Jafari, A. and Babadagli, T.: "Relationship between Percolation-Fractal Properties and Fracture Network Permeability of 2-D Fracture Networks," 2010.

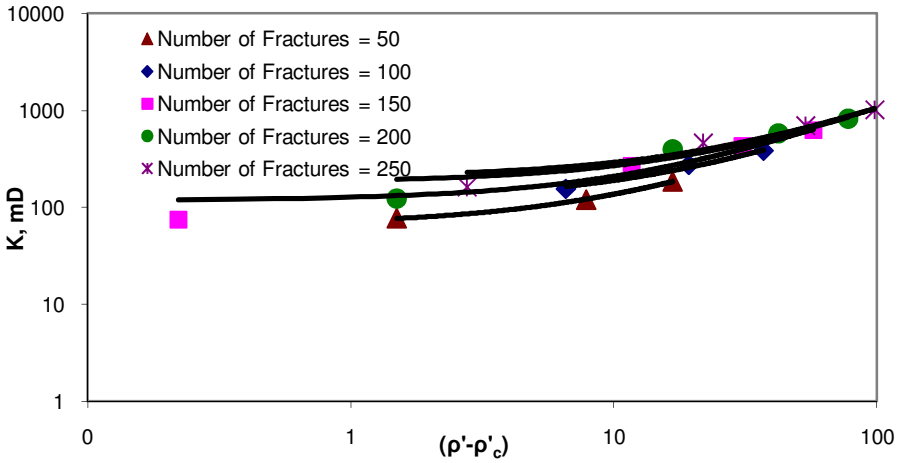

Figure 7.6 Equivalent fracture network permeability vs. the difference between dimensionless density and dimensionless percolation threshold ($\rho'-\rho'_c$) for different fracture densities and lengths.

In the final attempt, the above plot was split into five separate (log-log) plots for each curve (**Figure 7.7** through **Figure 7.11**) and a line was fitted to data in each plot which correlates the equivalent fracture network permeability to ($\rho'-\rho'_c$). The general form of this relationship is as follows:

$$K = A(\rho' - \rho'_c)^{\mu} \qquad \textbf{(7)}$$

where K is the equivalent fracture network permeability, A is the proportionality constant, μ is the permeability exponent and finally ρ' and ρ'_c are dimensionless density and percolation threshold, respectively (Zhang and Sanderson, 2002).

In all these plots (fracture patterns with different number of fractures), as

fracture length increases, the $(\rho'-\rho'_c)$ and accordingly the equivalent fracture network permeability increases. The value of the permeability exponent varies between 0.344 and 0.526 for each fracture pattern with a different number of fractures. However, as was mentioned earlier, two fracture permeability values were obtained as negative due to negative values of $(\rho'-\rho'_c)$, which could be attributed to the finite size effect on the fracture patterns. Those negative values were ignored and that is why only three points exist in **Figure 7.7** and **Figure 7.8**. If fact, this could be an indication that some systems with finite size start percolating with much lower probability density (or any other equivalent parameter) than the percolation threshold determined for infinite systems or even not do not percolate at a much higher probability density than the percolation threshold of infinite systems (King et al., 2002) due to the random nature of fracture networks.

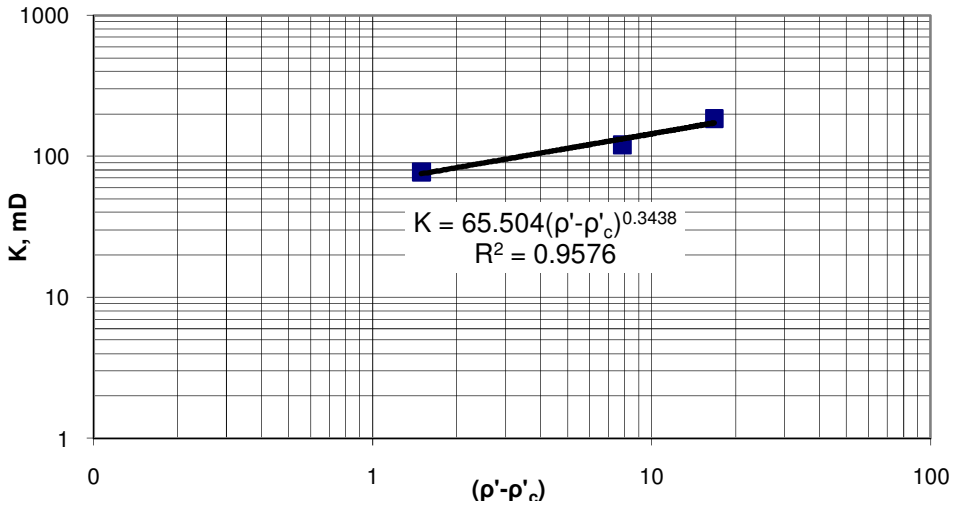

Figure 7.7 Equivalent fracture network permeability vs. the difference between dimensionless density and dimensionless percolation threshold $(\rho'-\rho'_c)$ for a fracture pattern with N_{fr}=50.

Jafari, A. and Babadagli, T.: "Relationship between Percolation-Fractal Properties and Fracture Network Permeability of 2-D Fracture Networks," 2010.

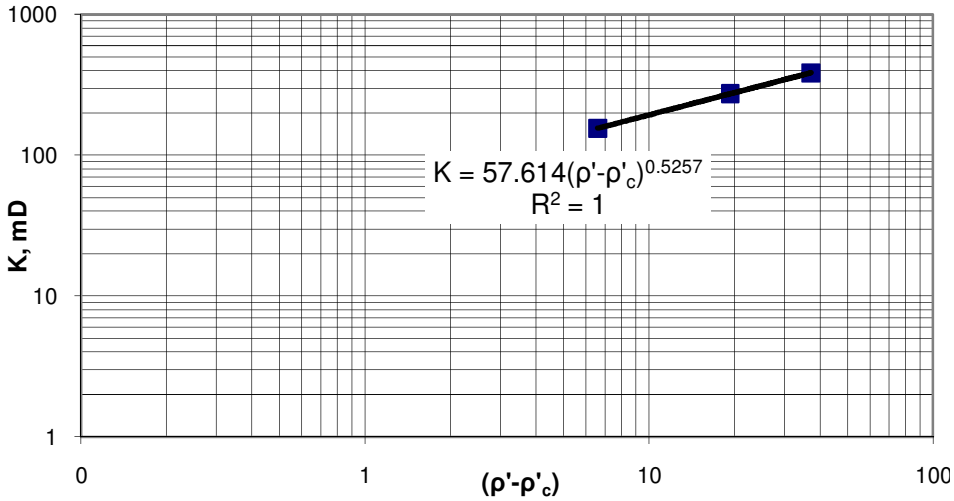

Figure 7.8 Equivalent fracture network permeability vs. the difference between dimensionless density and dimensionless percolation threshold ($\rho'-\rho'_c$) for a fracture pattern with N_{fr}=100.

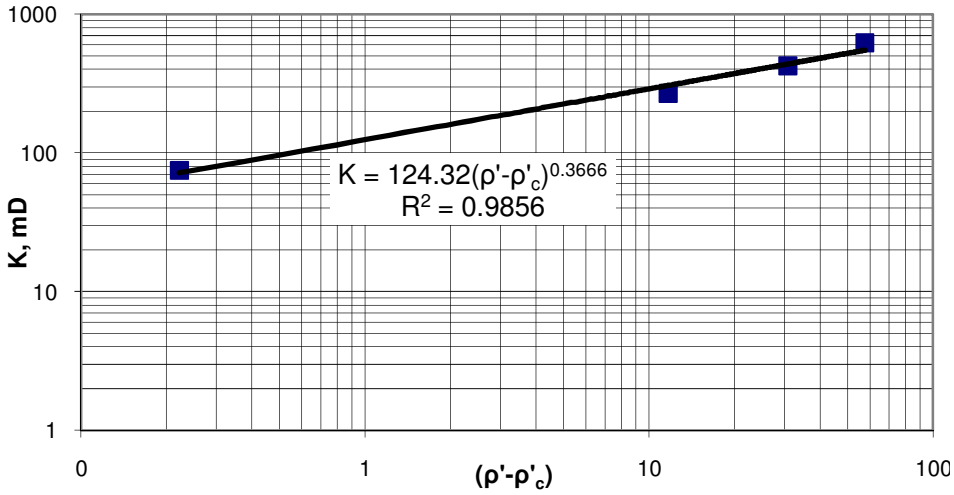

Figure 7.9 Equivalent fracture network permeability vs. the difference between dimensionless density and dimensionless percolation threshold ($\rho'-\rho'_c$) for a fracture pattern with N_{fr}=150.

Jafari, A. and Babadagli, T.: "Relationship between Percolation-Fractal Properties and Fracture Network Permeability of 2-D Fracture Networks," 2010.

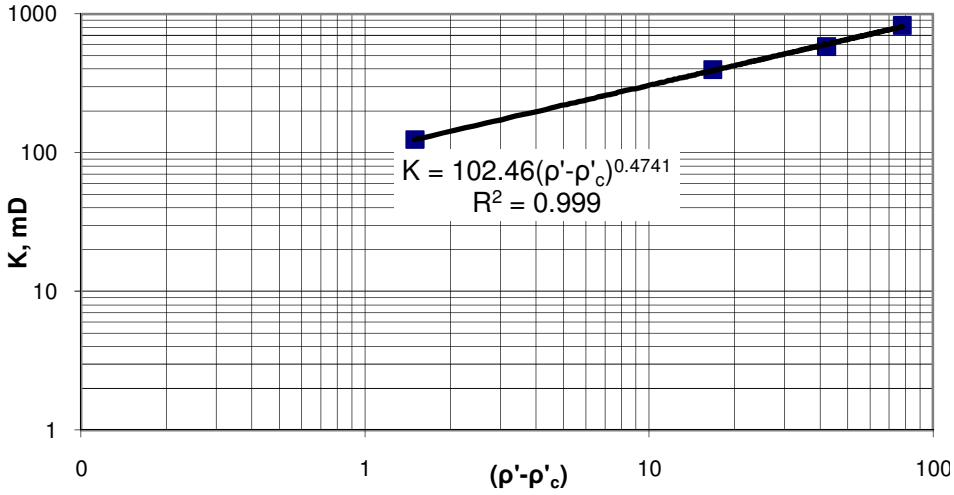

Figure 7.10 Equivalent fracture network permeability vs. the difference between dimensionless density and dimensionless percolation threshold ($\rho'-\rho'_c$) for a fracture pattern with N_{fr}=200.

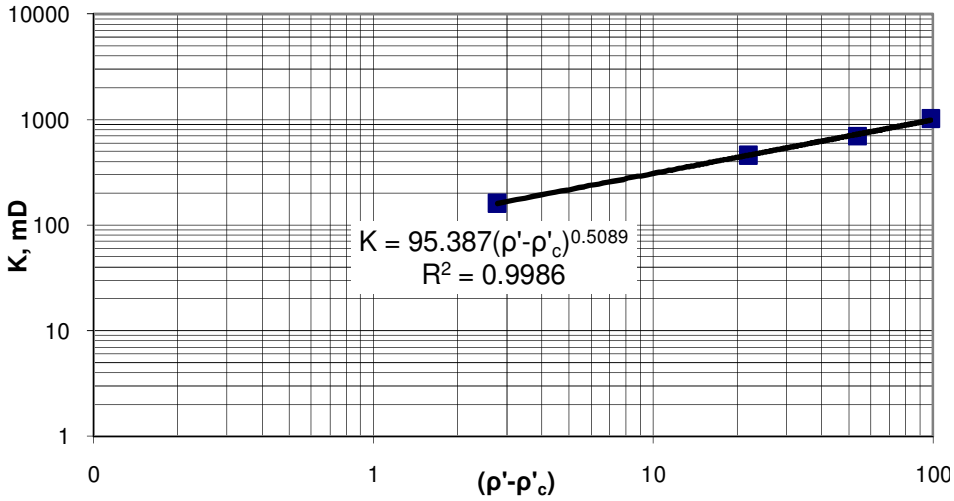

Figure 7.11 Equivalent fracture network permeability vs. the difference between dimensionless density and dimensionless percolation threshold ($\rho'-\rho'_c$) for a fracture pattern with N_{fr}=250.

Jafari, A. and Babadagli, T.: "Relationship between Percolation-Fractal Properties and Fracture Network Permeability of 2-D Fracture Networks," 2010.

One possible application of the joint characterization of 2-D fractal-percolation properties is that by correlating the fractal dimension of different features to $(\rho'-\rho'_c)$ and then $(\rho'-\rho'_c)$ to the equivalent fracture network permeability and deriving relationships, it would be possible to estimate the equivalent fracture network permeability of the fracture pattern of interest. In this case, the permeability estimation will be conditioned to both fractal and percolation properties of the systems which supposedly improve the accuracy of the estimation. Therefore, five parameters including the fractal dimension of intersection points (FDi), the fractal dimension of fracture lines (FDl), Connectivity index (CI), fractal dimension of scanning lines in the X-direction (FDx) and the fractal dimension of scanning lines in the Y-direction (FDy) were plotted against $(\rho'-\rho'_c)$. The equations for these correlations were presented in **Table 7.4** through **Table 7.8**. Note that in each table the first equation is for all fracture cases, i.e., all cases with a different number of fractures were put together to derive this equation. The other five equations in these tables were for different numbers of fractures, as shown by indices. If the number of fractures (in a sense, the fracture density) is known, one may select the particular equation corresponding to the known value of the number of fractures. This obviously increases the accuracy as indicated by a very high regression coefficient (the second column of the **Tables 7.4**) except in the case of the connectivity index value, which also yielded a very high value of regression coefficient for the all fracture cases (given as the first equation in the tables).

Jafari, A. and Babadagli, T.: "Relationship between Percolation-Fractal Properties and Fracture Network Permeability of 2-D Fracture Networks," 2010.

Table 7.4 Relationship between the fractal dimension of intersection points (FDi) for different numbers of fractures in the domain and $(\rho'-\rho'_c)$ along with the regression coefficient (R^2). The first equation is for all fracture densities (number of fractures).

Equation	R^2
$FDi = 0.0452Ln(\rho'-\rho'_c) + 1.7758$	0.5408
$FDi_{50} = 0.0949ln(\rho'-\rho'_c) + 1.5632$	0.992
$FDi_{100} = 0.0575ln(\rho'-\rho'_c) + 1.7362$	0.9914
$FDi_{150} = 0.0336ln(\rho'-\rho'_c) + 1.8284$	0.9989
$FDi_{200} = 0.0284ln(\rho'-\rho'_c) + 1.8579$	0.9982
$FDi_{250} = 0.0221ln(\rho'-\rho'_c) + 1.884$	0.9903

Table 7.5 Relationship between the fractal dimension of fracture lines (FDl) for different numbers of fractures in the domain and. $(\rho'-\rho'_c)$ along with the regression coefficient (R^2). The first equation is for all fracture densities (number of fractures).

Equation	R^2
$FDl = 0.0526Ln(\rho'-\rho'_c) + 1.5901$	0.6842
$FDl_{50} = 0.057ln(\rho'-\rho'_c) + 1.4764$	0.9948
$FDl_{100} = 0.0653ln(\rho'-\rho'_c) + 1.5232$	0.998
$FDl_{150} = 0.0381ln(\rho'-\rho'_c) + 1.6463$	0.978
$FDl_{200} = 0.0478ln(\rho'-\rho'_c) + 1.6362$	0.9993
$FDl_{250} = 0.0464ln(\rho'-\rho'_c) + 1.6537$	0.9999

Table 7.6 Relationship between the connectivity index (CI) for different numbers of fractures in the domain and. $(\rho'-\rho'_c)$ along with the regression coefficient (R^2). The first equation is for all fracture densities (number of fractures) .

Equation	R^2
$CI = 0.7003(\rho'-\rho'_c) + 2.0397$	0.9991
$CI_{50} = 0.6662(\rho'-\rho'_c) + 2.6196$	0.9984
$CI_{100} = 0.6755(\rho'-\rho'_c) + 2.3845$	0.9981
$CI_{150} = 0.7018(\rho'-\rho'_c) + 1.9868$	0.9979
$CI_{200} = 0.701(\rho'-\rho'_c) + 1.9081$	0.9996
$CI_{250} = 0.7003(\rho'-\rho'_c) + 2.0397$	0.9991

Jafari, A. and Babadagli, T.: "Relationship between Percolation-Fractal Properties and Fracture Network Permeability of 2-D Fracture Networks," 2010.

Table 7.7 Relationship between the fractal dimension of scanning lines in the X-direction (FDx) for different numbers of fractures in the domain and $(\rho'-\rho'_c)$ along with the regression coefficient (R^2). The first equation is for all fracture densities (number of fractures).

Equation	R^2
$FDx = -0.119\ln(\rho'-\rho'_c) + 1.4671$	0.7761
$FDx_{50} = -0.084\ln(\rho'-\rho'_c) + 1.2126$	0.9995
$FDx_{100} = -0.136\ln(\rho'-\rho'_c) + 1.472$	0.9822
$FDx_{150} = -0.139\ln(\rho'-\rho'_c) + 1.5435$	0.9945
$FDx_{200} = -0.146\ln(\rho'-\rho'_c) + 1.6103$	0.9941
$FDx_{250} = -0.131\ln(\rho'-\rho'_c) + 1.5765$	0.9973

Table 7.8 Relationship between the fractal dimension of scanning lines in the Y-direction (FDx) for different numbers of fractures in the domain and $(\rho'-\rho'_c)$ along with the regression coefficient (R^2). The first equation is for all fracture densities (number of fractures).

Equation	R2
$FDy = -0.114\ln(\rho'-\rho'_c) + 1.4468$	0.7876
$FDy50 = -0.099\ln(\rho'-\rho'_c) + 1.2411$	0.9961
$FDy100 = -0.139\ln(\rho'-\rho'_c) + 1.4817$	0.995
$FDy150 = -0.128\ln(\rho'-\rho'_c) + 1.5084$	0.9912
$FDy200 = -0.142\ln(\rho'-\rho'_c) + 1.5952$	0.9918
$FDy250 = -0.122\ln(\rho'-\rho'_c) + 1.5307$	0.9956

Finally, to obtain the effective fracture network permeability values using **Eq. 7**, the equivalent permeability of all cases was plotted against $(\rho'-\rho'_c)$ and the corresponding relationship in the form of an equation was presented in **Figure 7.12**.

Jafari, A. and Babadagli, T.: "Relationship between Percolation-Fractal Properties and Fracture Network Permeability of 2-D Fracture Networks," 2010.

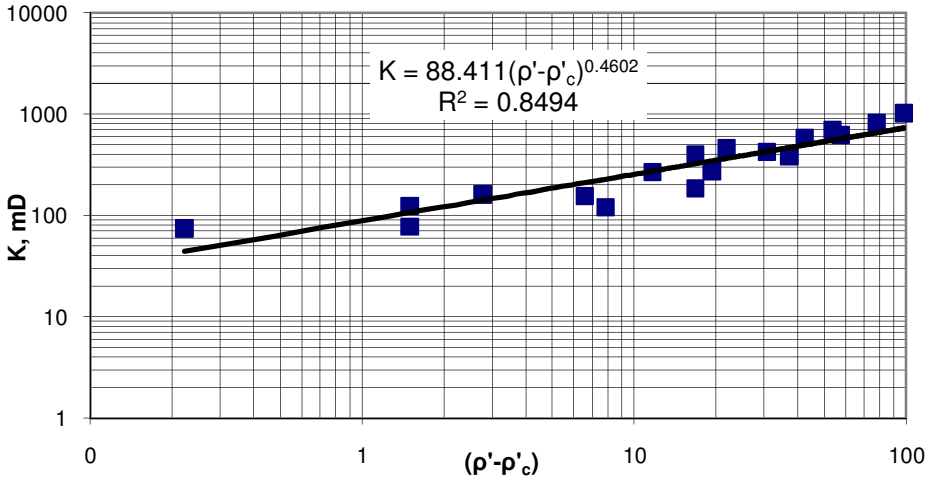

Figure 7.12 Equivalent fracture network permeability of all cases vs. the difference between dimensionless density and dimensionless percolation threshold ($\rho'-\rho'_c$).

Also, by manipulation of the **Eq. 3**, the following equation can be derived to determine the shortest (or minimum) fracture length required for a given specific number of fractures and domain size to be percolating:

$$l_{\min} = sqrt\left(\left(\rho'_c . L^2 . \pi\right)/\left(2N_{fr}\right)\right) \qquad \textbf{(8)}$$

where $l_{\min}$ is the shortest or minimum fracture length required to be percolating, L^2 is the area of domain and N_{fr} is the number of fractures in the domain. These minimum fracture lengths were calculated for a different number of fractures but the same domain size and are given in **Figure 7.13**.

Jafari, A. and Babadagli, T.: "Relationship between Percolation-Fractal Properties and Fracture Network Permeability of 2-D Fracture Networks," 2010.

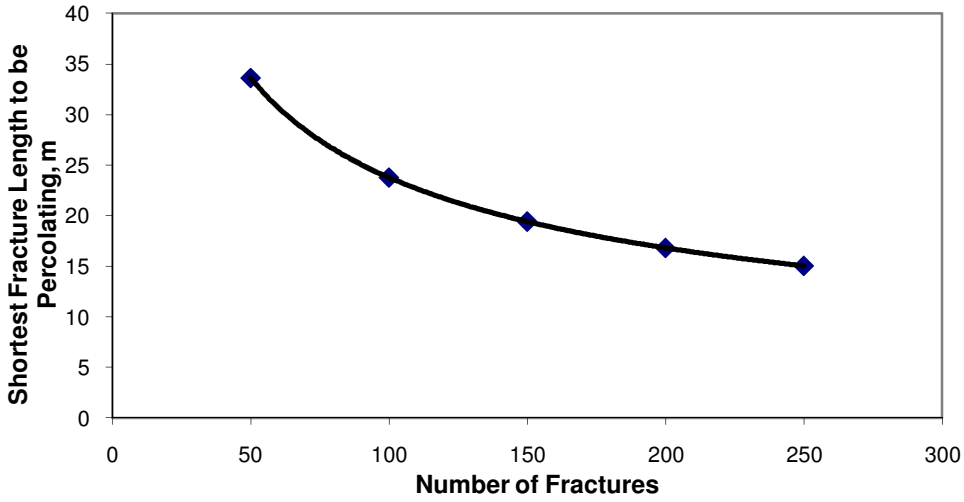

Figure 7.13 Minimum required fracture length to be percolating versus number of fractures.

As obvious from **Figure 7.13**, the lower the number of fractures in the domain, the longer the required fracture length. It is also essential to mention that this minimum required fracture length depends on both the number of fractures and also the size of the domain or system. This observation and **Eq. 8** has practical importance to determine the shortest length of fracture to have a percolating (or conductive) fracture network system for a given fracture density (number of fractures).

7.6 Validation of results

To validate the methodology introduced and the equations, a set of new fracture patterns with different random realizations were considered. Their properties (fractal dimension of intersection points, fractal dimension of

Jafari, A. and Babadagli, T.: "Relationship between Percolation-Fractal Properties and Fracture Network Permeability of 2-D Fracture Networks," 2010.

fracture line, connectivity index and also fractal dimension of scanning lines in the X- and Y-directions) were calculated and the equivalent fracture network permeability values for each pattern were computed using FRACA software. The results are presented in **Table 7.9**.

Table 7.9 Fractal dimension of different features of the fracture networks used for validation.

Length	Number of Fractures	FD of intersection points	FD of scanning line in X-direction	FD of scanning line in Y-direction	Connectivity Index	FD of fracture lines	Permeability mD
20	100	1.573	1.503	1.527	1.730	1.505	27.346
20	200	1.875	1.396	1.520	2.700	1.664	132.320
40	100	1.835	1.289	1.275	6.180	1.654	150.122
40	200	1.950	1.304	1.288	13.530	1.766	413.981
60	100	1.917	1.020	1.017	16.570	1.715	298.754
60	200	1.969	1.028	1.020	31.730	1.814	552.036
80	100	1.953	1.017	1.004	25.550	1.764	367.481
80	200	1.972	0.975	0.977	57.605	1.844	858.655

Then, using the first equation of each table presented in **Table 7.4** through **Table 7.8**, $(\rho'-\rho'_c)$ of each fracture pattern was calculated. Here, we assumed that there is no information available on the number of the fractures in each case (pattern) and as a result the first equation of each table, which represents an average values of all fracture patterns, were used to estimate $(\rho'-\rho'_c)$. Once again, if the number of fractures in the domain is known, one can use the related equation for that specific number of fractures (as shown by indices) instead of using the general equation (the first equation in each table). In this case, the error of the estimated $(\rho'-\rho'_c)$ would be much lower. Next, these values were plugged into the equation given in **Figure 7.12** and the equivalent permeability of each pattern was computed. The results are presented in **Table 7.10** for five different fracture network properties. In this table, the value of $(\rho'-\rho'_c)$ obtained using the

connectivity index in the first row was negative; thus, the permeability calculation was omitted.

Table 7.10 Calculated ($\rho'-\rho'_c$) values using different equations presented in Tables 7.4 through 7.8 and their corresponding equivalent fracture network permeability using the equation given in Figure 7.15.

Length	Number of Fractures	($\rho'-\rho'_c$) using FDi	K	($\rho'-\rho'_c$) using FDl	K	($\rho'-\rho'_c$) using Cl	K	($\rho'-\rho'_c$) using FDx	K	($\rho'-\rho'_c$) using FDy	K
20	100	0.011	11.239	0.197	41.895	-0.442	-	0.739	76.914	0.497	64.072
20	200	8.968	242.622	4.074	168.743	0.943	86.050	1.819	116.430	0.525	65.734
40	100	3.686	161.154	3.338	153.959	5.912	200.292	4.485	176.383	4.499	176.626
40	200	47.576	522.925	28.341	412.008	16.408	320.384	3.939	166.146	4.034	167.974
60	100	22.677	371.834	10.760	263.846	20.749	356.932	42.723	497.662	43.400	501.278
60	200	72.350	634.189	71.112	629.174	42.397	495.911	40.083	483.266	42.329	495.547
80	100	50.069	535.360	27.061	403.341	33.572	445.410	43.825	503.532	48.834	529.245
80	200	76.079	649.030	123.890	812.309	79.345	661.706	62.458	592.700	61.598	588.932

A comparison of the predicted and actual (FRACA values) EFNPs is given in **Figure 7.14**. Although the general equation for ($\rho'-\rho'_c$) was used for each case (given as the first equation in **Table 7.4** through **Table 7.8**), the correlation between the predicted and actual values of EFNPs is very strong. It is interesting to note that the best correlation was obtained when the fractal dimensions of fracture lines were used to estimate the ($\rho'-\rho'_c$) values for any fracture length and density values. Corresponding regression coefficients for each case are given in **Table 7.11**. To improve the accuracy of estimation one may choose an average value of EFNPs estimated using these five (or fewer) network properties. If one has to choose only one property, the fractal dimension of fracture lines obtained through the box counting method would yield the most accurate estimation. The correlation between these two EFNP values is reasonably good, indicating that the approach presented can be used for practical purposes.

Jafari, A. and Babadagli, T.: "Relationship between Percolation-Fractal Properties and Fracture Network Permeability of 2-D Fracture Networks," 2010.

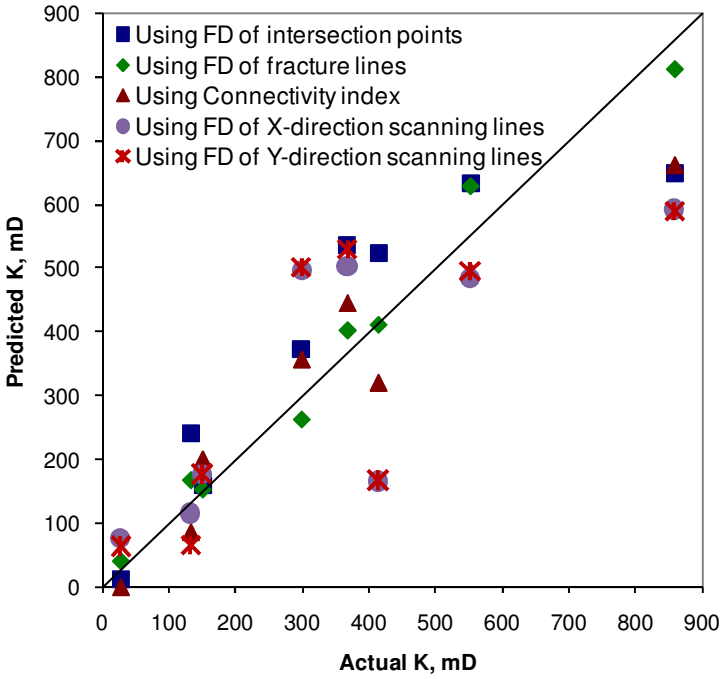

Figure 7.14 Predicted equivalent fracture network permeability vs. the actual permeability obtained using FRACA software.

Table 7.11 Correlation coefficients for the comparison of actual and predicted EFNP's (Figure 7.14) obtained through five different fractal-statistical properties.

$(\rho'-\rho'_c)$ obtained using	R^2
FD of intersection points	0.81
FD of fracture lines	0.98
Connectivity index	0.9
FD of X-direction scanning lines	0.61
FD of Y-direction scanning lines	0.59

Jafari, A. and Babadagli, T.: "Relationship between Percolation-Fractal Properties and Fracture Network Permeability of 2-D Fracture Networks," 2010.

7.7 Conclusions and remarks

(1) The relationships between different fracture network properties, i.e., fractal and percolation properties, and their equivalent fracture network permeability were investigated and analyzed. It was found that a nonlinear-direct relationship exists between the fractal dimension of fracture intersection points and fracture lines (using the box counting technique) and the dimensionless density. In these cases, at close to percolation threshold, patterns with different number of the fractures have different fractal dimension of intersection points and fracture lines; however, at higher dimensionless density, all curves relating to different numbers of fractures diverge into a single value, which is the maximum fractal dimension of two in each case. This is attributed to an increase in the number of the fractures and also the fracture length in the domain, which eventually causes an increase in both fractal dimension and dimensionless density.

(2) The connectivity index shows a direct relation against $(\rho'-\rho'_c)$ because both are mostly being controlled by the number of the fractures, the fracture length and the domain size.

(3) It was also shown that there is a non-linear inverse relationship between the fractal dimension of scanning lines in the X- and Y-directions and $(\rho'-\rho'_c)$. While $(\rho'-\rho'_c)$ continuously increases with an increase in fracture length for a given number of fractures, the fractal dimension of scanning lines in the X- and Y-directions decreases starting at the percolation threshold.

Jafari, A. and Babadagli, T.: "Relationship between Percolation-Fractal Properties and Fracture Network Permeability of 2-D Fracture Networks," 2010.

(4) Correlations between equivalent fracture network permeability and (ρ'-ρ'_c) for different number of fractures (fracture density) were developed. It was found that for the finite size fracture patterns, the permeability exponent (μ) varies between 0.344 and 0.526. This variation could be explained with regard to the size of each fracture pattern through the finite size effect on percolation properties.

(5) The relationship between the number of fractures in the domain and the minimum size of the fracture length was presented to have a percolating system for 2-D randomly distributed fractures. A correlation was introduced, for a given fracture domain, to quickly estimate the possibility of connectivity (percolation).

(6) A methodology and correlations were presented to estimate the equivalent fracture network permeability (EFNP) of 2-D fracture networks using fractal properties of 2-D fracture networks and percolation properties, i.e., percolation density and threshold. The validation exercise confirmed that the technique can be used to estimate the EFNP practically. The fractal dimension of fracture lines (obtained using the box counting technique) yielded a more accurate estimation compared to the fractal dimension of intersection points, connectivity index, and fractal dimension of scanning lines in X- and Y-directions used to calculate the (ρ'-ρ'_c) values and the EFNP from it.

Jafari, A. and Babadagli, T.: "Relationship between Percolation-Fractal Properties and Fracture Network Permeability of 2-D Fracture Networks," 2010.

8 Contributions and recommendations

As this is a paper-based thesis, conclusions were provided at the end of each chapter. Here, the major contributions out of this dissertation and also recommendations for future works were presented.

8.1 Major contributions to the literature and industry

The major contributions of this dissertation to the literature and industry are listed below:

8.1.1 Specific contributions to the literature

- In general, the fracture network properties (mainly fracture density and length) dominate over the single fracture conductivity for the permeability of fracture networks. Even, if the density and length are low, this observation is satisfied as long as single fracture conductivity is not very high. The conductivity of individual fractures starts becoming the dominating term over the network properties as the density and length values decrease, reaching a certain -low- range and when the conductivity is high enough. The limiting ranges of the values of these properties were defined in chapter 2. The common practice in the industry is to use single fracture conductivity in the estimation of effective fracture network permeability (EFNP), based on the density values obtained from

core or image logs. Our observations showed that one should be careful about this as fracture network properties dominate the EFNP over single fracture conductivity in many circumstances, as they are the parameters which have a direct impact on obtaining a percolating network.

- Relationships between the fractal-statistical properties of networks and EFNP were quantitatively determined. It was shown that strong relationships exist between the EFNP values and five fractal-statistical parameters (among a total of 10 parameters) representing different fracture network features including the fractal dimension of intersection points, the fractal dimension fracture lines and the fractal dimension of X-and Y- directions scanning lines, as well as a statistical parameter, i.e., connectivity index.

- It was also shown that there are strong relationships between the fractal-statistical parameters and the percolation properties of fracture networks. Then, using these relationships, and also a relationship between the percolation properties and the EFNP which was shown as a power law term, a few correlations for predicting EFNP were proposed. In fact, fractal and percolation properties were combined to reduce any possible error in the estimation of EFNP due to lack of data, especially on the connectivity of the network. Using the fractal properties of fracture networks and their presented relationships with the percolation properties, the percolation properties of the system were calculated and from the latter, the EFNP was estimated. Also, a criterion was presented to determine the minimal fracture length for a given number of

fractures (fracture density) and domain size to have a percolating (or permeable) fracture network.

- An artificial neural network (ANN) with the back-propagation algorithm was presented which takes five fractal-statistical inputs and then gives (predicts) the EFNP as the output. It was found that a supervised back propagation network with five inputs and one hidden layer consisting of five neurons and a sigmoid transfer function would be able to capture the highly complex and nonlinear relationships among the fractal and statistical properties of fracture networks (five of them was observed to be the most critical ones out of twelve).

8.1.2 General Contributions to the industry

- The conditions to obtain EFNP for practical applications based on the available data (1-D well, 2-D outcrop, and 3-D welltest) were presented. It was shown that honoring all three types of data results in the best estimate of the actual EFNP. The accuracy of using only 1-D well data and 3-D well test data was surprisingly comparable to the situation where five 2-D fractal-statistical parameters from outcrop studies and the permeability obtained from a single well pressure transient (3-D) data are used. Hence, 1-D single well data could be useful when it is used along with the permeability obtained from a single well pressure transient test. However, for better accuracy, this can be supported by additional fractal-statistical measurements on 2-D patterns obtained from outcrop studies. Fracture network characteristics (or types) that require the

incorporation of 2-D data were identified. Once the practitioners have a certain degree of information on fracture network characteristics, based on the observations summarized above, they can develop an optimal data collection strategy to minimize the data cost for mapping fracture networks accurately.

- A simple methodology was proposed to quickly analyze whether or not the fracture system of interest is capable of having permeability (being above the percolation threshold based on number of fractures, domain size and fracture length).

- It is believed that the new methodology and results presented in this dissertation will be useful for practitioners in the static model development of naturally fractured reservoirs and will shed light on further studies on modeling, as well as understanding the transmissibility characteristics of fracture networks.

8.2 Recommendations for future work

This research work was done on 2-D fracture networks which could be extended to 3-D models. This, however, requires further algorithm development to utilize 2-D fractal characteristics for 3-D systems and/or the development of fractal measurement techniques for 3-D systems in different planes (not only in the X-Y plane but also, in the X-Z and Y-Z planes). This work will provide a guideline for this type of research. In this research, it was assumed that all fractures are vertically oriented by intersecting the top and bottom of each layer; taking the fracture dips in the network into account is also recommended.

9 Bibliography

Acuna, J.A., Ershaghi, I., Yortsos, Y.C., 1992. Fractal analysis of pressure transients in the Geysers geothermal field. In Proceedings: Seventeenth Workshop on Geothermal Reservoir Engineering, Stanford University, Stanford, California, Jan. 29-31, 87-93.

Acuna, J. A., Ershaghi, I., Yortsos, Y. C., 1995. Practical application of fractal pressure-transient analysis in naturally fractured reservoirs. SPE Formation Evaluation, 10(3): 173-179.

Addison, P. S., 1997. Fractals and chaos: An illustrated course. Institute of Physics Publishing, Bristol and Philadelphia, pp. 256.

Adler, P.M., 1992. Porous media. Butterworth-Heinemann, Stoneham, MA.

Adler. P.M. and Thovert, J.-F., 1999. Fracture and Fracture Networks. Kluwer Academic, Dordrecht.

Arkan, S., Akin, S. and Parlaktuna, M., 2002. Effect of calcite scaling on pressure transient analysis of geothermal wells. Proceedings, Twenty-Seventh Workshop on Geothermal Reservoir Engineering, Stanford University, Stanford, California, January 28-30.

Babadagli, T., 2002. Scanline method to determine the fractal nature of 2-D fracture networks. Mathematical Geology, 34(6): 647-670.

Babadagli, T., 2000. Evaluation of outcrop fracture patterns of geothermal reservoirs in southwestern Turkey. Proceedings World Geothermal Congress, Kyushu, Tohoku, Japan, May 28 - June 10.

Babadagli, T., 2001. Fractal analysis of 2-D fracture networks of geothermal reservoirs in south-western Turkey. J. of Volcanology and Geothermal Research, 112: 83-103.

Balberg, I., Anderson C.H., Alexander, S. and Wagner, N., 1984. Excluded Volume and its Relation to the Onset of Percolation. Physical Review B, 30, 3933.

Barenblatt, G. I., and Zheltov, Y. P., 1960. Fundamental equations of filtration of homogenous liquids in fissured rocks. Sov. Dokl. Akad. Nauk., Engl. Transl., 13: 545-548.

Barenblatt, G. I., Zheltov, Y. P. and Kochina, I. K., 1960. Basic concepts in the theory of seepage of homogenous liquids in fissured rocks. Sov. Appl. Math. Mech., Engl. Transl., 24: 852-864.

Barton, C.C., Larson, E., 1985. Fractal geometry of two-dimensional fracture networks at Yucca Mountain, south-western Nevada. Proceedings of International Symposium on Fundamentals of Rock Joints, Bjorkliden, Sweden, 77-84.

Barton, C. C. and Hsieh, P. A., 1989. Physical and hydrologic-flow properties of fractures. Field Trip Guidebook, T385, 28th Int. Geol. Cong. Washington D.C.

Barton, C. C., 1995. Fractal analysis of scaling and spatial clustering of fractures. In: Barton, C. C, La Pointe, P. R. (Eds.), Fractals in the earth sciences. Plenum Press, New York, pp. 168.

Berkowitz, B. and Balberg, I., 1993. Percolation theory and its application to groundwater hydrology. Water Resources Research, 29(4): 775-194.

Berkowitz, B. and Ewing, R.P., 1998. Percolation theory and network modeling applications in soil physics. Surveys in Geophysics, 19: 23-72.

Bogdanov, I.I., Mourzenko, V.V., Thovert, J.-F. and Adler, P.M., 2003b. Two-phase flow through fractured porous media. Physical Review E, 68, 026703.

Berkowitz, B., 1995. Analysis of Fracture Network Connectivity Using Percolation Theory. Mathematical Geology, 27(4).

Berkowitz, B., 1994. Modeling and contaminant transport in fractured media. in Advances in Porous Media, 2, edited by. Y. Corapcioglu, 397-451, Elsevier, New York.

Berkowitz, B. and Hadad, A., 1997. Fractal and multifractal measures of natural and synthetic fracture networks. J. of Geophysical Research,

102(B6): 205-218, June 10.

Bogdanov, I. I., Mourzenko, V. V., Thovert, J. F. and Adler, P. M., 2003a. Effective permeability of fractured porous media in steady state flow. Water Resources Research, 39(1), 1023, doi: 10.1029/2001WR000756.

Bonnet, E., Bour, O., Odling, N. E., Davy, P., Main, I., Cowie, P. and Berkowitz, B., 2001. Scaling of fracture systems in geological media. Rev. of Geoph., 39 (3): 347-383.

Bourbiaux, B., Cacas, M. C., Sarda, S. and Sabathier, J. C., 1998. A rapid and efficient methodology to convert fractured reservoir images into a dual-porosity model. Oil & Gas Science and Technology Rev. IFP, 53(6): 785-799, DOI:10.2516/ogst:1998069.

Bourbiaux, B., Granet, S., Landereau, P., Noetinger, B., Sarda, S. and Sabathier, J. C., 1999. Scaling up matrix-fracture transfers in dual-porosity models: Theory and Application. SPE 56557, Annual Technical Conference and Exhibition held in Houston, Texas, 3–6 October.

Bunde, A. and Havlin, S., 1995. Brief introduction to fractal geometry. In: Bunde, A., Havlin, S. (Eds), Fractals in Science. Springer, Berlin, 298 pp.

Cacas, M. C., Sarda, S., Bourbiaux, B. and Sabathier, J. C., 2000. Method for determining the equivalent fracture permeability of a fracture

network in a subsurface multi-layerd medium. United States Patent, Patent Number: 6,023,656.

Cacas, M. C., Ledoux, E. and De Marsily, G., 1990. Modeling fracture flow with a stochastic discrete fracture network: Calibration and Validation**.** Water Resources Research, 26(3): 479-500.

Cox, D. R. and Reid, N., 2000. The theory of the design of experiments. Chapman & Hall/CRC Press.

Dershowitz, B., La Pointe, P., Eiben, T. and Wei, L., 2000. Integration of Discrete Feature Network Methods with Conventional Simulator Approaches. SPE Res. Eval. & Eng., 3 (2), April.

Ferreira, T. A., Rasband, W., 2010. The ImageJ User Guide Version 1.43. U. S. National Institutes of Health, Bethesda, Maryland, USA. Available on World Wide Web at http://rsb.info.nih.gov/ij/

FRACA, 2005. User's technical manual. BeicipFranlab, Rueil-Malmaison, France.

Hamida, T., Babadagli, T., 2005. Effects of ultrasonic waves on immiscible and miscible displacement in porous media. SPE 95327, presented at SPE Annual Technical Conference and Exhibition, Dallas, Texas, USA.

Hamida, T., Babadagli, T., 2007. Fluid-fluid interaction during miscible and immiscible displacement under ultrasonic waves. European Physical J. B, 60: 447–462.

Huseby, O., Thovert, J.-F. and Adler, P.M., 1997. Geometry and topology of fracture systems. J. Physics A, 30, 1415.

Huseby, O., Thovert, J.-F. and Adler, P.M., 2001. Dispersion in three-dimensional fracture networks. Phys. Fluids, 13, 594.

Itasca Consulting Group Inc., 2000. UDEC user's guide. City, Minnesota, USA.

Jafari, A. and Babadagli, T., 2008. A sensitivity analysis for effective parameters on fracture network permeability. SPE 113618, Western Regional and Pacific Section AAPG Joint Meeting, Bakersfield, California, U.S.A., 31 March–2 April 2008.

Jafari, A. and Babadagli, T., 2009a. A sensitivity analysis for effective parameters on 2-D fracture network permeability. SPE Res. Eval. and Eng., 12(3): 455-469.

Jafari, A. and Babadagli, T., 2009b. Generating 3-D permeability map of fracture networks using well, outcrop and pressure transient data. SPE 124077, SPE/EAGE Reservoir Characterization and Simulation Conference. Also accepted for publication in SPE Res. Eval. and Eng.

Jafari, A. and Babadagli, T., 2010a. Practical estimation of equivalent fracture network permeability of geothermal reservoirs. in proceedings World Geothermal Congress, Bali, Indonesia, 20-25 April, 10 pp.

Jafari, A. and Babadagli, T., 2010b. Calculating equivalent fracture

network permeability of multi-layer-complex naturally fractured reservoirs. SPE 132431, presented at SPE Western Regional Meeting, Anaheim, California, U.S.A., 27-29 May.

Jafari, A. and Babadagli, T., 2010c. Effective Fracture Network Permeability of Geothermal Reservoirs. Accepted for publication in Geothermics.

Karperien, A., 2005. FracLac V.2, Charles Stuart University, NSW, Australia. 38 pp.

King, P.R., Andrade Jr., J.S., Buldyrev, S.V., Dokholyan, N.V., Lee, Y., Havlin, S., and Stanley, H.E., 1999. Predicting Oil Recovery using Percolation. Physica A, 266: 107-114.

Kirkpatrick, S., 1971. Classical transport in disordered media: Scaling and Effective-Medium Theories. Pyhs. Rev. Lett., 27: 1722-1725.

Khamforoush, K., Shams, K., Thovert, J.-F. and Adler, P. M., 2008. Permeability and Percolation of Anisotropic Three-Dimensional Fracture Networks. Physical Review E, 77, 056307.

King, P.R., Buldyrev, S.V., Dokholyan, N.V., Havlin, S., Lopez, E., Paul, G. and Stanley, H.E., 2002. Percolation Theory. DIALOG [London Petrophysical Society Newsletter] 10/3.

Koudina, N., Gonzales Garcia, R., Thovert, J.-F. and Adler, P.M., 1998. Permeability of Three-Dimensional Fracture Networks. Physical Review E, 57, 4466.

La Pointe, P. R., 1988. A method to characterize fracture density and connectivity through fractal geometry. Int. J. Rock Mech. Min. Sci. Geomech. Abstr., 25: 421-429.

La Pointe, P. R., 1997. Flow compartmentalization and effective permeability in 3D fractal fracture networks. Int. J. Rock Mech. Min. Sci., 34 (3/4), 171.

Lee, J., 1982. Well Tesing. SPE Textbook Series, 1.

Long, J. C. S., Remer, J. S., Wilson, C. R. and Witherspoon, P. A., 1982. Porous media equivalents for networks of discontinuous fractures. Water Resources Research, 18(3): 645-658.

Long, J. C. S., Gilmour, P. and Witherspoon, P. A., 1985. A model for steady fluid flow in random three-dimensional networks of disk-shaped fractures. Water Resources Research, 21(8): 1105-1115.

Long, J.C.S. and Billaux, D. M., 1987. From field data to fracture network modeling: An example incorporating spatial structure. Water Resources research, 23(7): 1201-1216.

Lough, M. F., Lee, S. H. and Kamath, J., 1996. A new method to calculate the effective permeability of grid blocks used in the simulation of

naturally fractured reservoirs. SPE 36730, SPE Annual, Technical Conference and Exhibition, Denver, Colorado, U.S.A.

Lough, M. F., Lee, S. H., Kamath, J., 1997. A new method to calculate the effective permeability of grid blocks used in the simulation of naturally fractured reservoirs. SPE Res. Eng., 12(3): 219-224.

Mandelbrot, B. B., 1982. The fractal geometry of nature. W. H. Freeman and Co., San Francisco, 460.

Mardia, K.V. and Jupp, P.E., 2000. Directional Statistics. John Wily & Sons, Chichester, U.K.

Margolin, G., Berkowitz, B. and Scher, H., 1998. Structure, flow and generalized conductivity scaling in fracture networks. Water Resour. Res., 34: 2103-2121.

Masihi, M, King, P.R. and Nurafza, P., 2007. Fast Estimation of Connectivity in Fractured Reservoirs using Percolation Theory. SPE Journal, June.

Masihi, M, King, P.R. and Nurafza, P., 2005. Fast Estimation of Performance Parameters in Fractured Reservoirs using Percolation Theory. SPE 94186, SPE Europe/EAGE Annual Conference, Madrid Spain.

Mason, R. L., Gunst, R. F. and Hess, J. L., 2003. Statistical design and analysis of experiments with applications to engineering and science. John Wiley & Sons, Inc.

Massonnat, G. and Manisse, E., 1994. Modelisation des reservoirs fractures et recherché de parameters equivalents: etude de l'anisotropie verticale de permeability. Bull. Centres Rech. Explor. Prod. Elf Aquitaine, 18: 171-209.

MATLAB User's Guide Version 4: Neural Network Toolbox for Use with MATLAB.

Matsumoto, N., Yomogida, K. and Honda, S., 1992. Fractal analysis of fault systems in Japan and the Philippines. Geophys. Res. Lett., 19(4): 357-360.

Min, K.B., Jing, L., Stephansson, O., 2004. Determining the equivalent permeability tensor for fractured rock masses using a stochastic REV approach: method and application to the field data from Sellafield, UK. Hydrogeology Journal, 12(5): 497-510.

Montgomery, D. C., 2005. Design and analysis of experiments. Sixth edition, John Wiley & Sons, Inc.

Mourzenko, V. V., Thovert, J. F. and Adler, P. M., 2001. Permeability of self-affine fractures. Transport in Porous Media, 89-103.

Mourzenko, V.V., Thovert, J.-F. and Adler, P.M., 2005. Percolation and

Permeability of Three Dimensional Fracture Networks with a Power Law Size Distribution. Fractals in Engineering, Springer London.

Mourzenko, V.V., Thovert, J.-F. and Adler, P.M., 2004. Macroscopic permeability of three-dimensional fracture networks with power-law size distribution. Physical Review E, 69, 066307.

Murphy, H., Huang, C., Dash, Z., Zyvoloski, G. and White, A., 2004. Semianalytical solutions for fluid flow in rock joints with pressure-dependent openings. Water Resources Research, 40, W12506, doi: 10.1029/2004WR003005.

Nakashima, T., Arihar, N. and Sato, K. 2001. Effective Permeability Estimation for Modeling Naturally Frcatured Reservoirs. SPE 68124, SPE Middle East Oil Show held in Bahrain, 17–20 March.

Nakashima, T., Sato, K., Arihar, N. and Yazawa, N., 2000. Effective Permeability Estimation for Simulation of Naturally Fractured Reservoirs. SPE Asia Pacific Oil and Gas Conference and Exhibition held in Brisbane, Australia, 16–18 October.

Narr, W., Schechter, D. W. and Thompson, L. B., 2006. Naturally fractured reservoir characterization. Society of Petroleum Engineers, Printed in USA, Pages 112.

Nelson, R. A., 2001. Geological analysis of naturally fractured reservoirs. Second edition, Golf Professional Publishing Company, pp. 332.

Nikravesh, M., Aminzadeh, F. and Zadeh, L. A., 2003. Soft computing and intelligent data analysis in oil exploration. Elsevier, First Edition.

Nolte, D.D., Pyrak-Nolte, L.J. and Cook, N.G.W., 1989. The Fractal Geometry of Flow Paths in Natural Fractures in Rocks and the Approach to Percolation. PAGEOPH, 131, Nos. 1/2.

Odagaki, T., Kawai, H. and Toyofuku, S., 1999. Percolation in Correlated Systems. Physica A, 266: 49-54.

Odeh, A. S., 1981. Comparison of solutions to a three-dimensional black-oil reservoir simulation problem. SPE 9723.

Oda, M., 1985. Permeability tensor for discontinuous rock mass. Geotechnique, 35(4): 483-495.

Odling, N.E., 1992a. Permeability of natural and simulated fracture patterns, structural and tectonic modelling and its application to petroleum geology. NPF Special Publication 1, Norwegian Petroleum Society (NPF), 365-380.

Odling, N. E., 1992b. Network properties of a two-dimensional natural fracture pattern. PAGEOPH, 138(1): 95-114.

Odling, N. E., Webman, I., 1991. A "conductance" mesh approach to the permeability of natural and simulated fracture patterns. Water Resources Research, 27(10): 2633-2643.

Onur, M., Zeybek, A. D., Serpen, U. and Gok, I. M., 2003. Application of modern well test analysis techniques to pressure transient tests in Kizildere geothermal field, Turkey. Geothermics, 32: 147-170.

Parney, P., Cladouhos, T., La Pointe, P., Dershowitz, W. and Curran, B., 2000. Fracture and Production Data Integration Using Discrete Fracture Network Models for Carbonate Reservoir Management, South Oregon Basin Field, Wyoming. SPE 60306, SPE Rocky Mountain Reg./Low Perm. Res. Symp. And Exh., 12-15 March, Denver, CO.

Petrel Manual, 2007. Petrel Processes. Schlumberger.

Pruess, K., Narasimhan, T.N., 1985. A practical method for modeling fluid and heat flow in fractured porous media. SPE Journal, 25(1) 14-26.

Rezaee, M. R., Jafari, A. and Kazemzadeh, E., 2006. Relationships between permeability, porosity and pore throat size in carbonate rocks using regression analysis and neural networks. Journal of Geophysics and Engineering, 370–376.

Rossen, W. R., Gu, Y. and Lake, L. W., 2000. Connectivity and permeability in fracture networks obeying power-law statistics. SPE 50720, paper presented at the SPE Permian Basin Oil and Gas Rec. Conf., Midland, TX, 21-23 March.

Sahimi, M., 1993. Flow phenomena in rocks: From continuum models to fractals, percolation, cellular automata, and simulated annealing. Rev. of Modern Phys., 65(4), Oct., 1392-1537.

Sammis, C., An, L.J., Ershaghi, I., 1991. Fracture patterns in Graywacke outcrops at the Geysers geothermal field. In: Proceedings Sixteenth Workshop on Geothermal Reservoir Engineering, Stanford University, Stanford, California, 107-111.

Sammis, C., An, L., Ershaghi, I., 1992. Determining the 3-D fracture structure in the Geysers geothermal reservoir. In: Proceedings Seventeenth Workshop on Geothermal Reservoir Engineering, Stanford University, Stanford, California, 79-85.

Saxena, U. and Vjekoslav, P., 1971. Factorial designs as an effective tool in mining and petroleum engineering. SPE 3333, unsolicited paper available in SPE Library.

Stauffer, D. and Aharony, A., 1994. Introduction to Percolation Theory. 2nd ed. Taylor and Francis, London.

Stauffer, D. and Aharony, A., 1992. Introduction to Percolation Theory. Taylor and Francis, Bristol, PA.

Stauffer, D., 1979. Scaling Theory of Percolation Clusters. Physics Reports (Review Section of Physics Letters). 54:1-74.

Teimoori, A., Chen, Z., Rahman, S. S. and Tran, T., 2003. Calculation of permeability tensor using boundary element method provides a unique tool simulate naturally fractured reservoirs. SPE 84545, Annual Technical Conference and Exhibition held in Denver, Colorado, USA.

Vaentini, L., Perugini, D. and Poli, G., 2007. The small-world topology of rock fracture networks. Physica A. 377: 323-328.

Veire, H.H., Wennberg, O.P., Basquet , R. and Ingsøy, P., 2007. Integration of wide azimuth seismic with static and dynamic well data for fractured reservoir characterization. EAGE 69th Conference & Exhibition, London, UK, 11 - 14 June.

Warren, J. E. and Root, P. J., 1963. The behavior of naturally fractured reservoirs. SPE Journal, September, 245-255.

Whitaker, S., 1998. The method of volume averaging. Kluwer, Dordrecht.

White, A. C., Monlar, D., Aminian, K., Mohaghegh, S., Ameri, S. and Esposito, P., 1995. The application of ANN for zone identification in a complex reservoir. SPE 30977, SPE Eastern Reg. Conf. and Exh., 18-20 Sept., Morgantown, WV.

Wiener, J., 1995. Predict permeability from wire line logs using neural networks. Petroleum Engineering International, May18–24.

Wong, P. M. and Nikravesh, M., 2001. Introduction: Field applications of intelligent computing techniques. Journal of Petroleum Geology, 24(4): 381-387.

Zhang, X. and Sanderson, D.J., 2002. Numerical modelling and analysis of fluid flow and deformation of fractured rock masses. Oxford, UK, Elsevier.